Valuation of Some Nonlinear Financial Contracts by Finite Element Method

NAZARBAYEV
UNIVERSITY

A thesis presented by
Rakhymzhan Kazbek

to

The School of Sciences and Humanities in partial fulfillment of the requirements for the degree of

Doctor of Philosophy in Mathematics Nazarbayev University

Astana, Kazakhstan
June 14, 2024

Acknowlegements

To My Supervisors

The inspiration for this dissertation began six years ago during my master's studies with my supervisor, Prof. Dongming Wei. I deeply appreciate his patience, active involvement, and motivational words, especially when I was close to losing my drive to continue the research.

I am also grateful to him for organizing the dream team by inviting Professor Yerlan Amanbek and Professor Yogi Ahmad Erlangga. Their dedication was priceless.

Special thanks to Professor Yerlan, who was always open to discussions and concerned about my performance, always providing key advice and pushing me to follow the high standards. To be honest, I did not always understand the advice at that moment, but later, I came to appreciate its value, which contributed significantly to my PhD journey.

To Professor Yogi. The deeper understanding I gained during my PhD is closely associated with him. His dedication to my academic and personal growth has been a cornerstone of my PhD journey, and I am profoundly thankful for his role in my journey. Besides our job, his mentorship was invaluable. My gratitude towards Professor Yogi is beyond words.

I would like to express my gratitude to my external and internal examiners, Prof. Yerkin Kitapbayev, Prof Jichun Li, Prof. Ardak Kashkynbayev, and Prof. Rustem Takhanov, for their insightful comments and feedback, which have significantly enhanced the overall quality of my thesis. Additionally, I appreciate the support and guidance from the PhD program director, Prof. Durvudkhan Suragan.

To My Family

I express my endless love and gratitude to my mother, who never lost faith in my abilities. I am also deeply thankful to my siblings, Bakhytkul, Meruert, and Baurzhan,

for their support and encouragement throughout my life.

I am incredibly thankful to my wife, Assel, and my small, beautiful daughter, Amina, for their unwavering support, belief, and patience.

This accomplishment was only possible with the involvement of God's willing and the people I listed.

In conclusion, I dedicate this thesis work to the memory of my father, who passed away during the pandemic. He was an expert in the investment and banking industry, and in his prime, he served as the Chief Executive Officer of a bank in Kazakhstan. Undoubtedly, he is my lifelong idol, whom I always respected and loved. He is the one who has always inspired and motivated me to follow my dreams. We miss him a lot!

Supervisory Committee

Lead Supervisor: Dongming Wei
Full Professor, Department of Mathematics
Nazarbayev University
email: dongming.wei@nu.edu.kz

Co-Supervisor: Yerlan Amanbek
Assistant Professor, Department of Mathematics
Nazarbayev University
email: yerlan.amanbek@nu.edu.kz

External Supervisor: Yogi Ahmad Erlangga
Associate Professor, College of Natural and Health
Zayed University
email: yogi.erlangga@zu.ac.ae

Abstract

This thesis proposes a methodology for dealing with nonlinear financial derivative models using the finite element method (FEM). Financial engineering solutions are in high demand to mimic realistic market scenarios. Significantly, the nonlinear partial differential equations (PDE) seen in security pricing theory make it almost impossible to develop explicit solutions. Therefore, one resorts to numerical approximations. The literature contains articles dealing with nonlinear contracts using the finite difference method (FDM), which practitioners frequently use. This thesis aims to provide some computational gain in time and an accurate solution to nonlinear contracts in the derivative market. The generality of the approach is extendable to other types of American and European nonlinear contracts.

For nonlinear models, conventional FEM and Isogeometric analysis (IGA) are designed to be compared with benchmark results. The second-order P2-FEM performs better convergence properties than FDM and P1-FEM for convertible bond models. Moreover, the incorporation of an adaptive grid leads to the use of a few spatial discretizations.

Usually, PDE models seen in financial engineering consist of convection-dominated or degenerate terms. The naive approach relies on stabilization techniques, as they allow for mitigating spurious oscillations. Alternatively, we use a relatively new approach, demonstrated by IGA-NURBS-based finite element technology, where the monotonic convergence is achieved with uniform and non-uniform grids without any stabilization techniques and validated within the benchmark region. Numerical experiments were conducted among well-known conventional FEM and FDM methods. The presence of the IGA framework has showcased the classical results by using fitted curve approximation. IGA demonstrates notable results based on the linear case, where the exact solution was achieved using a lesser number of grids than those by FEM and/or FDM.

The post-processing Greek values are essential, as is the price of the contracts. The literature on computing the Greek values by FDM or finite volume methods (FVM) is

vast. Specific models that consider frictionless markets may encounter challenges in accurately representing real-world scenarios. To satisfy the request of the derivative market, one shall consider the nonlinear pricing models that incorporate the specific request seen in financial derivative markets. The use of standard FDM or/and FEM leads to instability in the post-processing Greeks. In principle, a possible mitigation of such oscillations could be resolved using stabilization techniques. Employing NURBS basis functions with high compact support offers smoother Greek values, which may contribute to more reliable investment and trading strategies for hedging purposes.

Абстракт

Бұл диссертация соңғы элементтер әдісін (FEM) қолданатын сызықтық емес қаржылық туынды модельдермен жұмыс істеу әдістемесін ұсынады. Қаржылық инженерия шешімдері нарықтың шынайы сценарийлеріне қайталау үшін жоғары сұранысқа ие. Маңыздысы, бағалы қағаздардың баға теориясында көрінетін сызықты емес ішінара дифференциалдық теңдеулер (PDE) айқын шешімдерді әзірлеуді қиындатады. Сондықтан сандық жуықтауларға жүгінеді. Әдебиетте практиктер жиі қолданатын шекті айырмашылықтар әдісін (FDM) қолданатын сызықтық емес келісімдерге қатысты мақалалар бар. Бұл дипломдық жұмыс уақытында белгілі бір есептеу табысын және туынды нарықтағы сызықтық емес келісім-шарттардың дәл шешімін қамтамасыз етуге бағытталған. Әдістің мәні американдық және еуропалық сызықтық емес келісімшарттардың басқа түрлеріне де қолдануға қолайлы.

Сызықты емес модельдер үшін әдеттегі FEM және изогеометриялық талдау (IGA) эталондық нәтижелермен салыстыруға арналған. Екінші ретті P2-FEM конвергенциялық қасиеттерді айырбасталатын байланыс үлгілері үшін FDM және P1-FEM-ге қарағанда жақсырақ орындайды. Сонымен қатар, адаптивті торды енгізу бірнеше кеңістіктік дискретизацияларды қолдануға әкеледі.

Әдетте, қаржылық инженерияда көрінетін PDE үлгілері конвекция басым немесе азғындалған мүшелерден тұрады. Аңғал тәсіл тұрақтандыру әдістеріне сүйенеді, өйткені олар жалған тербелістерді азайтуға мүмкіндік береді. Балама ретінде біз IGA-NURBS негізіндегі соңғы элементтер технологиясы арқылы орын алған салыстырмалы түрде жаңа тәсілді қолданамыз, мұнда монотонды шешімге жету ешқандай тұрақтандыру әдістерінсіз біркелкі және біркелкі емес торлармен қол жеткізілді және эталондық аймақта расталады. Сандық тәжірибелер белгілі дәстүрлі FEM және FDM әдістерінің арасында жүргізілді. IGA құрылымының болуы бекітілген қисық жуықтауды қолдану арқылы классикалық нәтижелерді көрсетті. IGA сызықтық жағдайға негізделген елеулі нәтижелерді көрсетеді,

мұнда нақты шешім FEM және/немесе FDM-мен салыстырғанда торлардың аздау саны арқылы қол жеткізілді.

Келісімшарттардың бағасы сияқты өңдеуден кейінгі грек мәндері өте маңызды. Грек мәндерін FDM немесе соңғы көлемді әдістермен (FVM) есептеу туралы әдебиетте өте кең таралған. Үйкеліссіз нарықтарды қарастыратын арнайы үлгілер нақты әлемдегі сценарийлерді дәл көрсетуде қиындықтарға тап болуы мүмкін. Туынды нарықтың сұранысын қанағаттандыру үшін туынды қаржы нарығында байқалатын нақты сұранысты қамтитын сызықтық емес баға модельдерін қарау қажет. Стандартты FDM немесе/және FEM пайдалану кейінгі өңдеу гректерінде тұрақсыздыққа әкеледі. Негізінде мұндай тербелістердің ықтимал жұмсартылуын тұрақтандыру әдістерін қолдану арқылы шешуге болады. Жоғары ықшам қолдауы бар NURBS негізгі функцияларын пайдалану хеджирлеу мақсаттары үшін сенімді инвестициялық және сауда стратегияларына ықпал етуі мүмкін біркелкі грек құндылықтарын ұсынады.

Contents

1 Introduction **1**

1.1 Historical background 1
1.2 Literature review 2
1.3 Aim of this work 5
1.4 Financial derivative models 6
1.5 Contributions 9
1.6 Outline 10

2 FEM for Black-Scholes equations **11**

2.1 European call option 11
2.1.1 Derivation of the Black-Scholes PDE 12
2.2 Finite Element Method 16
2.2.1 Linear polynomial bases 19
2.2.2 Quadratic polynomial bases 21
2.3 Isogeometric analysis 22
2.3.1 B-spline and NURBS 23
2.3.2 Gauss-Legendre quadrature 26
2.4 Time integration scheme 27
2.5 Stability analysis 28
2.6 Absolute stability of the time integration scheme 30
2.7 Numerical results 33
2.7.1 Uniformly generated mesh 33
2.7.2 Non-uniformly generated mesh 34

3 Leland model for option pricing with transactions **40**

3.1 Introduction 40
3.1.1 Leland model as European contract 41
3.1.2 Transformation 42

3.2 Isogeometric analysis . . . 43
3.2.1 Weak formulation for Leland model . . . 43
3.3 Time integration scheme . . . 45
3.4 Numerical results . . . 46
3.4.1 Absolute stability region . . . 49
3.5 Greeks . . . 49

4 TF model for Convertible bonds **55**
4.1 Introduction . . . 55
4.2 The transformed TF model . . . 59
4.3 Finite element method . . . 62
4.3.1 Treating the constraints by Penalty method . . . 65
4.4 Time integration scheme . . . 65
4.4.1 Boundary solutions . . . 67
4.4.2 Interior solutions . . . 69
4.4.3 Summary of the time integration method . . . 71
4.5 Numerical solution of the TF model . . . 72
4.5.1 Comparison with FDM . . . 72
4.5.2 Absolute stability region . . . 77
4.5.3 The Greeks . . . 78
4.6 Accuracy of the approximations . . . 81

5 AFV model for Convertible bonds **84**
5.1 Introduction . . . 84
5.1.1 Derivation of the AFV model . . . 86
5.1.1.1 Convertible bond with no credit risk . . . 86
5.1.1.2 Risky bond . . . 88
5.1.1.3 The Hedge Model . . . 89
5.1.1.4 Equity component upon default . . . 92
5.1.2 AFV model as American contract . . . 93
5.1.3 Transformation of the models . . . 95
5.1.3.1 AFV model . . . 95
5.2 Isogeometric analysis . . . 97
5.2.1 Weak formulation for AFV model . . . 97
5.2.2 Treatment of nonlinear term by *group* FEM . . . 101
5.3 Time integration scheme . . . 102
5.3.1 Boundary solutions . . . 104

5.3.2 Interior solutions 105
5.4 Numerical results 106
5.4.1 Absolute stability region 113
5.5 Greeks 113

6 Conclusions **116**
6.1 European contract: Call option 116
6.2 European contract: Call option with transaction costs by Leland . . . 117
6.3 American contract: Convertible bonds by TF model 118
6.4 American contract: Convertible bonds by AFV model 118
6.5 Future work 119

Bibliography **121**

List of Figures

2.1 Two different stock price behaviors over the time $[t_o, T]$ 12

2.2 Solution of the European call option with $S_0 = \$10$, $r = 0.05$, $\sigma = 0.4$, $T = 1$, $K = \$10$. Left figure: Stock price evolution over time; Right figure: Option price surface with the projection of the stock price. 15

2.3 Solution of the European call option with $S_0 = \$10$, $r = 0.05$, $\sigma = 0.4$, $T = 1$, $K = \$10$. Left figure: Delta; Right figure: Gamma. . . . 15

2.4 Left figure: Cubic B-spline with uniform knot vector as $\Xi = \{0, 0, 0, 0, 1, 2, 3, 4, 5, 5, 5, 5\}$; Right figure: Cubic B-spline with non-uniform knot vector $\Xi = \{0, 0, 0, 0, 1, 2, 3, 3, 3, 4, 5, 5, 5, 5\}$. 24

2.5 Left figure: Cubic NURBS with uniform knot vector and unequal weight vector as $\Xi = \{0, 0, 0, 0, 1, 2, 3, 4, 5, 5, 5, 5\}$, $\omega = \{1, 1, 1, 4, 3, 5, 1, 1\}$; Right figure: Cubic NURBS with non-uniform knot vector and unequal weight vector as $\Xi = \{0, 0, 0, 0, 1, 2, 3, 3, 3, 4, 5, 5, 5, 5\}$, $\omega = \{1, 1, 1, 1, 4, 3, 5, 1, 1, 1\}$. 25

2.6 Absolute stability region of the time integration scheme for backward Euler, when $\theta = 1$ 32

2.7 Absolute stability region of the time integration scheme for Crank-Nicolson, when $\theta = 1/2$ 32

2.8 Solution of the European call option with $S_0 = \$100$, $r = 0.05$, $\sigma = 0.2$, $T = 1$, $K = \$100$. Left figure: Stock price evolution over time; Right figure: Option price surface with the projection of the stock price. . . 33

2.9 Solution of the European call option with $S_0 = \$100$, $r = 0.05$, $\sigma = 0.2$, $T = 1$, $K = \$100$. Left figure: Stock price evolution over time; Right figure: Option price surface with the stock price projection. 34

2.10 Solution of the European call option with $S_0 = \$100$, $r = 0.05$, $\sigma = 0.2$, $T = 1$, $K = \$100$. Left figure: Stock price evolution over time; Right figure: Option price surface with the projection of the stock price. . . 34

2.11 Solution of the European call option with $S_0 = \$100$, $r = 0.05$, $\sigma = 0.2$, $T = 1$, $K = \$100$. Left figure: Stock price evolution over time; Right figure: Option price surface with the projection of the stock price. . . 35
2.12 Solution of the European call option $t = 0$, $r = 0.05$, $\sigma = 0.2$, $\hat{K} = \$100$. Left figure: Uniform meshing with $nE = 2^8$, $n_\tau = 6 * 10^4$; Right figure: Non-uniform meshing with $nE = 2^8$, $n_\tau = 6 * 10^4$. 35
2.13 Solution of the European call option $t = 0$, $r = 0.05$, $\sigma = 0.2$, $\hat{K} = \$100$. Left figure: Uniform meshing with $nE = 2^8$, $n_\tau = 6 * 10^4$; Right figure: Non-uniform meshing with $nE = 2^8$, $n_\tau = 6 * 10^4$. 36
2.14 Solution of the European call option $t = 0$, $r = 0.05$, $\sigma = 0.2$, $\hat{K} = \$100$. Left figure: Non-uniform meshing with $nE = 2^5$, $n_\tau = 2 * 10^4$; Right figure: NURBS weights. 38
2.15 Solution of the European call option $t = 0$, $r = 0.05$, $\sigma = 0.2$, $\hat{K} = \$100$. Left figure: Non-uniform meshing with $nE = 2^6$, $n_\tau = 2 * 10^4$; Right figure: NURBS weights. 38
2.16 Solution of the European call option $t = 0$, $r = 0.05$, $\sigma = 0.2$, $\hat{K} = \$100$. Left figure: Non-uniform meshing with $nE = 2^7$, $n_\tau = 2 * 10^4$; Right figure: NURBS weights. 39

3.1 Solution of the Leland's model $t = 0$, $r = 0.1$, $\sigma = 0.2$, $\hat{K} = \$100$, $Le \approx 0.8$. Left figure by Cubic-NURBS: $\Delta\tau/h = 0.02$, $\Delta\tau/h^2 = 0.8$; Right figure by Cubic-NURBS: $\Delta\tau/h = 0.05$, $\Delta\tau/h^2 = 0.1$. 47
3.2 Solution of the Leland's model $t = 0$, $r = 0.1$, $\sigma = 0.2$, $\hat{K} = \$100$, $Le \approx 0.8$. Left figure by Cubic-NURBS: $\Delta\tau/h = 0.02$, $\Delta\tau/h^2 = 0.8$; Right figure by Cubic-NURBS: $\Delta\tau/h = 0.05$, $\Delta\tau/h^2 = 0.1$. 47
3.3 Solution of the Leland's model $t = 0$, $r = 0.1$, $\sigma = 0.2$, $\hat{K} = \$100$, $Le \approx 0.8$. Left figure by Cubic-NURBS: $\Delta\tau/h = 0.02$, $\Delta\tau/h^2 = 0.8$; Right figure by Cubic-NURBS: $\Delta\tau/h = 0.05$, $\Delta\tau/h^2 = 0.1$. 48
3.4 Solution of the Leland's model $t = 0$, $r = 0.1$, $\sigma = 0.2$, $\hat{K} = \$100$. Left figure: $Le \approx 0.8$, $h = 0.0017$, $\Delta\tau = 0.0000007$, therefore, $\Delta\tau/h = 0.0004$, $\Delta\tau/h^2 = 0.2$; Right figure: $Le \approx 1.33$, $h = 0.05$, $\Delta\tau = 0.00025$, therefore, $\Delta\tau/h = 0.005$,$\Delta\tau/h^2 = 0.1$. 49
3.5 Absolute stability region of the time integration scheme for Crank-Nicolson method, when $\theta = 1/2$ 50

3.6 Greeks for European call option with the parameters $t = 0$, $r = 0.1$, $r_c = 0.02$, $\sigma = 0.2$, $\hat{K} = \$100$. For Cubic-NURBS: $n_E = 2^{12}$, $n_\tau = 20000$; For P2-FEM: $n_E = 2^{11}$, $n_\tau = 20000$; Left figure: Delta Δ; Right figure: Gamma Γ; Middle figure: Theta Θ. 51
3.7 Greeks for Leland model with $t = 0$, $r = 0.1$, $\sigma = 0.2$, $\hat{K} = \$100$, $Le \approx 0.8$. For NURBS: $h = 0.005$, $\Delta\tau = 10^{-6}$, therefore, $\Delta\tau/h = 0.0001$, $\Delta\tau/h^2 = 0.02$; For P2-FEM: $h = 0.013$, $\Delta\tau = 5 * 10^{-7}$, therefore, $\Delta\tau/h = 3.6 * 10^{-5}$, $\Delta\tau/h^2 = 0.02$. Left figure: Delta Δ; Right figure: Gamma Γ; Middle figure: Theta Θ. 53
3.8 Greeks for Leland model with $t = 0$, $r = 0.1$, $\sigma = 0.2$, $\hat{K} = \$100$, $Le \approx 0.8$, $h = 0.0017$, $\Delta\tau = 0.0000007$, therefore, $\Delta\tau/h = 0.0004$, $\Delta\tau/h^2 = 0.2$. Left figure: Delta Δ; Right figure: Gamma Γ; Middle figure: Theta Θ. 54

4.1 Finite difference solution of the penalty TF model over time $t \in [0, 5]$, with $r = 0.05$, $r_c = 0.02$, $\sigma = 0.2$, $F = \$100$, $K = \$4$, $\rho = 10^6$; Left figure: $n = 100$, $n_t = 100$; Right figure: $n = 200$, $n_t = 200$. 73
4.2 P1-FEM solution of the penalty TF model over time $t \in [0, 5]$, with $r = 0.05$, $r_c = 0.02$, $\sigma = 0.2$, $F = \$100$, $K = \$4$, $\rho = 10^6$; Left figure: $n_E = 100$, $n_t = 100$; Right figure: $n_E = 200$, $n_t = 200$. 74
4.3 P2-FEM solution of the penalty TF model at $t \in [0, 5]$, with $r = 0.05$, $r_c = 0.02$, $\sigma = 0.2$, $F = \$100$, $K = \$4$, $\rho = 10^6$; Left figure: $n_E = 100$, $n_t = 100$; Right figure: $n_E = 200$, $n_t = 200$. 74
4.4 Solution of the TF model at $t = 0$, with $r = 0.05$,$r_c = 0.02$, $\sigma = 0.2$, $F = \$100$, $K = \$4$, $\rho = 10^6$; Left figure: for P1-FEM and P2-FEM, $n_E = 100$, $n_t = 100$, and for FDM $n = 200$; Right figure: for P1-FEM and P2-FEM, $n_E = 200$, $n_t = 200$, for FDM, $n = 400$. 75
4.5 Solution of the TF model at $t = 0$, with $r = 0.05$,$r_c = 0.02$, $\sigma = 0.2$, $F = \$100$, $K = \$4$, $\rho = 10^6$; Left figure: for P1-FEM and P2-FEM, $n_E = 400$, $n_t = 400$, for FDM $n = 800$; Right figure: for P1-FEM and P2-FEM, $n_E = 800$, $n_t = 800$, for FDM $n = 1600$. 75
4.6 Absolute stability region of the time integration scheme for Crank-Nicolson method, when $\theta = 1/2$ 78
4.7 Greeks by with the parameters $t = 0$, $r = 0.05$, $r_c = 0.02$, $\sigma = 0.2$, $F = \$100$, $K = \$4$, $\rho = 10^6$, $n_E = 1600$, $n_t = 1000$ by P2-FEM; Left figure: Delta Δ; Right figure: Gamma Γ; Right figure: Theta Θ. . . . 80

4.8 Greeks by with the parameters $t = 0$, $r = 0.05$, $r_c = 0.02$, $\sigma = 0.2$, $F = \$100$, $K = \$4$, $\rho = 10^6$, $n_E = 1600$, $n_t = 1000$ by P2-FEM; Left figure: Delta Δ; Right figure: Gamma Γ. 81
4.9 Error estimates of the model problem in $\tau \in [0, 1]$, with $r = 0.05$,$r_c = 0.02$, $\sigma = 0.2$, $h_{P1} = 3 \times 10^{-4}$, and $h_{P2} = 10^{-3}$. 82
4.10 Error estimates of the MMS model in $x \in [0, 1]$, with $r = 0.05$,$r_c = 0.02$, $\sigma = 0.2$, and $\Delta\tau = 10^{-4}$. 83

5.1 Solution of the AFV model $t = 0$, $r = 0.05$, $\sigma = 0.2$, $F = \$100$, $\rho = 10^6$. Left figure: $nE = 2^7$, $n_\tau = 100$, CB price by FDM; Right figure: $nE = 2^7$, $n_\tau = 100$, CB price by P1-FEM. 108
5.2 Solution of the AFV model $t = 0$, $r = 0.05$, $\sigma = 0.2$, $F = \$100$, $\rho = 10^6$. Left figure: $nE = 2^7$, $n_\tau = 100$, CB price by P2-FEM; Right figure: $nE = 2^7$, $n_\tau = 100$, CB price by Linear-NURBS. 108
5.3 Solution of the AFV model $t = 0$, $r = 0.05$, $\sigma = 0.2$, $F = \$100$, $\rho = 10^6$. Left figure: $nE = 2^7$, $n_\tau = 100$, CB price by Quadratic-NURBS; Right figure: $nE = 2^7$, $n_\tau = 100$, CB price by Cubic-NURBS. 109
5.4 Solution of the AFV model $t = 0$, $r = 0.05$, $\sigma = 0.2$, $F = \$100$, $\rho = 10^6$. Left figure: $nE = 2^8$, $n_\tau = 200$; Right figure: $nE = 2^9$, $n_\tau = 400$. 109
5.5 Solution of the AFV model $t = 0$, $r = 0.05$, $\sigma = 0.2$, $\hat{K} = \$100$. Left figure: Non-uniform meshing with $nE = 2^5$, $n_\tau = 100$; Right figure: NURBS weights. 111
5.6 Solution of the AFV model $t = 0$, $r = 0.05$, $\sigma = 0.2$, $\hat{K} = \$100$. Left figure: Non-uniform meshing with $nE = 2^6$, $n_\tau = 100$; Right figure: NURBS weights. 112
5.7 Solution of the AFV model $t = 0$, $r = 0.05$, $\sigma = 0.2$, $\hat{K} = \$100$. Left figure: Non-uniform meshing with $nE = 2^7$, $n_\tau = 100$; Right figure: NURBS weights. 112
5.8 Solution of the AFV model $t = 0$, $r = 0.05$, $\sigma = 0.2$, $\hat{K} = \$100$. Left figure: Non-uniform meshing with $nE = 2^8$, $n_\tau = 100$; Right figure: NURBS weights. 112
5.9 Absolute stability region of the time integration scheme for Crank-Nicolson method, when $\theta = 1/2$ 113

5.10 Greeks for AFV model with $t = 0$, $r = 0.05$, $\sigma = 0.2$, $F = \$100$. For NURBS: $nE = 2048$, $n_\tau = 2000$; For P2-FEM: $nE = 1000$, $d\tau = 2000$. Left figure: Delta Δ; Right figure: Gamma Γ; Middle figure: Theta Θ. 115

List of Tables

2.1 European call option at $t = 0$ and $\hat{K} = \$100$ computed by NURBS. Exact price is \$10.4505. During the refinement $n_\tau = 6 * 10^4$ is fixed. 37

3.1 Solution of the Leland's model $t = 0$, $r = 0.1$, $\sigma = 0.2$, $\hat{K} = \$100$, $Le \approx 0.8$ and $\Delta\tau/h^2 = 0.1$ throughout the refinement (with Rannacher start). 50

4.1 Modeling and computational parameters 73
4.2 Convertible bond price at $t = 0$ and $S = 100$ computed by P1-FEM, P2-FEM, and FDM with $n, n_E = n_t$ 76
4.3 Number of Newton's iterations for the results in Table 4.2 with $n, n_E = n_t$ 77

5.1 Modeling and computational parameters. 107
5.2 Convertible bond price based on the AFV model at $t = 0$ ans $S = 100$, computed using cubic NURBS. The numerical parameters are given in Table 5.1 111
5.3 Convertible bond price based on the AFV model at $t = 0$ ans $S = 100$, computed using cubic NURBS with optimal weights. 111

List of Symbols

Chapter 2

$\boldsymbol{K_j}$	FE stiffness matrix
$\boldsymbol{M_j}$	FE mass matrix
$\boldsymbol{N_j}$	FE convective matrix
Δ	Delta hedging parameter
$\Delta\tau$	Size of time step
Γ	Gamma
$\hat{\mu}$	Nodes of Gauss-Legendre quadrature
$\hat{\omega}$	Weights of Gauss-Legendre quadrature
$\hat{z}$	Normally distributed random number
$\mathbb{1}$	Indicator function
$\mathbb{E}$	Expected value
$\mathbb{Q}$	Probabilistic measure
$\mathbb{R}$	Set of real numbers
μ	Drift parameter
Ω	Physical domain
ω	Weight of the NURBS
Π	Portfolio value
ψ	FE basis function
σ	Volatility
τ	Transformed time variable
θ	Value of theta-scheme
ς	Root of Legendre polynomial
Ξ	IGA knot vector
ξ	Knot value
C^p	Differentiable up tp order p
F	Cumulative distribution function
H	Pay-off function
h	Mesh size between each element
K	Strike price
m	Multiplicity of knot
$M(t)$	Money-savings
N	B-spline basis function
n_E	Number of elements
n_τ	Number of time steps
n_{gp}	Number of Gaussian points
p	Order of B-Spline

P_L	Legendre polynomial
R	NURBS basis function
r	Risk-free interest rate
S	Stock price
T	Maturity time
t	Time
V	Value of European call option
V_h	FE approximation
v_i	FE nodal value
W	Stochastic term
x	Transformed log coordinates
z	Test function in the weak formulation

Chapter 3

$\boldsymbol{K_j}$	FE stiffness matrix
$\boldsymbol{M_j}$	FE mass matrix
$\boldsymbol{N_j}$	FE convective matrix
δt	The transaction frequency
$\Delta\tau$	Size of time step
Γ	Gamma
$\hat{K}$	Strike price
$\hat{u}$	Transformed slack vector
$\mathbb{R}$	Set of real numbers
$\mathcal{H}$	Subset of Hilbert space for test function
$\mathcal{S}$	Subset of Hilbert space for trial solution
Ω	Physical domain
ω	Weight of the NURBS
ψ, ϕ	FE basis function
τ	Transformed time variable
θ	Value of theta-scheme
$\tilde{u}$	Transformed value of option
$\tilde{u}_h$	FE approximation
$\tilde{u}_i$	FE nodal value
Ξ	IGA knot vector
ξ	Knot value
C^p	Differentiable up tp order p
h	Mesh size between each element
H^1	Hilbert space
Le	Leland number
N	B-spline basis function
n_E	Number of elements
n_τ	Number of time steps
n_{gp}	Number of Gaussian points
p	Order of B-Spline
R	NURBS basis function

r	Risk-free interest rate
S	Stock price
S_{int}	Initial stock price
T	Maturity time
t	Time
V	Value of European call option with transaction costs
w, q	Test function in the weak formulation
x	Transformed log coordinates
c	The round trip of transaction costs

Chapter 4

$\boldsymbol{K_j}$	FE stiffness matrix
$\boldsymbol{M_j}$	FE mass matrix
$\boldsymbol{N_j}$	FE convective matrix
Δ	Delta Greek
$\Delta\tau$	Size of time step
Γ	Gamma Greek
$\mathbb{R}$	Set of real numbers
$\mathcal{P}_{call}$	Penalty matrix of callability term
$\mathcal{P}_{put}$	Penalty matrix of puttability term
Ω	Physical domain
ψ	FE basis function
ρ	Penalty parameter
τ	Transformed time variable
Θ	Theta Greek
θ	Value of theta-scheme
$AccI$	Accrued Interest
B_{call}	Dirty call price
B_{put}	Dirty put price
F	Face value
h	Mesh size between each element
K	Coupon payment
k	Conversion ratio
n_E	Number of elements
n_τ	Number of time steps
r_c	Credit spread reflecting payoff default risk
r_c	Growth rate or risk-free rate
S	Stock price
S_{int}	Initial stock price
T	Maturity time
U	Convertible bond value
U_h, V_h	FE approximation
u_i, v_i	FE nodal value
V	Cash-only convertible bond value
x	Transformed space variable
z, w	Test functions in the weak formulation

P1-FEM Linear basis function

P2-FEM Quadratic basis function

Chapter 5

$\boldsymbol{K_j}$ FE stiffness matrix

$\boldsymbol{M_j}$ FE mass matrix

$\boldsymbol{N_j}$ FE convective matrix

Δ Delta Greek

$\Delta\tau$ Size of time step

η Indicator of partial and total default

Γ Gamma Greek

$\hat{R}$ Recovery factor

$\mathbb{R}$ Set of real numbers

$\mathcal{P}_{call}$ Penalty matrix of callability term

$\mathcal{P}_{put}$ Penalty matrix of puttability term

Ω Physical domain

ρ Penalty parameter

τ Transformed time variable

Θ Theta Greek

θ Value of theta-scheme

$AccI$ Accrued Interest

B Value of bond component

B_{call} Dirty call price

B_{put} Dirty put price

C Value of equity component

F Face value

h Mesh size between each element

K Coupon payment

k Conversion ratio

n_E Number of elements

n_τ Number of time steps

p Hazard rate

r Risk-free rate

R_i NURBS basis functions

S Stock price

S_{int} Initial stock price

T Maturity time

t Time variable

U Value of convertible bond

U_h, B_h, C_h FE approximation

u_i, v_i, c_i FE nodal values

w, q, z Test functions in the weak formulation

x Transformed space variable

Chapter 1

Introduction

1.1 Historical background

The revolutionary contribution to Financial Mathematics that the dynamic of fair option price follows stochastic processes was first reported by the mathematician Louis Bachelier in his doctoral thesis in 1900 Bachelier (1900) under the supervision of Henri Poincaré. The idea of this work was the incorporation of the Brownian Motion Brown (1828) into option price dynamics; indeed, underlying stock price theoretically follows the same behavior as a random movement of pollen grains of a plant in liquid. Five years after Bachelier's work, Albert Einstein Einstein (1905) proposed to use the same Brownian motion theory for modeling the movement of small particles. The theory of Bachelier has a counterpart as a negative value of the underlying assets, which, in reality, is mostly unlikely to happen. The work of Louis Bachelier was the driving model theory in Financial mathematics until 1973, when Fischer Black and Myron Scholes Black and Scholes (1973), published their groundbreaking work known today is the Black-Scholes model.

Derivative pricing theory is divided into two eras. The first work was done by Bachelier, but its negativity property inherited from arithmetic Brownian motion was evolved by the Black-Scholes-Merton (BSM) model, where they used geometric Brownian motion. We refer to BS as the original work and model by Black and Scholes in Black and Scholes (1973). The use of the Bachelier model nowadays has arisen again due to the crisis in 2008 with negative interest rate values in the market Choi et al. (2022). The recent COVID-19 collapse in the world with a historically low level of oil demand caused a negative price. Due to these facts, the original BS model has too restrictive an assumption the interest rate or stock prices(e.g. they follow the lognormal distribution), therefore, the model could not essentially fit some market requirements. Moreover, the BS model cannot deal with negative prices, unlike the

Bachelier model. Nevertheless, the BS model has given rise to several generations of researchers who have successfully applied the idea of the BS model in mathematical finance directions. Scientific and industrial communities have been applying these financial instruments in areas such as derivative pricing theory, operational research, real options, decision-making, and management strategies.

According to the financial market evaluation reports, as of 2022, the stock market in the world is $109 trillion, whereas the derivatives market costs about $20 trillion. The financial derivative market requires deep quantitative analysis and investment strategies worldwide every day.

1.2 Literature review

Quantitative finance is a huge branch of financial mathematics, and pricing derivatives is one of its main interests. The real-life advantage of quantitative finance can not be imagined without derivative pricing theory, which deals with stochastic differential equations (SDE), partial differential equations (PDE), and numerical simulations. The fair price of the derivative deduced from either a SDE or a PDE is a key information for financial institutions in terms of risk management and contract price evolution, as it can be utilized for trading strategies. Throughout this work, we have suggested several finite element frameworks for nonlinear derivative pricing theory in the context of American and European style contracts. There are two main approaches to defining the fair price of the derivative:

- PDE approach using Black Scholes based models Black and Scholes (1973).
- The martingale approach, which considers certain assumptions and the fair price, can be defined via expected value Harrison and Pliska (1981).

These two approaches are connected via the Feynman-Kac theorem Oosterlee and Grzelak (2019). However, this dissertation focuses on developing numerical techniques for PDEs based on the BS model. Particularly, we focus on European and American derivatives. A European option is a type of contract where the holder of the option can exercise only at maturity time, whereas American contract can be exercised during the whole contract life before the expiration date. One of the breakthrough inventions for PDE simulations for the variety of BS type problems was suggested by the group of Peter Forsyth in a series of papers, specifically in Forsyth et al. (1999); Forsyth and Vetzal (2002). The established methodology is widespread among the scientific and industrial community of numerical methods for BS type of

PDEs. Essentially, the PDEs in option pricing theory suffers from being convection dominated in the original form, however, this phenomenon can be handled by stabilization techniques from several decades ago at 1980s. The presence of the convection dominance nature makes the PDE unstable and more likely to produce spurious oscillations Forsyth et al. (1999), especially in the range where the gradient is strong by given initial data. In the context of the finite difference method (FDM), this kind of issue is handled by an upwinding scheme, which controls the flow on the convection term. However, the Finite Volume Method (FVM) is more natural to capture spurious oscillation as it allows them to describe the non-smooth initial data Forsyth et al. (1999). One should pay attention to the fact that the original Black Scholes PDE has variable coefficients on diffusion and convection terms, which makes it difficult to control the Peclet number throughout the space domain. However, this problem can be treated by subdividing into local and global domains, which entails more control over varying Peclet numbers. However, as in Zvan et al. (1999), this problem is treated by using FVM with the modified convective term, which incorporates the usage of Vanleer flux limiters paired with Rannacher start-in-time integration scheme. Note that flux limiters are introducing nonlinearity into PDE. However, this hybrid and brutal force approach guarantees the monotonic convergence to the solution using relatively fewer degrees of freedom (DOF). Moreover, it allows for mitigating the spurious oscillation that might be caused by a higher Peclet number. Finally, this approach is applied to the original PDE without using any change of variables, therefore, it is a tedious scheme from implementation point of view, as the scheme constructed by FVM and flux limiter needs to be adapted to each particular problem, especially with multidimensional problems. Not that this approach secures a high-resolution scheme, being accurate up to 6-8 decimal place precision Forsyth and Vetzal (2002).

In the context of Finite Element Method (FEM), as in Kozpınar et al. (2020), the discontinuous Galerkin method can effectively deal with convection dominant problems. Another approach is to use Cottrell et al. (2009) Streamline Upwinding Petrov Galerkin (SUPG) method to alleviate the spurious oscillations by modifying the weak formulation according to the specific task. However, this kind of problem can always be handled by the above-mentioned approaches. However, some research groups resort to transformation techniques that convert the variable coefficients into constant ones. Nevertheless, this transformation is exact, and the newly transformed problem will have an exact transition between the original and the transformed, which answers the question of whether the numerical results are inconsistent after the transformation. The transformation can not avoid the nature of the problem being convection

dominant; it only simplifies the existence of local Peclet numbers into global ones. Therefore, during the refinement process, one could spend more effort to capture the areas where the gradient is stronger. After the transformation, the only region where the problem can be faced is piecewise continuous or even discontinuous grids in initial data for our purpose. One of the widely used is the Landau transformation Zhu and Zhang (2011), which originates from fluid mechanics and all other methods involved in BS type of problems. Stabilization techniques were first introduced for continuum and structural or fluid mechanics. Stabilization techniques preserve high-resolution schemes or mitigate spurious oscillations Forsyth et al. (1999). However, the commonality is that those validated techniques are suited to financial problems.

Equally important, the numerical technique that is widely used and serves as a robust and fast technique is FDM. In general, FDM is a powerful technique compared to many other complicated methods, such as FEM or FVM, because of its simplicity and efficiency. However, it is plagued by the inability to handle some complicated geometries or nonlinear terms faced in PDEs. Moreover, the error analysis from the FDM perspective is hard to achieve for nonlinear models, while FEM suggests a richer arsenal to deal with different complicated models. Considering that the fundamental results of FEM are grounded in appropriate Hilbert and Sobolev spaces, which provide a broader architecture for addressing various issues, it's worth noting that, in practice, the challenges encountered in the financial sector are comparatively less intricate due to the simplicity of the geometry than those encountered in the field of engineering Cottrell et al. (2009). However, FDM is successfully applied to many nonlinear problems, showing a competitive result by modifying the scheme using nonlinear smooth mapping functions for a non-uniform grid Christara and Wu (2022). In FEM, the treatment of some nonlinearities are not straightforward as in FDM, therefore, wide range of financial derivative solutions are available in FDM context. The literature on FDM is vast and rich; however, the research is still active in using FDM for financial problems, where they utilize more complicated schemes such as adaptive mesh or non-uniform grids.

Up to this point, we covered a literature review consistent with this thesis's scope. However, some exotic numerical techniques are rarely used numerical techniques which use the B-spline collocation method for pricing the option Christara and Leung (2016) for jump-diffusion models as well as B-spline wavelets Ortiz-Gracia and Oosterlee (2013). The spectral method is Zhu and Kopriva (2009) used for European options, yielding superior results to benchmark FDM solutions. Radial basis

functions are used for the jump-diffusion model Cont et al. (2011). The review paper Saedi and Tularam (2018) provides a recent account on methodologies for option pricing under the Black-Scholes equation, such as the R3C scheme Ankudinova and Ehrhardt (2008), cubic spline wavelets and multiwavelet bases methods Černá and Fiňková (2024), FDM Dremkova and Ehrhardt (2011), FVM Forsyth and Vetzal (2002), and FEM Forsyth et al. (1999); Barone-Adesi et al. (2003); de Frutos (2005); Kovalov and Linetsky (2008). Another series of papers on the integral equation approach, which is defined in Fourier space, was produced by Zhu et al. (2018). As it was concluded, by comparing all other methods, FEM was the choice because of its convergence and mesh adaptivity opportunity.

These paragraphs serve as a concise literature review on some numerical methods for Black Scholes problems and motivation for applying the IGA for financial derivatives Pospíšil and Švígler (2018); Christara and Leung (2016); Mohammadi (2015). However, one could say that there have been relatively limited research papers published by FEM, particularly by IGA no papers for European or American nonlinear models.

1.3 Aim of this work

In the spirit of the gap in the literature and IGA's privilege, this thesis aims to provide a fundamental framework using IGA for European and American type nonlinear contracts, which, to the best of the author's knowledge, remains unexplored in the literature. A financial derivative is a contract containing two or more sides who are allowed to buy or sell this contract within a specified period and under specific regulations. Nowadays, the trend involves more than one risk factor, making the PDE approach less efficient as the several risk factors are presented as a multidimensional problem. It is well-known that once the dimension is higher than three in PDE, the computational cost to obtain a satisfactory solution is extremely high. Therefore, nowadays, the martingale approach Harrison and Pliska (1981) for finding the expected value of SDEs is more efficient for dealing with multifactor pricing problems Oosterlee and Grzelak (2019). Financially, it makes good sense to be capable of working with multifactor risk sources. Especially in option pricing problems, the portfolio content can vary depending on different types of instruments such as derivatives, stocks, commodities, features, swaps, etc. However, the ability to calculate the expected value of derivative price out of these factors is promising a serious structure to control, hedge, and rebalance the portfolio for better trading strategies. Famous

methodologies to deal with SDEs are Monte-Carlo or Fourier based approach and Euler-Maruyama scheme for asset integration, however, the research in this direction, involves a usage of Deep Learning to deal with multidimensional problems, which is presented as forward or backward SDEs Andersson et al. (2023). Nevertheless, many specific tasks in quantitative finance require a few risk factors, and it is still efficient to be solved by the PDE approach, which suggests a richer roaster of tools that can deal with up to three dimensions quite effectively and accurately than those by SDE models.

As was described in Section 1.2, the majority of the numerical methods in the derivative pricing area are FDM and FVM. There are relatively less number of FEM papers that discusses derivative pricing problems. Moreover, to the author's knowledge, IGA was not applied for nonlinear American and European contracts. Our proposed methodology is to handle the nonlinear problems using variational methods, such as FEM and Isogeometric Analysis (IGA). As FEM suggests, there is a wealth of theoretical and practical modifications that can deal with nonlinearity and convection dominance situations that are common in financial engineering. Depending on the specific problem, the methods vary to capture the models' nontrivial difficulties. For our purpose, we employ an IGA with NURBS, capable of effectively handling selected models, with the potential for extension to other issues commonly encountered in European or American style derivatives.

In the first part of this thesis, we introduce a hybrid of *group* FEM Fletcher (1983) with the system of PDEs, which involves a penalty term that is formulated from a Linear Complementarity Problem (LCP). Together with this spatial discretization, we use a modified Crank-Nicolson scheme for time integration. Moreover, the Newton-Raphson iterative method for non-smooth function is utilized at each time step to deal with nonlinearity coming from penalty terms. The second part introduces a more sophisticated IGA for nonlinear American and European contracts. IGA is a technique Cottrell et al. (2009) which falls into the FEM family as it involves the variational methods with different test functions compared to those by conventional FEM with Lagrangian polynomials. Specific techniques that do not have counterparts in conventional FEM are applied for different problems, suggesting a promising result.

1.4 Financial derivative models

Financially, there has been a rise in the usage of CBs in Europe in the past several years, as banking institutions are forced to suggest higher interest rates. This stimu-

lated the people to invest money into CBs as they offered lower interest rates but a safe environment for their activities. Therefore, the demand for CBs was raised again in Europe, however, after the financial crisis in 2008, the demand for CBs in China's derivative market went suddenly up as investors could save the money in CBs rather than traditional financial institutions. It is worth noting that the CBs are an old and specific type of derivatives that require advanced analytics before making any investments. Over the decades, the CB contracts in real life Jan De Spiegeleer (2014) have become more challenging and difficult to control the risks without puttability constraints. One could say that CBs are suggesting a stable investment vehicle, but it is plagued by being less effective from a profit point of view. Therefore, investments in CBs require a first round of investment to be a notable amount of money to get a prompt profit in a short window. Therefore, these are notable cons of CBs compared to traditional derivatives such as options or swaps, which suggest more risk but correspondingly more profit. Another motivation to study the CBs is that the literature is not saturated by CBs investigations, what one can not say about options. To fill this gap, we aim to study some CB models' fair prices and suggest relatively better techniques to overcome the gap.

Throughout the thesis work, we present the three main problems that, to the best of the author's knowledge, remained unexplored using FEM. Firstly, the Leland Leland (1985) model describes the impact of transaction costs when one exercises the derivatives. In previous work Wei et al. (2024), a European call option with transaction costs was handled using P1-P2 FEM, suggesting a comparable and stable solution for specific spatial-temporal grid choices. From a mathematical point of view, the Leland model in the PDE approach is a challenging task due to its strong nonlinearity created by diffusion terms. The stability of these kinds of strong diffusion terms is well posed in certain parameter settings. Therefore, the parameters need to be calibrated to avoid blow-up solutions and avoid falling into the range of ill-posed problems. Nevertheless, we consider both cases to show how different methodologies deal with it. A very important quantity in investigating the fair price is post-processing Greeks, which gives priceless information about the model's behavior according to each variable in the model. For a strongly nonlinear problem, the smooth Greeks are likely to be non-smooth or have shocks and spikes. However, this is of great importance, as those nonlinear models suggests real life benefits, therefore accurate Greeks are crucial and advantageous for practitioners. To remedy this issue, we have adapted the IGA with NURBS, which performs significantly better than other conventional methods.

The second problem is the Tsiveriotis and Fernandes (TF) model for pricing the convertible bonds Tsiveriotis (1998). A convertible bond is a financial derivative that allows the holder to convert it into the underlying asset during its lifetime. Indeed, CB is a complicated financial instrument that allows to manage the risk from above and below by controlling the asset price behavior. It belongs to the sort of American style derivatives, which is supposed to be described as LCP Forsyth and Vetzal (2002). Key constraints, such as callability, puttability and conversion constraints are the driving inequalities that must be imposed at each time step, either explicitly or implicitly. The literature on TF model is not vast, as it is more common in industrial software vendors. England's company called FINCAD&Numerix, and a French company called ITO33, are active users of this model and other models. Initially, we were inspired to suggest a better numerical method than standard FDM. The CBs are involving versatile parameters that are strongly connected within a parametric setting, therefore, it suggests a challenging task to implement them correctly from implementation point of view. Especially, the key constraints, which are only natural for CBs, have an impact on a solution which is computed at each time step. This makes the problem more sophisticated, as those parameters will beneficially change the penalized matrices during the Newton-Raphson iteration method. Therefore, computational time for this particular problem requires a huge amount of time when we use the fine grid in time and space.

The last considered problem is Ayache, Forsyth and Vetzal (AFV) model which has significantly improved the TF model as it was demonstrated to be inconsistent with default strategies of underlying assets. Incorporating partial and default cases has resulted in a new AFV model, which is actively used for convertible bond tasks worldwide, especially by ITO33 in France. This model is presented as a system of triple PDEs that has to be solved simultaneously at each time step, involving the Newton-Raphson method for the same penalty terms discussed for the TF model. We do provide a detailed comparison of different methods applied to this model, such as FDM, FEM and IGA. This model is convection dominated in its nature, as certain parameter configurations according to CB properties make this problem difficult to control in the numerical sense. However, an approach to overcome these nuances is presented in the following sections. Note that, for academic purposes, many key properties of CBs are shortlisted for the sake of simplicity and validation. Nevertheless, those properties can always be incorporated into the model properly once the fundamental model is performed by a numerical method in a satisfactory way.

1.5 Contributions

The notable results and improvements are highlighted in the following, which may deserve the reader's attention:

- P2-FEM is successfully applied to the TF model, resulting in better results than the traditional FDM benchmark problem using reduced grid points.
- Corresponding Greeks are computed taking advantage of P2-FEM, which resulted in the obtained explicit formula.
- P2-FEM Greeks are compared favorably with FDM Greeks for the TF model.
- The *group* FEM is applied for nonlinear terms under P1-P2-FEM and IGA NURBS as well.
- It was the first instance when IGA-NURBS was applied to nonlinear European and American contracts, suggesting an extendable structured methodology to other nonlinear problems.
- A fundamental framework for treating nonlinear European and American contracts is presented under IGA-NURBS.
- AFV model is solved accurately with monotonic convergence where the result falls into the benchmark range.
- Fitted NURBS results, where the weights are calibrated according to closed form or reference solution, has performed exceptional results both for the linear and nonlinear model, using a few grids to obtain a noteworthy similar result.
- A full-stage post-processing algorithm for computing the Greeks under IGA-NURBS is also presented. IGA-NURBS performs promising Greek solutions with previously obtained P2-FEM Greeks.
- Nonlinear Leland model is solved by IGA-NURBS precisely comparing to reference solution by P1-P2-FEM showing stability for a certain choice of time-space grid sizes.
- The Greeks from the Leland model by IGA-NURBS have outperformed the P2-FEM results. P2-FEM produces an oscillation in second-order Gamma Greek, while IGA-NURBS produces smooth Greeks throughout the whole surface.

1.6 Outline

In chapter 1, the introduction is carried out by considering the notable works and discussions of viable important moments that motivated us to make these investigations. In chapter 2, we have considered detailed information about the methodology and some numerical algorithms to demonstrate the fundamental aspects. Then, we provide the main results based on the European call option with transaction costs discussed in chapter 3. The TF model for pricing the convertible bonds by P1-P2-FEM is presented in chapter 4. Finally, the AFV model, which incorporates the default strategy, is solved by IGA-NURBS in chapter 5.

Chapter 2

FEM for Black-Scholes equations

2.1 European call option

In financial engineering, an option is a contract that gives the holder the right, not obligation, to trade (buy or sell) an asset (e.g. such as stock prices, swaps, futures, interest rates, foreign exchange rates, or commodity prices, etc.) at a predetermined strike price. The performance of the contract then depends on underlying assets. If the option can only be exercised at the expiry date, then it is called a European option Higham (2004). If the option can be exercised at any time, then it is called an American option Higham (2004). A call option gives a right but not an obligation to buy the underlying asset at a predetermined price, while a put option gives a right but not an obligation to sell the asset. In this section, we shall consider the European call option by FEM. We shall describe the underlying asset's behavior, which follows the Geometric Brownian Motion (GBM) Hull (2014). In this case, the underlying asset price can be written as a stochastic differential equation:

$$\mathrm{d}S(t) = \mu S(t)\mathrm{d}t + \sigma S(t)\mathrm{d}W(t) \quad \text{with} \quad S(t_0) = S_0,$$

where $S(t)$ is the stock price dynamic (normally distributed random variable) with $\mathcal{N}(0,1)$, μ is the drift parameter, σ is the volatility, and W is the Brownian motion. Therefore, the stochastic integral which handles the above SDE can be written as follows:

$$S(t) = S_0 + \int_{t_0}^{t} \mu S(\hat{z})\mathrm{d}\hat{z} + \int_{t_0}^{t} \sigma S(\hat{z})\mathrm{d}W(\hat{z})$$

where $\hat{z}$ is time variable. For illustration purposes, we have simulated the above SDE for two different stocks to observe their stochastic behavior. In particular, we consider a call option. In Figure 2.1, the blue stock at the time T is higher than the red one, initially the strike price is \$150. Therefore it is reasonable to buy this

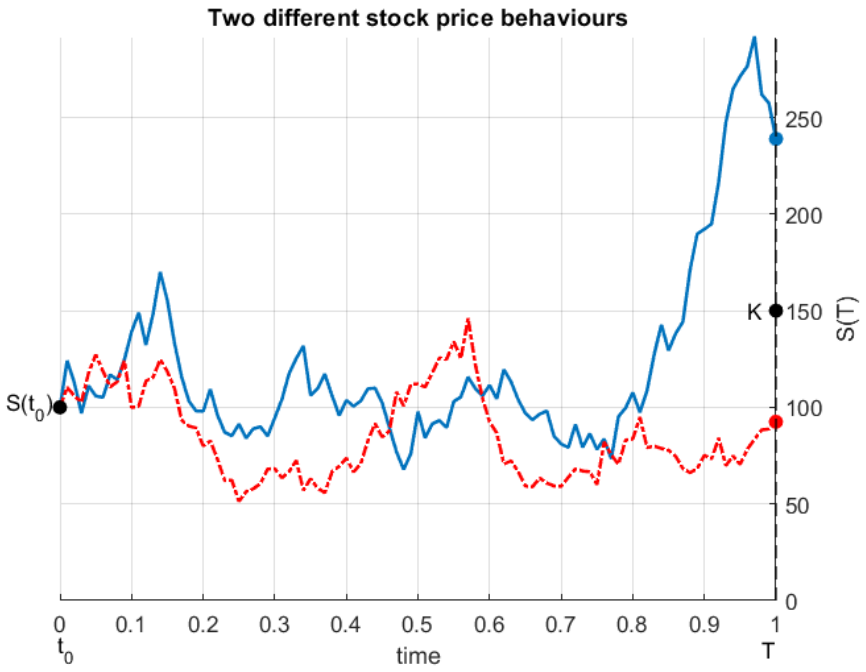

Figure 2.1: Two different stock price behaviors over the time $[t_o, T]$

stock because one can sell it promptly in the market for \$250, making the pay-off $\max(S - K, 0) = \$100$. The option becomes valueless in the red labeled asset, as $S(T) < K$. Hence, there is no need to exercise the right to call.

2.1.1 Derivation of the Black-Scholes PDE

This section serves to derive the BS PDE and analytical solutions. The celebrated BS PDE is a most famous model in financial engineering, where the authors Black and Scholes (1973) have used the idea that the underlying stock price follows the GBM. Moreover, they assume that the concept of replicating the portfolio is to obtain the Black-Scholes. They follow the dynamic Delta hedge by updating the portfolio at each time step. Stochastic process $S(t)$ is

$$\mathrm{d}S(t) = \mu S(t)\mathrm{d}t + \sigma S(t)\mathrm{d}W(t).$$

$V(S,t)$ is the price of European option. Then by means of Ito's lemma Ito (1951), one could come up with the following SDE:

$$\begin{aligned}\mathrm{d}V(t,S) &= \frac{\partial V}{\partial t}\,\mathrm{d}t + \frac{\partial V}{\partial S}\,\mathrm{d}S + \frac{1}{2}\frac{\partial^2 V}{\partial S^2}(\,\mathrm{d}S)^2 \\ &= \left(\frac{\partial V}{\partial t} + \mu S\frac{\partial V}{\partial S} + \frac{1}{2}\sigma^2 S^2\frac{\partial^2 V}{\partial S^2}\right)\mathrm{d}t + \sigma S\frac{\partial V}{\partial S}\,\mathrm{d}W.\end{aligned}$$

Now, we construct a portfolio that consists of a one long position option V and a short position in Δ number of shares of S:

$$\Pi(S,t) = V(S,t) - \Delta S(t).$$

By Ito's lemma, the change in the portfolio:

$$\begin{aligned} \mathrm{d}\Pi &= \mathrm{d}V - \Delta \mathrm{d}S \\ &= \left(\frac{\partial V}{\partial t} + \mu S\frac{\partial V}{\partial S} + \frac{1}{2}\sigma^2 S^2\frac{\partial^2 V}{\partial S^2}\right)\mathrm{d}t + \sigma S\frac{\partial V}{\partial S}\,\mathrm{d}W - \Delta\left[\mu S\,\mathrm{d}t + \sigma S\,\mathrm{d}W\right]. \\ &= \left[\frac{\partial V}{\partial t} + \mu S\left(\frac{\partial V}{\partial S} - \Delta\right) + \frac{1}{2}\sigma^2 S^2\frac{\partial^2 V}{\partial S^2}\right]\mathrm{d}t + \sigma S\left(\frac{\partial V}{\partial S} - \Delta\right)\mathrm{d}W \end{aligned}$$

At this position, the portfolio has accumulated all the necessary ingredients. For the dynamic Delta-hedging re-balancing strategy, we have to consider $\Delta = \dfrac{\partial V}{\partial S}$ which gives:

$$\mathrm{d}\Pi = \left(\frac{\partial V}{\partial t} + \frac{1}{2}\sigma^2 S^2\frac{\partial^2 V}{\partial S^2}\right)\mathrm{d}t. \tag{2.1.1}$$

This replicating portfolio approach converts the initial stochastic nature to deterministic one, since the form with stochastic random variable W vanishes under Delta-hedging. The final important component involves the interest rate on savings accounts, which provides us with another portfolio where the same Delta-hedging is applied:

$$\mathrm{d}\Pi = r\left(V - S\frac{\partial V}{\partial S}\right)\mathrm{d}t. \tag{2.1.2}$$

Equating (2.1.1) and (2.1.2) results in the Black-Scholes partial differential equation:

$$\frac{\partial V}{\partial t} + \frac{1}{2}\sigma^2 S^2\frac{\partial^2 V}{\partial S^2} + rS\frac{\partial V}{\partial S} - rV = 0 \tag{2.1.3}$$

which is supplemented by specific terminal conditions identifying the nature of the problem. The PDE is well-posed because of the positive diffusion term. The use of Feynman-Kac theorem Oosterlee and Grzelak (2019) in Financial mathematics is crucial as it suggests a wider opportunity to make a transition between a stochastic and a deterministic world.

Theorem 2.1.1 (Feynman-Kac). *Assume that money-savings according to constant interest rate r is given by $\mathrm{d}M(t) = rM(t)\mathrm{d}t$ and $V(S,t)$ is a price of the option as a function of time t and stock price S. Suppose that $V(S,t)$ satisfies the following PDE, with general drift term, $\bar{\mu}$, and volatility term, $\bar{\sigma}$:*

$$\frac{\partial V}{\partial t} + \bar{\mu}\frac{\partial V}{\partial S} + \frac{1}{2}\bar{\sigma}^2\frac{\partial^2 V}{\partial S^2} - rV = 0,$$

with a final condition given by $V(S,T) = H(S_T, T)$. *The price* $V(S,t)$ *at any time* t *and stock price* S *can be written as:*

$$V(S,t) = \mathrm{e}^{-r(T-t)}\mathbb{E}^{\mathbb{Q}}[H(T,S_T) \mid \mathcal{F}(t)] =: M(t)\mathbb{E}^{\mathbb{Q}}\left[\frac{H(T,S_T)}{M(T)} \mid \mathcal{F}(t)\right]$$

where the expectation is taken under the measure $\mathbb{Q}$ *(risk-neutral probability measure), with respect to a process* S*, which is defined by:*

$$\mathrm{d}S(t) = \bar{\mu}(t,S)\mathrm{d}t + \bar{\sigma}(t,S)\mathrm{d}W^{\mathbb{Q}}(t), \quad t > t_0.$$

Through Theorem 2.1.1, one could obtain the solution for European call option PDE (2.1.3) as follows:

$$\begin{aligned} V(S,t) &= \mathrm{e}^{-r(T-t)}\mathbb{E}^{\mathbb{Q}}[\max(S(T)-K,0) \mid \mathcal{F}(t)] \\ &= \mathrm{e}^{-r(T-t)}\mathbb{E}^{\mathbb{Q}}\left[S(T)\mathbb{1}_{S(T)>K} \mid \mathcal{F}(t)\right] - \mathrm{e}^{-r(T-t)}\mathbb{E}^{\mathbb{Q}}\left[K\mathbb{1}_{S(T)>K} \mid \mathcal{F}(t)\right]. \end{aligned}$$

The exact solution for the European call option reads:

$$V(t,S) = S(t)F_{\mathcal{N}(0,1)}(d_1) - K\mathrm{e}^{-r(T-t)}F_{\mathcal{N}(0,1)}(d_2),$$

where

$$\begin{aligned} d_1 &= \frac{\log\frac{S(t)}{K} + \left(r + \frac{1}{2}\sigma^2\right)(T-t)}{\sigma\sqrt{T-t}}, \\ d_2 &= d_1 - \sigma\sqrt{T-t}, \end{aligned}$$

and $F_{\mathcal{N}(0,1)}(\cdot)$ is the cumulative distribution function of the standard normal variable. A naive approach to check this solution, by the Feynman-Kac theorem, by substituting into the BS PDE to verify its correctness.

The derivatives of the exact solution, called Greeks, can be derived. The first derivative, called Delta Δ:

$$\Delta = \frac{\partial}{\partial S}V(S,t) = F_{\mathcal{N}(0,1)}(d_1),$$

Delta Δ shows us the option price's sensitivity to the stock price change. The second derivative, the Gamma Γ shows the sensitivity of Delta in the stock price change.

$$\Gamma = \frac{\partial\Delta}{\partial S} = F_{\mathcal{N}(0,1)}(d_1)\frac{\partial d_1}{\partial S} = \frac{F'_{\mathcal{N}(0,1)}(d_1)}{S\sigma\sqrt{T-t}}.$$

Using one-dimensional BS PDE, it is also possible to obtain the Theta Θ, which will be shown later 3. An alternative way to find the Theta is from BS PDE directly, as we already accumulated Delta and Gamma.

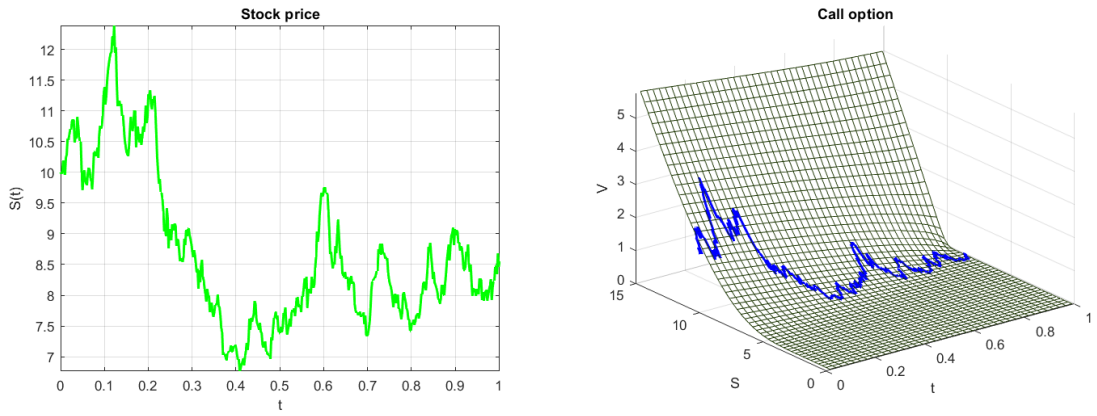

Figure 2.2: Solution of the European call option with $S_0 = \$10$, $r = 0.05$, $\sigma = 0.4$, $T = 1$, $K = \$10$. Left figure: Stock price evolution over time; Right figure: Option price surface with the projection of the stock price.

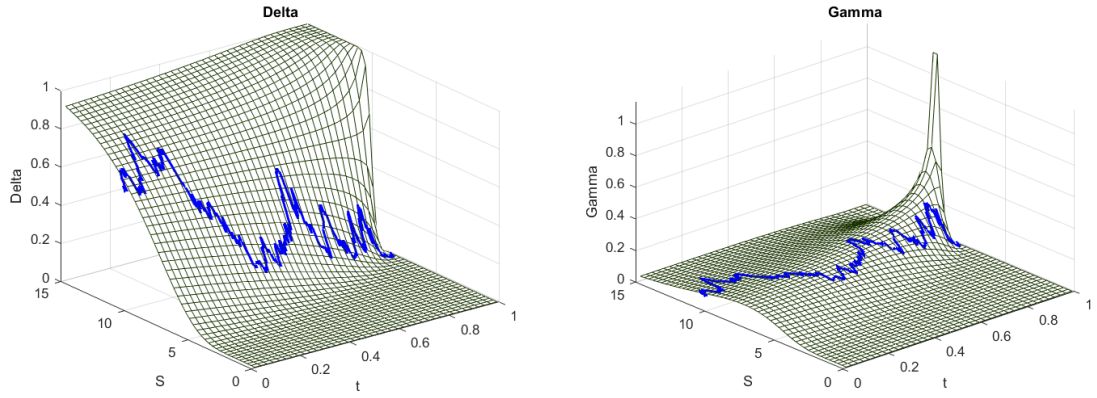

Figure 2.3: Solution of the European call option with $S_0 = \$10$, $r = 0.05$, $\sigma = 0.4$, $T = 1$, $K = \$10$. Left figure: Delta; Right figure: Gamma.

Figure 2.2 shows the exact solution of European call option. The stock price path is generated using the Monte-Carlo integration with the Euler-Maruyama scheme. The projection of the stock movement was superimposed on the option price surface. The solution of the BS PDE does not represent any randomness as the Delta-hedging strategy cancels out the stochastic term W. Nevertheless, the nature of BS is stochastic, and when the size of spatial dimension $d \leq 3$, the PDE approach is capable of producing high-quality results. In Figure 2.3, exactly obtained Delta and Gamma surfaces are plotted with stock projection. We have presented certain figures to give readers general information about the simplest cases.

2.2 Finite Element Method

The first invention of the family of variational methods is associated with Alexander Hrennikoff Liu et al. (2022). During his thesis work at MIT, he invented a similar approach to handle the structural mechanics problem, but due to the lack of computational opportunity, this idea could not be realized. Later in 1941, his first work, which is nowadays accepted as a starting point of FEM, is the extension of his doctoral thesis, where he made a great contribution to the design of metal structures. In the same year, Richard Courant from NYU gave a talk on numerical techniques that uses the Rayleigh-Ritz variational principle using a triangular subdomain, which is a primitive type of modern FEM. After two years, this work has been published. Over 80 years from the first papers of Hrennikoff and Courant, there has been an enormous development of FEM, which has made engineer's life much simpler. However, a detailed literature survey on FEM history can be found in Liu et al. (2022).

What does FEM represent nowadays? It is a universal tool used in many applied mathematics problems, from engineering to biological sciences, and providing an approximated numerical solution for the models. Throughout this work, the focus of the main methodology is FEM. This work is far away from being the one of the first application of FEM into financial world, however, a concise literature survey on FEM for Financial engineering can be found in section 1.2.

Now, we can represent the Finite Element formulation for the above-mentioned linear European call option (2.1.3). Before we start with the weak formulation, we will use the following transformation techniques:

- $x = \log\left(\frac{S}{S_{int}}\right)$, where S_{int} is initial stock price.
- $\tau = T - t$,
- $\frac{\partial V}{\partial t} = -\frac{\partial V}{\partial \tau}$,
- $\frac{\partial V}{\partial S} = \frac{1}{S}\frac{\partial V}{\partial x}$,
- $\frac{\partial^2 V}{\partial S^2} = \frac{1}{S^2}\left(\frac{\partial^2 V}{\partial x^2} - \frac{\partial V}{\partial x}\right)$.

Applying the transformation to (2.1.3), results in initial-boundary value problem as:

$$\begin{cases} \dfrac{\partial V}{\partial \tau} = \dfrac{1}{2}\sigma^2 \dfrac{\partial^2 V}{\partial x^2} + \left(r - \dfrac{1}{2}\sigma^2\right)\dfrac{\partial V}{\partial x} - rV \quad \text{in } \Omega. \\ V(x,0) = \max(S_{int}e^x - K, 0), \\ \lim_{x\to\infty} V(x,\tau) \approx S_{int}e^x \quad \text{on } \Gamma_D, \\ \lim_{x\to-\infty} V(x,\tau) = 0 \quad \text{on } \Gamma_D, \end{cases} \tag{2.2.1}$$

where $\Gamma_D = \Gamma \equiv \partial\Omega$.

The transformation, that converts S to x variable takes the origin from mechanics when one shall proceed with the numerical discretization in logarithmic coordinates, which is the so-called Landau technique, see e.g. Zhu and Zhang (2011). Reducing a variable coefficient of diffusion and convection terms to the constant coefficients is reasonable because, technically, the variable coefficients are closer to causing unpredictable behavior in the solution, such as spurious oscillations or numerical instability. The BS equation can always be treated in its original form using the numerical quadrature rule if we stay under the FEM framework. This approach will create another source of error in the FE element matrices, while some quadrature rule is supposed to approximate the integral term. In the current weak formulation setting, constant coefficients will be beneficial to result as exactly computed integral, consequently exactly obtained element matrices, which directly affects the quality of the FEM solution.

Let us consider a family of trial solutions as we construct finite-element methods to approximately discretize the BS PDE (2.2.1). To do so, one may characterize the two classes of functions: trial solutions and weighting functions. These functions shall satisfy the Dirichlet boundary condition. One may define the space of square-integrable functions on Ω, which is called $L^2(\Omega)$. Consider the space of square integrable functions on Ω, defined by $L^2(\Omega)$, where for any $f : \Omega \to \mathbb{R}$ such that

$$\int_\Omega f^2 d\Omega < +\infty.$$

There is a multi-index $\boldsymbol{\alpha} \in \mathbb{N}^d$ where d is the number of spatial dimensions. For $\boldsymbol{\alpha} = \{\alpha_1, \ldots, \alpha_d\}$, we define $|\boldsymbol{\alpha}| = \sum_{i=1}^d \alpha_i$. Let $D^\alpha = D_1^{\alpha_1} D_2^{\alpha_2} \ldots D_d^{\alpha_d}$, where $D_i^j = \dfrac{\partial^j}{\partial x_i^j}$. The requirement is that the derivatives of trial and weighting functions are square-integrable. If $f : \Omega \to \mathbb{R}$ is a trial solution, then it must satisfy the following expression:

$$\int_\Omega \nabla f \cdot \nabla f d\Omega < +\infty$$

this function belongs to the Sobolev space $\mathcal{H}^1(\Omega)$:

$$\mathcal{H}^1(\Omega) = \left\{ V \,\middle|\, D^{\boldsymbol{\alpha}} f \in L^2(\Omega), \middle| \, \boldsymbol{\alpha} \, \middle| \leq 1 \right\}.$$

The next step is to define the space for trial solutions $\mathcal{S}$, the requirement to be square integrable for the functions and satisfaction of Dirichlet boundary condition:

$$f|_{\Gamma_D} = g$$

thus

$$\mathcal{S} = \left\{ f \,\middle|\, f \in \mathcal{H}^1(\Omega), f\big|_{\Gamma_D} = g \right\}.$$

Now we are in the position to formulate the space for the class of weighting functions $\mathcal{V}$. However, the formulation of this class is likely to have a similar form to the latter, except the Dirichlet boundary condition is homogeneous. Then, it is defined as

$$\mathcal{V} = \left\{ z \,\middle|\, z \in \mathcal{H}^1(\Omega), z\big|_{\Gamma_D} = 0 \right\}.$$

The weak formulation of (2.2.1) is then defined as follows. Find $V \in \mathcal{S}$ such that for all $z \in \mathcal{V}$.

$$\int_\Omega z \frac{\partial V}{\partial \tau} = \frac{\sigma^2}{2} \int_\Omega z \frac{\partial^2 V}{\partial x^2} + \left(r - \frac{\sigma^2}{2} \right) \int_\Omega z \frac{\partial V}{\partial x} - r \int_\Omega zV,$$

where the integration is carried out along the x-direction (dx is not included to save space). Integration by parts and applying the homogeneous property of the function z at the boundary results in the weak formulation

$$\frac{\partial}{\partial \tau} \int_\Omega zV = -\frac{\sigma^2}{2} \int_\Omega \frac{\partial z}{\partial x} \frac{\partial V}{\partial x} - \left(r - \frac{\sigma^2}{2} \right) \int_\Omega \frac{\partial z}{\partial x} V - r \int_\Omega zV, \quad \forall z \in \mathcal{V}.$$

Note that the Neumann boundary (natural boundary condition in FE) conditions are not needed to supplement the well-posedness of the problem, therefore, addition term standing for Neumann condition vanishes after the integration by parts in diffusion term as it is homogeneous for most of the BS problems.

To build the finite-element approximation, consider the finite-dimensional subspace $S_0^h \subset \mathcal{H}_0^1$, spanned by the basis $\{\psi_1, \psi_2, \ldots, \psi_n\}$. The finite-element approximation to the solution V is the function

$$V_h = \sum_{i=1}^{n} v_i \psi_i + \sum_{i \in \mathcal{I}_\partial} v_i \psi_i \simeq V, \quad v_i \in \mathbb{R}.$$

where $\psi_{i\in\mathcal{I}_\partial}$ are additional functions needed to interpolate the given solutions at the boundaries. The use of the above approximations results in the weak formulation in the finite-dimensional space:

$$\begin{aligned}\frac{\partial}{\partial\tau}\left(\sum_{i=1}^{n} v_i \int_\Omega z\psi_i + \sum_{i\in\mathcal{I}_\partial} v_i \int_\Omega z\psi_i\right) &= -\frac{\sigma^2}{2}\left(\sum_{i=1}^{n} v_i \int_\Omega \frac{\partial z}{\partial x}\frac{\partial \psi_i}{\partial x} + \sum_{i\in\mathcal{I}_\partial} v_i \int_\Omega \frac{\partial z}{\partial x}\frac{\partial \psi_i}{\partial x}\right) \\ &\quad - \left(r - \frac{\sigma^2}{2}\right)\left(\sum_{i=1}^{n} v_i \int_\Omega \frac{\partial z}{\partial x}\psi_i + \sum_{i\in\mathcal{I}_\partial}^{n} v_i \int_\Omega \frac{\partial z}{\partial x}\psi_i\right) \\ &\quad - r\left(\sum_{i=1}^{n} v_i \int_\Omega z\psi_i + \sum_{i\in\mathcal{I}_\partial} v_i \int_\Omega z\psi_i\right).\end{aligned} \tag{2.2.2}$$

In the Galerkin method Kythe and Wei (2004), the test function z is chosen to coincide with the basis function ψ_i. Imposing this condition for $z = \psi_j$, $j = 1, \ldots, n$ results in the system of equations

$$\begin{aligned}\frac{\partial}{\partial\tau}\left(\sum_{i=1}^{n} v_i \int_\Omega \psi_j\psi_i + \sum_{i\in\mathcal{I}_\partial} v_i \int_\Omega \psi_j\psi_i\right) &= -\frac{\sigma^2}{2}\left(\sum_{i=1}^{n} v_i \int_\Omega \frac{\partial \psi_j}{\partial x}\frac{\partial \psi_i}{\partial x} + \sum_{i\in\mathcal{I}_\partial} v_i \int_\Omega \frac{\partial \psi_j}{\partial x}\frac{\partial \psi_i}{\partial x}\right) \\ &\quad - \left(r - \frac{\sigma^2}{2}\right)\left(\sum_{i=1}^{n} v_i \int_\Omega \frac{\partial \psi_j}{\partial x}\psi_i + \sum_{i\in\mathcal{I}_\partial}^{n} v_i \int_\Omega \frac{\partial \psi_j}{\partial x}\psi_i\right) \\ &\quad - r\left(\sum_{i=1}^{n} v_i \int_\Omega \psi_j\psi_i + \sum_{i\in\mathcal{I}_\partial} v_i \int_\Omega \psi_j\psi_i\right).\end{aligned} \tag{2.2.3}$$

In practice, systems of equations (2.2.3) is constructed via an assembly process using (local) element matrices, whose structures depend on the choice of the basis functions ψ_i. The common choice for the basis functions is a class of functions satisfying the nodal condition,

$$\psi_i(x_j) = \begin{cases} 1, & i = j, \\ 0, & \text{otherwise}, \end{cases} \tag{2.2.4}$$

where x_j is the nodal point. This choice leads to global systems of linear equations with sparse and banded coefficient matrices.

2.2.1 Linear polynomial bases

Consider partition of the spatial domain Ω into n_E non-overlapping elements $\Omega_j = [x_{j-1}, x_j]$, with $|\Omega_j| = x_j - x_{j-1} = h$, x_j, $j = 0, \ldots, n_E$, the nodal points, $x_0 = x_{\min}$

and $x_{n_E} = x_{\max}$. In the basic element $\Omega_j = [x_{j-1}, x_j]$, we define two linear interpolation basis functions on parametric coordinates, ξ, which will later be transformed to physical coordinates x

$$\phi_1(\xi) = \xi \quad \text{and} \quad \phi_2(\xi) = 1 - \xi, \quad 0 \le \xi \le 1,$$

which are called the local linear shape functions in the parametric coordinate ξ associated with $\phi_1^{(e)}(x)$ and $\phi_2^{(e)}(x)$. Where

$$\xi(x) = \frac{x - x_1^{(e)}}{x_2^{(e)} - x_1^{(e)}}, \quad x \in \left[x_1^{(e)}, x_2^{(e)}\right].$$

The inverse of $\xi(x)$ is $x(\xi) = x_1^{(e)} + \left(x_2^{(e)} - x_1^{(e)}\right)\xi$. After transformation, linear basis functions are:

$$\psi_{j-1}(x) = (x - x_j)/(x_{j-1} - x_j) = -(x - x_j)/h,$$
$$\psi_j(x) = (x - x_{j-1})/(x_j - x_{j-1}) = (x - x_{j-1})/h,$$

Evaluating the integrals in (2.2.3) using the above-stated basis functions over the element Ω_j results in the following local (element) matrices:

- For the $\int \psi_j \psi_i dx$ term, the element matrix reads

$$\boldsymbol{M}_j = \begin{bmatrix} \int_{\Omega_j} \psi_{j-1}\psi_{j-1}dx & \int_{\Omega_j} \psi_{j-1}\psi_j dx \\ \int_{\Omega_j} \psi_j\psi_{j-1}dx & \int_{\Omega_j} \psi_j\psi_j dx \end{bmatrix} = \frac{h}{6}\begin{bmatrix} 2 & 1 \\ 1 & 2 \end{bmatrix}.$$

- For the $-\int \psi_{j,x}\psi_{i,x}dx$ term, the element matrix reads

$$\boldsymbol{K}_j = -\begin{bmatrix} \int_{\Omega_j} \psi_{j-1,x}\psi_{j-1,x}dx & \int_{\Omega_j} \psi_{j-1,x}\psi_{j,x}dx \\ \int_{\Omega_j} \psi_{j,x}\psi_{j-1,x}dx & \int_{\Omega_j} \psi_{j,x}\psi_{j,x}dx \end{bmatrix} = -\frac{1}{h}\begin{bmatrix} 1 & -1 \\ -1 & 1 \end{bmatrix}.$$

- For the $\int \psi_j \psi_{i,x} dx$ term, the element matrix reads

$$\boldsymbol{N}_j = \begin{bmatrix} \int_{\Omega_j} \psi_{j-1}\psi_{j-1,x}dx & \int_{\Omega_j} \psi_{j-1}\psi_{j,x}dx \\ \int_{\Omega_j} \psi_j\psi_{j-1,x}dx & \int_{\Omega_j} \psi_j\psi_{j,x}dx \end{bmatrix} = \frac{1}{2}\begin{bmatrix} -1 & -1 \\ 1 & 1 \end{bmatrix}.$$

2.2.2 Quadratic polynomial bases

In this approach, we add a midpoint $x_{j-\frac{1}{2}} = (x_{j-1} + x_j)/2$ in the basic element Ω_j, giving three nodal points: x_{j-1}, $x_{j-1/2}$, and x_j, and define three quadratic interpolation polynomials satisfying the nodal condition (4.3.5) on parametric coordinates, ξ which will later be transformed to physical coordinates x:

$$\phi_1(\xi) = \frac{-\xi(1-\xi)}{2}, \quad \phi_2(\xi) = (1-\xi)(1+\xi), \quad \phi_3(\xi) = \frac{\xi(1+\xi)}{2}$$

resulting in P2-FEM.

$$x = \frac{x_3^{(e)} + x_1^{(e)}}{2} + \frac{\left(x_3^{(e)} - x_1^{(e)}\right)}{2}\xi$$

be the linear transformation, and for simplicity also let $x_2^{(e)} = \dfrac{x_3^{(e)} + x_1^{(e)}}{2}$. Once the transformation is done, we have:

$$\begin{aligned}
\psi_{j-1}(x) &= \frac{(x - x_{j-\frac{1}{2}})(x - x_j)}{(x_{j-1} - x_{j-\frac{1}{2}})(x_{j-1} - x_j)} = 2(x - x_{j-\frac{1}{2}})(x - x_j)/h^2, \\
\psi_{j-\frac{1}{2}}(x) &= \frac{(x - x_{j-1})(x - x_j)}{(x_{j-\frac{1}{2}} - x_{j-1})(x_{j-\frac{1}{2}} - x_j)} = -4(x - x_{j-1})(x - x_j)/h^2, \\
\psi_j(x) &= \frac{(x - x_{j-1})(x - x_{j-\frac{1}{2}})}{(x_j - x_{j-1})(x_j - x_{j-\frac{1}{2}})} = 2(x - x_{j-1})(x - x_{j-\frac{1}{2}})/h^2,
\end{aligned}$$

The local element matrices are as follows:

- the $\int \psi_j \psi_i dx$ term:

$$\boldsymbol{M}_j = \begin{bmatrix}
\int_{\Omega_j} \psi_{j-1}\psi_{j-1}dx & \int_{\Omega_j} \psi_{j-1}\psi_{j-\frac{1}{2}}dx & \int_{\Omega_j} \psi_{j-1}\psi_j dx \\
\int_{\Omega_j} \psi_{j-\frac{1}{2}}\psi_{j-1}dx & \int_{\Omega_j} \psi_{j-\frac{1}{2}}\psi_{j-\frac{1}{2}}dx & \int_{\Omega_j} \psi_{j-\frac{1}{2}}\psi_j dx \\
\int_{\Omega_j} \psi_j\psi_{j-1}dx & \int_{\Omega_j} \psi_j\psi_{j-\frac{1}{2}}dx & \int_{\Omega_j} \psi_j\psi_j dx
\end{bmatrix} = \frac{h}{30}\begin{bmatrix} 4 & 2 & -1 \\ 2 & 16 & 2 \\ -1 & 2 & 4 \end{bmatrix}.$$

- the $-\int \psi_{j,x}\psi_{i,x}dx$ term:

$$\boldsymbol{K}_j = -\begin{bmatrix} \int\limits_{\Omega_j} \psi_{j-1,x}\psi_{j-1,x}dx & \int\limits_{\Omega_j} \psi_{j-1,x}\psi_{j-\frac{1}{2},x}dx & \int\limits_{\Omega_j} \psi_{j-1,x}\psi_{j,x}dx \\ \int\limits_{\Omega_j} \psi_{j-\frac{1}{2},x}\psi_{j-1,x}dx & \int\limits_{\Omega_j} \psi_{j-\frac{1}{2},x}\psi_{j-\frac{1}{2},x}dx & \int\limits_{\Omega_j} \psi_{j-\frac{1}{2},x}\psi_{j,x}dx \\ \int\limits_{\Omega_j} \psi_{j,x}\psi_{j-1,x}dx & \int\limits_{\Omega_j} \psi_{j,x}\psi_{j-\frac{1}{2},x}dx & \int\limits_{\Omega_j} \psi_{j,x}\psi_{j,x}dx \end{bmatrix} = -\frac{1}{3h}\begin{bmatrix} 7 & -8 & 1 \\ -8 & 16 & -8 \\ 1 & -8 & 7 \end{bmatrix}.$$

- the $\int \psi_j\psi_{i,x}dx$ term:

$$\boldsymbol{N}_j = \begin{bmatrix} \int\limits_{\Omega_j} \psi_{j-1}\psi_{j-1,x}dx & \int\limits_{\Omega_j} \psi_{j-1}\psi_{j-\frac{1}{2},x}dx & \int\limits_{\Omega_j} \psi_{j-1}\psi_{j,x}dx \\ \int\limits_{\Omega_j} \psi_{j-\frac{1}{2}}\psi_{j-1,x}dx & \int\limits_{\Omega_j} \psi_{j-\frac{1}{2}}\psi_{j-\frac{1}{2},x}dx & \int\limits_{\Omega_j} \psi_{j-\frac{1}{2}}\psi_{j,x}dx \\ \int\limits_{\Omega_j} \psi_j\psi_{j-1,x}dx & \int\limits_{\Omega_j} \psi_j\psi_{j-\frac{1}{2},x}dx & \int\limits_{\Omega_j} \psi_j\psi_{j,x}dx \end{bmatrix} = \frac{1}{6}\begin{bmatrix} -3 & -4 & 1 \\ 4 & 0 & -4 \\ -1 & 4 & 3 \end{bmatrix}.$$

2.3 Isogeometric analysis

Isogeometric analysis is a recently developed numerical tool that incorporates the elements of computer-aided design (CAD) utilizing the splines as a test function. IGA was first introduced by Thomas Hughes in 2005 Hughes et al. (2005), Later, publication of IGA monorgaphy by Cottrell et al. (2009) has raised its further development and popularity. The core idea behind the IGA is to use splines functions approximate complicated geometries. Moreover, IGA is a strong tool that has proved its advantageous properties compared to conventional FEM Cottrell et al. (2009). Initially, the splines were invented in the middle of the last century by Isaac Jacob Schoenberg. Carl De Boor de Boor (1980) developed a recursive algorith and made it numerically stable with parametric representation. First crucial usage was related to the car manufacturing industry. Carl De Boor has made a crucial contribution by suggesting new approaches to control and use of splines. One of the most flexible types of spline is non-uniform rational B-splines (NURBS), where he has invented and implemented its practical power into the design of the car body. Afterward, the first time it was used for classical engineering problems was associated with the IGA. Nevertheless,

choosing a spline is always challenging, depending on the specific task that must be addressed. As we demonstrate later in this section, IGA also has weaker points than the traditional FEM approach.

FEM is not always a choice among practitioners of the Financial industry as its implementation and realization need more dedicated and advanced attention because of its complexity in implementation and mathematics. Another noteworthy point is that FEM is way more complicated than FDM, especially for nonlinear models. Although, IGA is a more sophisticated method compared to conventional FEM. The reasonable arguing point is that applying IGA for not-so-complex geometries seen in Financial derivative problems seems like a rough force to simulate something that can be done using other traditional simple-to-implement methods. Response to this moment will be more detailed later in this section.

For the European call option, we use the NURBS as a test function following the Galerkin method.Let $\Xi = \{\xi_1, \xi_2, \ldots, \xi_m\}$, with $m = n + p + 1$, be the knot vector, where the knot values $\xi_i \in \mathbb{R}$ are non-decreasing, i.e., $\xi_i \leq \xi_{i+1}$, defined in the so-called parameter space, and p be the polynomial order. The knot vector is said to be open if the knot value ξ_1 and ξ_m are repeated $p + 1$ times. Furthermore, the knot vector is said to be uniform if the knot values partition the parameter space into equal elements.

2.3.1 B-spline and NURBS

According to recursive Cox-De Boor's algorithm de Boor (1980), univariate B-spline basis function for $p = 0$ is defined on the parametric domain

$$N_{i,0} = \begin{cases} 1, \text{ if } \xi_i \leq \xi < \xi_{i+1} \\ 0, \text{ otherwise} \end{cases} \tag{2.3.1}$$

and for any $p \geq 1$,

$$N_{i,p} = \frac{\xi - \xi_i}{\xi_{i+p} - \xi_i} N_{i,p-1}(\xi) + \frac{\xi_{i+p+1} - \xi}{\xi_{i+p+1} - \xi_{i+1}} N_{i+1,p-1}(\xi). \tag{2.3.2}$$

Remarks on some properties of the B-Spline functions are in order:

1. $N_{i,p}$ are nonnegative, piecewise polynomial functions;
2. the sum of basis functions for a given order p is identically unity; and
3. for a uniform knot vector, the functions $N_{i,p} \in C^p$.

The latter property is of importance in the calculation of Greeks, the derivatives of the option price function. B-spline is always non-zero throughout the domain and only interpolatory at both ends. The continuity level within the knot vector is always C^p unless a non-uniform knot vector is introduced with C^{p-m_i} differentiability, where m_i is the multiplicity of knot ξ_i. For our purpose, both uniform and non-uniform knot vectors are used. A uniform open knot vector is interpolatory only at both ends, having distinct repeated knot values $p+1$ as in Figure 2.4. While a closed knot vector implies identical first and last knot values, which generates a closed loop. Note that B-splines are the particular case of the NURBS when the weights are distributed equally.

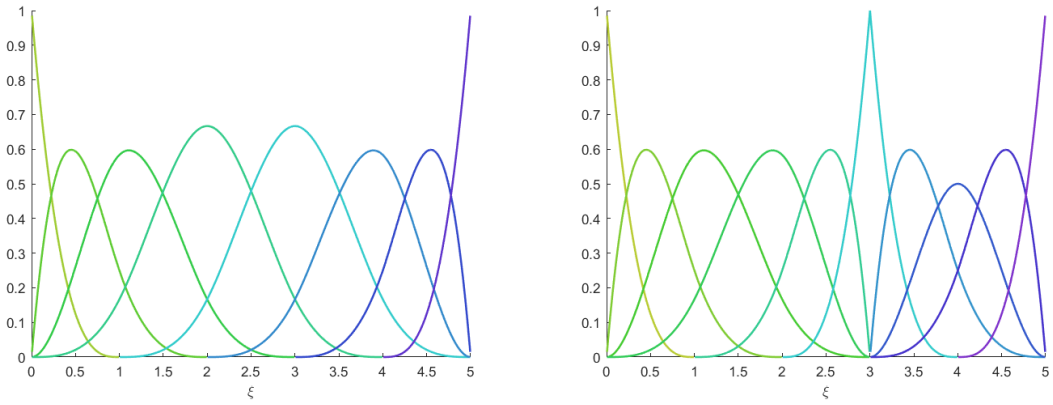

Figure 2.4: Left figure: Cubic B-spline with uniform knot vector as $\Xi = \{0, 0, 0, 0, 1, 2, 3, 4, 5, 5, 5, 5\}$; Right figure: Cubic B-spline with non-uniform knot vector $\Xi = \{0, 0, 0, 0, 1, 2, 3, 3, 3, 4, 5, 5, 5, 5\}$.

The NURBS inherits the beneficial properties of B-splines and is represented as a rational form of B-spline basis functions or sometimes referred to as a superset of B-splines:

$$R_{i,p}(\xi) = \frac{N_{i,p}(\xi)\omega_i}{\sum_{i=1}^{n} N_{i,p}(\xi)\omega_i} \tag{2.3.3}$$

where, $\{\omega_i\}_{i=1}^{n}$ are the NURBS weights. Compared to B-Splines, the NURBS basis functions are more flexible to capture non-smooth data. However, the choice of weights to perfectly capture different geometries is an open research question. The discussion of unequal weights will be discussed in the Section 4.5. Compared to B-Splines, the NURBS basis functions are more flexible (see Figure 2.5) to capture the complex geometries by an adjusted weight vector.

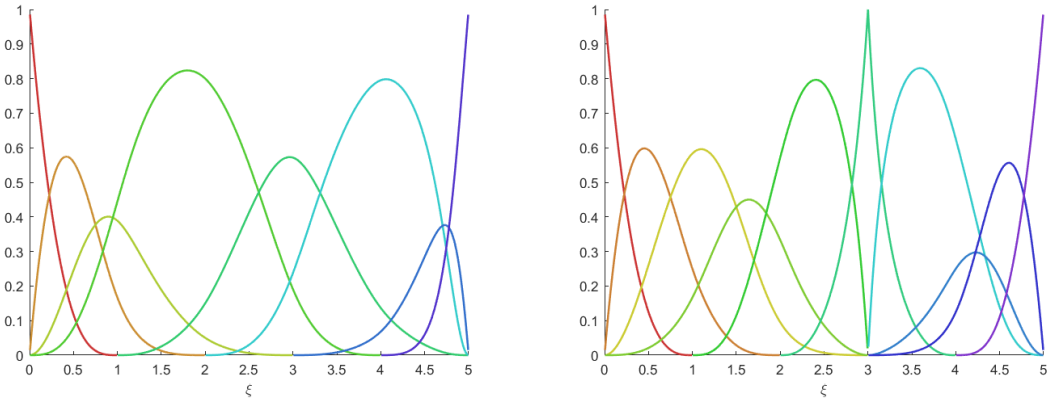

Figure 2.5: Left figure: Cubic NURBS with uniform knot vector and unequal weight vector as $\Xi = \{0,0,0,0,1,2,3,4,5,5,5,5\}$, $\omega = \{1,1,1,4,3,5,1,1\}$; Right figure: Cubic NURBS with non-uniform knot vector and unequal weight vector as $\Xi = \{0,0,0,0,1,2,3,3,3,4,5,5,5,5\}$, $\omega = \{1,1,1,1,4,3,5,1,1,1\}$.

The weights $w_i > 0, i = 1,2,\ldots,n$ need to be determined. The most appropriate fitting weights will be measured by the mean L^2 errors Pospíšil and Švígler (2018)

$$E_{\text{NURBS}} = \int_\Omega \left(V_{exact}(\xi) - V_{\text{h,NURBS}}(\xi)\right)^2 \, \mathrm{d}\xi$$

where E_{NURBS} is minimized with respect to the weights w_i.

In the same manner as we did for FEM, in IGA we are considering the family of trial solutions for spatial discretization:

$$V(x,\tau) \in \mathcal{S} = \left\{ V \,\middle|\, V \in \mathcal{H}^1(\Omega), V\big|_{\Gamma_D} = g \right\}.$$

and weighting functions are defined as

$$z \in \mathcal{V} = \left\{ z \,\middle|\, z \in \mathcal{H}^1(\Omega), z\big|_{\Gamma_D} = 0 \right\}.$$

Then the weak formulation is the same as we did for FEM except, now, the finite-dimensional subspace $S_0^h \subset \mathcal{H}_0^1$, spanned by the basis $\{R_1, R_2, \ldots, R_n\}$. The IGA NURBS-based finite-element approximation to the solution U is the function

$$V_h = \sum_{i=1}^{n} v_i R_i + \sum_{i \in \mathcal{I}_\partial} v_i R_i, \quad u_i \in \mathbb{R},$$

where $R_{i \in \mathcal{I}_\partial}$ are additional functions needed to interpolate the given solutions at the boundaries. The use of the above approximations results in the weak formulation in

the finite-dimensional space:

$$\begin{aligned}\frac{\partial}{\partial\tau}\left(\sum_{i=1}^{n} v_i \int_{\Omega} zR_i + \sum_{i\in\mathcal{I}_\partial} v_i \int_{\Omega} zR_i\right) &= -\frac{\sigma^2}{2}\left(\sum_{i=1}^{n} v_i \int_{\Omega} \frac{\partial z}{\partial x}\frac{\partial R_i}{\partial x} + \sum_{i\in\mathcal{I}_\partial} v_i \int_{\Omega} \frac{\partial z}{\partial x}\frac{\partial R_i}{\partial x}\right) \\ &\quad - \left(r - \frac{\sigma^2}{2}\right)\left(\sum_{i=1}^{n} v_i \int_{\Omega} \frac{\partial z}{\partial x} R_i + \sum_{i\in\mathcal{I}_\partial}^{n} v_i \int_{\Omega} \frac{\partial z}{\partial x} R_i\right) \\ &\quad - r\left(\sum_{i=1}^{n} v_i \int_{\Omega} zR_i + \sum_{i\in\mathcal{I}_\partial} v_i \int_{\Omega} zR_i\right),\end{aligned} \tag{2.3.4}$$

In the Galerkin method Cottrell et al. (2009), the test function z is chosen to coincide with the basis function R_i. Imposing this condition for $z = R_j$, $j = 1, \ldots, n$ results in the system of equations

$$\begin{aligned}\frac{\partial}{\partial\tau}\left(\sum_{i=1}^{n} v_i \int_{\Omega} R_jR_i + \sum_{i\in\mathcal{I}_\partial} v_i \int_{\Omega} R_jR_i\right) &= -\frac{\sigma^2}{2}\left(\sum_{i=1}^{n} v_i \int_{\Omega} \frac{\partial R_j}{\partial x}\frac{\partial R_i}{\partial x} + \sum_{i\in\mathcal{I}_\partial} v_i \int_{\Omega} \frac{\partial R_j}{\partial x}\frac{\partial R_i}{\partial x}\right) \\ &\quad - \left(r - \frac{\sigma^2}{2}\right)\left(\sum_{i=1}^{n} v_i \int_{\Omega} \frac{\partial R_j}{\partial x} R_i + \sum_{i\in\mathcal{I}_\partial}^{n} v_i \int_{\Omega} \frac{\partial R_j}{\partial x} R_i\right) \\ &\quad - r\left(\sum_{i=1}^{n} v_i \int_{\Omega} R_jR_i + \sum_{i\in\mathcal{I}_\partial} v_i \int_{\Omega} R_jR_i\right)\end{aligned} \tag{2.3.5}$$

Since the complexity of the NURBS functions entails the inevitable recourse to numerical quadrature, the actual integration of the element matrices is carried by the Gauss-Legendre quadrature rule, see, e.g., Cottrell et al. (2009). Although to increase the accuracy of the element matrices, one could increase the Gaussian points n_{gp}, as it was tested for a linear European call option, a large number of Gaussian n_{gp} does not affect the solution. The number of quadrature points is chosen to be $n_{gp} = p + 1$.

2.3.2 Gauss-Legendre quadrature

In piecewise polynomial-based FEM, the inner products can be evaluated relatively straightforwardly. This is typically done once on the so-called reference element. Evaluation of the inner products cannot however be done analytically due to the complexity of the NURBS basis functions and their derivatives. Numerical integration is therefore performed to approximately calculate the inner products. One popular

method for numerical integration is based on Gauss-Legendre quadrature Sevilla and Fernández-Méndez (2011); Jiang and Lin (2022).

The Gauss-Legendre quadrature rule for numerical integration of a function f over the interval $[-1, 1]$ is

$$\int_{-1}^{1} f(\zeta)d\zeta \approx \sum_{i=1}^{p_L} \overline{\omega}_i f(\zeta_i), \tag{2.3.6}$$

where ζ_i are the p zeros of the normalized Legendre polynomial of order p_L, $P_{L,p}$, and the weights $\overline{\omega}_i$ are given by

$$\overline{\omega}_i = \frac{b-a}{(1-\zeta_i^2)\left(P'_{L,p}(\zeta_i)\right)^2}.$$

Applying the rule to an arbitrary interval $[a, b] \subseteq [\xi_0, \xi_m]$ in, e.g., the parameter space, requires a change of interval of integration to $[-1, 1]$, yielding

$$\int_a^b f(\xi)d\xi = \int_{-1}^{1} f\left(\frac{b-a}{2}\zeta + \frac{b+a}{2}\right)\frac{d\xi}{d\zeta}d\zeta, \tag{2.3.7}$$

where $d\xi/d\zeta = (b-a)/2$. For accuracy, the rule is not applied over the entire interval $[\xi_1, \xi_m]$. Instead, the interval of integration is partitioned into subintervals, in each of which the Gauss-Legendre quadrature rule is applied.

2.4 Time integration scheme

Resulting FE element matrices can be written in a more general form. So far, we have provided details on how the space variable is discretized. To perform the time integration, we shall use θ-scheme, where the value of theta varies in the range $[0, 1]$. To approximate a time derivative, one could use a finite difference method. Finally, using global finite element matrices, the system of equations can be written as:

$$\frac{\partial}{\partial\tau}(\boldsymbol{M}\boldsymbol{v} + \hat{\boldsymbol{b}}_{M,v}) = -\frac{\sigma^2}{2}\boldsymbol{K}\boldsymbol{v} - \left(r - \frac{\sigma^2}{2}\right)\boldsymbol{N}\boldsymbol{v} - r\boldsymbol{M}\boldsymbol{v} - \boldsymbol{\beta}_1(\boldsymbol{v}) := F_1(\boldsymbol{v}), \tag{2.4.1}$$

where

$$\boldsymbol{\beta_1}(\boldsymbol{v}) = \frac{\sigma^2}{2}\boldsymbol{b}_{K,v} + \left(r - \frac{\sigma^2}{2}\right)\boldsymbol{b}_{N,v} + r\boldsymbol{b}_{M,v}, \tag{2.4.2}$$

is the boundary condition vector. Time integration of the system (2.4.1) is carried out by applying the θ-scheme on both equations, which results in the systems, $\Delta\tau = T/n_\tau$, and n_τ the number of time steps,

$$\boldsymbol{M}\boldsymbol{v}^{m+1} + \hat{\boldsymbol{b}}_{M,v}^{m+1} - \boldsymbol{M}\boldsymbol{v}^{m} - \hat{\boldsymbol{b}}_{M,v}^{m} = \theta\Delta\tau F_2(\boldsymbol{v}^{m+1}) + (1-\theta)\Delta\tau F_2(\boldsymbol{v}^{m}),$$

or

$$A_{11}\boldsymbol{v}^{m+1} = \widetilde{A}_{11}\boldsymbol{v}^{m} + \theta\Delta\tau\boldsymbol{\beta}_1^{m+1} + (1-\theta)\Delta\tau\boldsymbol{\beta}_1^{m} + \hat{\boldsymbol{b}}_{M,v}^{m} - \hat{\boldsymbol{b}}_{M,v}^{m+1}, \tag{2.4.3}$$

where

$$A_{11} = \boldsymbol{M} + \theta\Delta\tau\left(\frac{\sigma^2}{2}\boldsymbol{K} + \left(r - \frac{\sigma^2}{2}\right)\boldsymbol{N} + r\boldsymbol{M}\right)$$
$$\widetilde{A}_{11} = \boldsymbol{M} - (1-\theta)\Delta\tau\left(\frac{\sigma^2}{2}\boldsymbol{K} + \left(r - \frac{\sigma^2}{2}\right)\boldsymbol{N} + r\boldsymbol{M}\right).$$

Now, we can solve the FE system using the Crank-Nicolson method (when $\theta = 1/2$); during the process of solving the system, the algorithm is standard. Therefore, we did not provide the algorithm for this case. First, we start computing, $\boldsymbol{\beta}_1^{m+1}$ then using $\boldsymbol{v}^m$ compute the $\boldsymbol{v}^{m+1}$ from (2.4.3). Note that the time integration scheme is also valid for the IGA NURBS case, as it does not modify the equation's structure. The only difference can be found in local and global element matrices, which corresponds to a different choice of test functions that are used in the weak form.

2.5 Stability analysis

This section presents the stability analysis of the time integration scheme for the linear Black-Scholes equation for the European call option via Von Neumann analysis, sometimes called Fourier analysis. It is important to note that the Von Neumann stability analysis is the common approach when one deals with linear and constant coefficient systems. Even if the classical Von Neumann analysis has a limitation of applicable range, which is restricted by linear problems, it is still possible to create additional conditions for the amplification factor[1] so that the nonlinearity can be analyzed in terms of stability.

According to the Lax equivalence theorem Trefethen (1996), the convergence of the linearized scheme is equivalent to the stability of the scheme. Therefore, the convergence of the scheme is based on stability.

Theorem 2.5.1. *A linear, scalar, constant-coefficient finite difference formula is stable in L^2 norm if and only if the amplification factors ζ satisfy,*

$$|\zeta| \leq 1.$$

[1] Amplification factor describes how error perturbations are changing according to time.

The matrix equation (2.4.1) is considered for stability analysis. As the stability analysis is conducted on interior points, the boundary conditions here are omitted. Mass, stiffness, and convective matrices are based on P1-FEM basis functions. For the convenience of the analysis, the element matrices are rewritten in general form.

Theorem 2.5.2. *According to the Lax equivalence theorem, the stability of the consistent linear scheme implies convergence. The stability by Von Neumann analysis is* $(1-\theta) \leq \theta$ *which is pointed out in Theorem 2.5.1.*

Proof. From Fourier analysis, we need to assume that at the points (τ_m, x_n) the solution is defined as $\boldsymbol{v}_n^m = \zeta^m e^{in\phi}$. The proportion of $\frac{\zeta^{m+1}}{\zeta^m}$ is denoted as ζ. Now, by substituting the $\boldsymbol{v}_n^m$ into (2.4.1), one may obtain the characteristic equation as:

$$\zeta = \frac{\Delta\tau(1-\theta)D + h/3(2+\cos\phi)}{h/3(2+\cos\phi) - \Delta\tau\theta D} \tag{2.5.1}$$

where $D = \frac{\sigma^2}{h}(1-\cos\phi) + i(r - \frac{\sigma^2}{2})\sin\phi - \frac{rh}{3}(2+\cos\phi)$. The amplification factor's absolute value according to the Theorem 2.5.1 should be less than one; therefore, by taking the absolute value from (2.5.1)

$$\Delta\tau(1-\theta)D + h/3(2+\cos\phi) \leq h/3(2+\cos\phi) + \Delta\tau\theta D$$

this implies

$$(1-\theta) \leq \theta$$

which holds if and only if $\theta \geq 1/2$. Alternatively, the amplification factor can also be written as

$$\zeta = \frac{\mathcal{X}_1 + i\mathcal{Y}_1}{\mathcal{X}_2 + i\mathcal{Y}_2}$$

where

$$\mathcal{X}_1 = \frac{2+\cos\phi}{3}(h - \Delta\tau h(1-\theta)(r+r_c)) + \Delta\tau(1-\theta)\frac{\sigma^2}{h}(1-\cos\phi),$$

$$\mathcal{Y}_1 = \Delta\tau(1-\theta)(r - \frac{\sigma^2}{2})\sin\phi,$$

$$\mathcal{X}_2 = \frac{2+\cos\phi}{3}(h + \Delta\tau h\theta(r+r_c)) - \Delta\tau\theta\frac{\sigma^2}{h}(1-\cos\phi),$$

$$\mathcal{Y}_2 = -\Delta\tau\theta(r - \frac{\sigma^2}{2})\sin\phi.$$

By taking the magnitude from ζ as

$$|\zeta|^2 = \frac{\mathcal{X}_1^2 + \mathcal{Y}_1^2}{\mathcal{X}_2^2 + \mathcal{Y}_2^2}$$

and after some tedious calculations, one can conclude that $|\zeta| < 1$. This statement informs that the proposed scheme is unconditionally stable if the choice of θ is appropriate, which finalizes the proof. □

2.6 Absolute stability of the time integration scheme

Absolute stability ensures that the numerical method maintains stability across varying step sizes and refinement, preventing unbounded error growth and preserving the accuracy of the solution. The system of algebraic differential equation (2.4.1) is a constant coefficient problem which can be written as $\boldsymbol{u'(\tau)} = \boldsymbol{Au(t)}$. This system could be solved using various time-stepping techniques, which are zero-stable, in the sense that it will converge as $\tau \to 0$. However, in experiments, it is possible that instability may occur for the finite number of $\Delta\tau$, for example, in the Euler explicit method, when $\theta = 0$. Let us consider the eigenvalue decomposition $\boldsymbol{A} = \boldsymbol{VDV}^{-1}$, then

$$\begin{aligned} \boldsymbol{u}' &= \left(\boldsymbol{VDV}^{-1}\right)\boldsymbol{u}, \\ \left(\boldsymbol{V}^{-1}\boldsymbol{u}'\right) &= \boldsymbol{D}\left(\boldsymbol{V}^{-1}\boldsymbol{u}\right), \\ y' &= \boldsymbol{D}y \end{aligned}$$

where $y(\tau) = \boldsymbol{V}^{-1}\boldsymbol{u(\tau)}$. Since $\boldsymbol{D}$ is a diagonal matrix, the elements of the vector y are independent of each other. Then each $y_j' = \lambda_j y_j$, where λ_j is an eigenvalue of $\boldsymbol{A}$. Now, we are in the position to consider the eigenvalue problem

$$y' = \lambda y.$$

Let λ be a complex number. Therefore, $y(t)$ might be complex as well. The solution of the above eigenvalue problem can be seen as follows:

$$y(t) = e^{t\lambda}.$$

If we write λ in real and imaginary parts as $\lambda = \alpha + i\beta$, then by Euler's identity,

$$\left|e^{t(\alpha+i\beta)}\right| = \left|e^{t\alpha}\right| \cdot \left|e^{it\beta}\right| = e^{t\alpha}.$$

Hence, the solution of the eigenvalue problem is bounded when $\tau \to \infty$, if $\alpha = \operatorname{Re}\lambda \leq 0$. In the complex plane, one might easily see that the stability region is the left half of it.

Now let us consider the discrete solution of the proposed problem using the Euler method (explicit case when $\theta = 0$) provided with the given initial data (pay-off):

$$y_{k+1} = y_k + \tau\,(\lambda y_k) = (1 + \tau\lambda)y_k,$$

where $\lambda\tau$ is denoted as ζ. One could easily observe that $y_k = (1+\zeta)^k$, thus,

$$|y_k| = |1 + \zeta|^k,$$

from this expression, the conclusion can be deduced as follows: $|y_k|$ will be bounded as $k \to \infty$, if and only if $|1 + \zeta| \leq 1$ or $\{\zeta \in \mathbb{C}||1 + \zeta\ |< 1\}$. Geometrically, this can be written as:

$$|\zeta + 1| = |\zeta - (-1)| \leq 1,$$

this defines a closed disk of radius 1 centered at $(-1, 0)$, where within this disk the absolute stability region holds.

In the same manner, one can derive the region of absolute stability for the backward Euler method (when $\theta = 1$) as $y_k = (1-\zeta)^{-k}$. Therefore, the absolute stability needs to satisfy $|\zeta - 1| \geq 1$ or $\{\zeta \in \mathbb{C}||1 - \zeta\ |\geq 1\}$. Basically, we are moving to the counterpart of the Euler method, changing the absolute stability region to stay outside the unit circle on the left half of the complex plane.

However, it is important to note that, for our scope, one shall consider the so-called trapezoidal rule or Crank-Nicolson (when $\theta = 1/2$) method based on the absolute stability region. For this purpose, one could follow the above steps to derive a new inequality as $\left|\dfrac{1+\zeta/2}{1-\zeta/2}\right| < 1$ or $\{\zeta \in \mathbb{C}||\dfrac{1+\zeta/2}{1-\zeta/2}\ |< 1\}$. At this point, we must mention that the backward Euler and trapezoidal rules are unconditionally stable or A-stable in the sense that the absolute stability region lies on the left half plane. This can not be true for the Euler method, which is conditionally stable but also A-stable.

For both the backward Euler and Crank-Nicolson time-stepping methods for linear European call option problem, we demonstrate the eigenvalues in Figure 2.6, which are crucial for the determination of the absolute stability region. Moreover, one could see that for linear problems, there are no instability issues that can be posed based on absolute stability region for the time integrator and depicted eigenvalues that belong to the same stability range. One could find out that the Crank-Nicolson method has shared the same conclusion as Euler backward in Figure 2.7. It is important to note that based on realistic parameters of the model, such as r, h, σ, θ, and $\Delta\tau$, the eigenvalues meet the requirement of the absolute stability region; however, utilizing an impractical set of parameters the instability may occur.

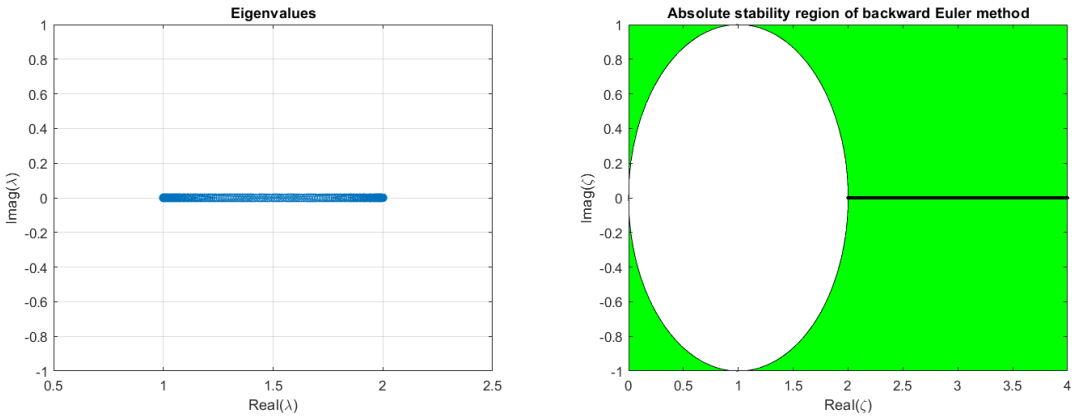

Figure 2.6: Absolute stability region of the time integration scheme for backward Euler, when $\theta = 1$

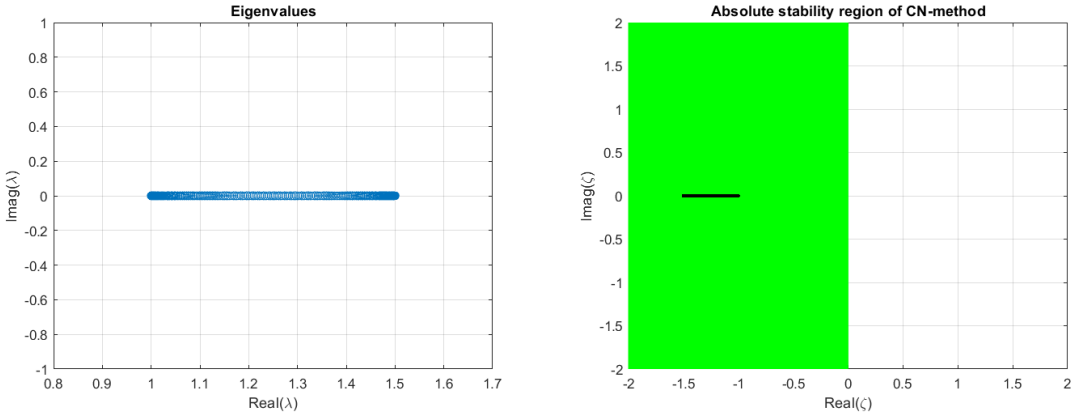

Figure 2.7: Absolute stability region of the time integration scheme for Crank-Nicolson, when $\theta = 1/2$

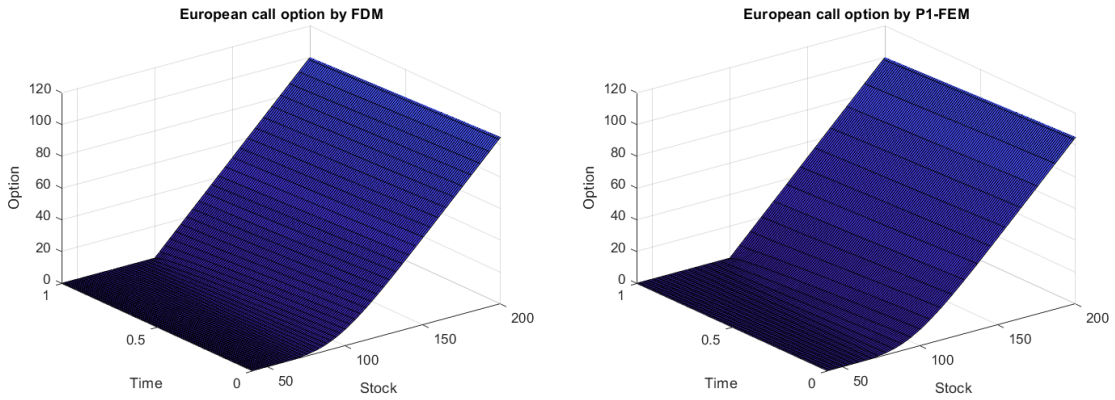

Figure 2.8: Solution of the European call option with $S_0 = \$100$, $r = 0.05$, $\sigma = 0.2$, $T = 1$, $K = \$100$. Left figure: Stock price evolution over time; Right figure: Option price surface with the projection of the stock price.

2.7 Numerical results

This section provides numerical examples based on P1-P2-FEM, Linear, Quadratic, and Cubic NURBS-based option prices. It is a common practice to provide some benchmarking range for the comparison, therefore, we have provided FDM based solutions. Note that there won't be any specific details on FDM implementation and scheme nuances, as we maintain the focus on FEM and IGA.

2.7.1 Uniformly generated mesh

Parameters for these examples, when $\sigma = 0.2,\ r = 0.05,\ K = \$100, T = 1$. Initially, the physical domain in S is semi-infinite, after Landau's transformation, it transformed to infinite domain, however, for computational convenience we truncate the domain in $x \in \Omega = [-6, 2]$. As was mentioned, for space discretization, we have provided weak formulations. Based on P1-P2 FEM, a system (2.2.3) is integrated analytically, which resulted in the above-mentioned local FE matrices. Based on Linear, Quadratic, and Cubic NURBS basis functions, we refer to (2.3.5) where the integration is resolved by the Gaussian Legendre quadrature rule. For time integration scheme, we derived a standard θ-scheme for European call option with $\theta = 1/2$ (Crank-Nicolson).

Firstly, we present a surface solution in three dimensions to see the general pattern. It can be observed that similar behavior could be detected between Figure 2.2(right) and Figures 2.8, 2.9, 2.10. In space and time, the mesh is generated uniformly, however, more sophisticated mesh types will be discussed in next sections 5. One

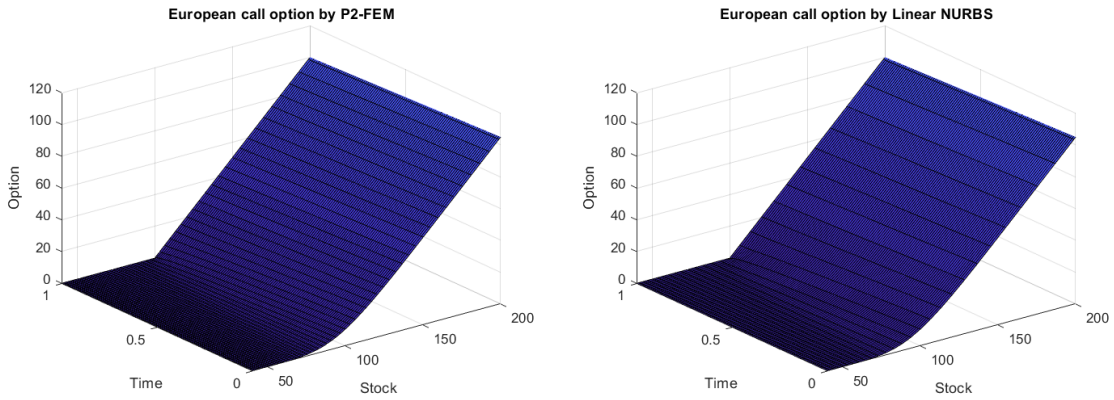

Figure 2.9: Solution of the European call option with $S_0 = \$100$, $r = 0.05$, $\sigma = 0.2$, $T = 1$, $K = \$100$. Left figure: Stock price evolution over time; Right figure: Option price surface with the stock price projection.

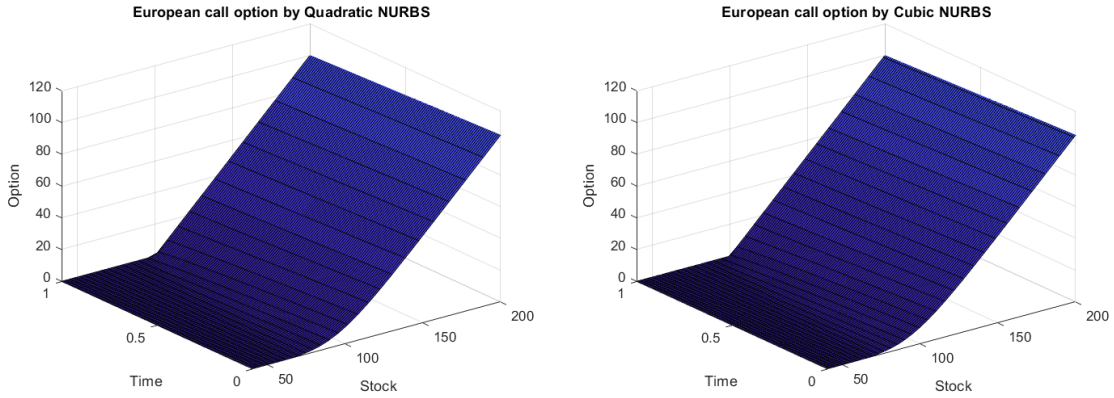

Figure 2.10: Solution of the European call option with $S_0 = \$100$, $r = 0.05$, $\sigma = 0.2$, $T = 1$, $K = \$100$. Left figure: Stock price evolution over time; Right figure: Option price surface with the projection of the stock price.

could easily see the similarity between all surfaces generated by different methods, especially, this sameness could be observed in Figure 2.11. When we double the number of nodes and time steps, we see the same behavior. However, this is the simplest case when boundary conditions are defined as constant, and the governing PDE is linear.

2.7.2 Non-uniformly generated mesh

Henceforth, NURBS_n denotes NURBS with non-uniform knot vector and NURBS_n^F is fitted NURBS with non-uniform knot vector. Error estimates Amanbek and Wheeler (2019); Amanbek et al. (2020) are provided for uniform, non-uniform NURBS and

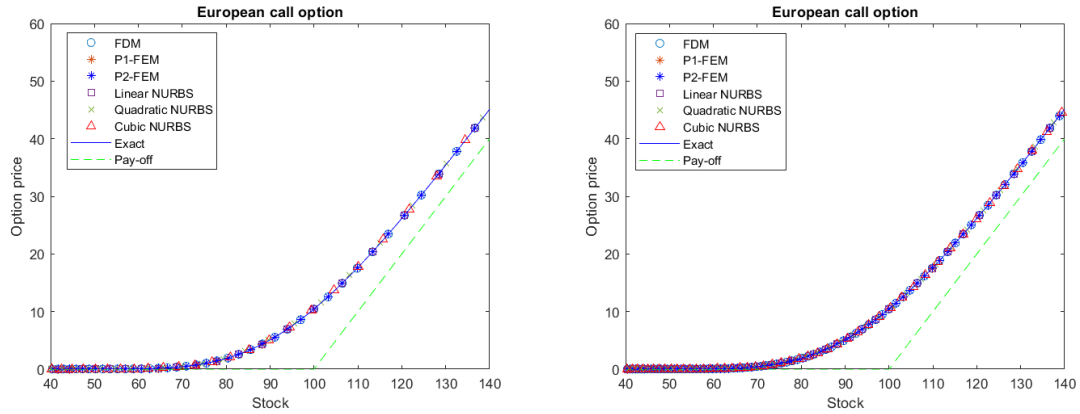

Figure 2.11: Solution of the European call option with $S_0 = \$100$, $r = 0.05$, $\sigma = 0.2$, $T = 1$, $K = \$100$. Left figure: Stock price evolution over time; Right figure: Option price surface with the projection of the stock price.

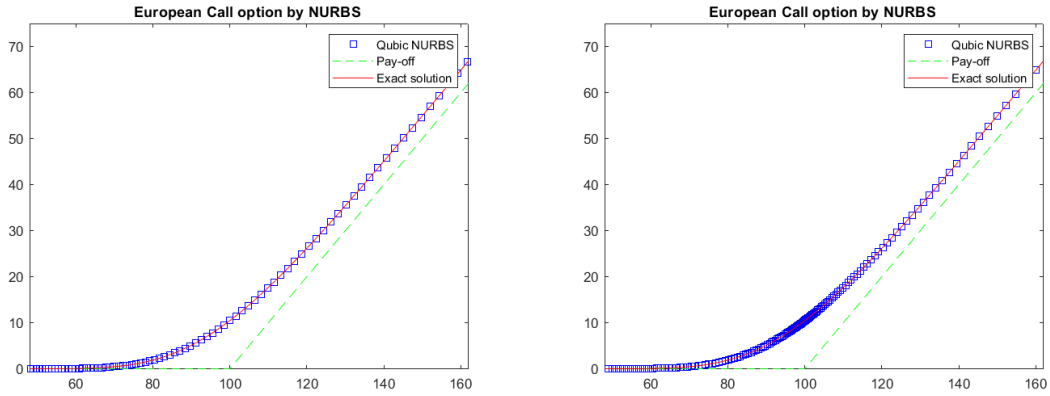

Figure 2.12: Solution of the European call option $t = 0$, $r = 0.05$, $\sigma = 0.2$, $\hat{K} = \$100$. Left figure: Uniform meshing with $nE = 2^8$, $n_\tau = 6 * 10^4$; Right figure: Non-uniform meshing with $nE = 2^8$, $n_\tau = 6 * 10^4$.

P2-FEM as $E_1 =\| E_{\text{NURBS}} \|_{L^2}$, $E_2 =\| E_{\text{NURBS}_\text{n}} \|_{L^2}$ and $E_3 =\| E_{P2} \|_{L^2}$, respectively.

In IGA, NURBS is well known to be a flexible tool that suggests effective treatment for non-smooth initial data. However, NURBS is defined in parametric space, where the knot vector is defined. As mentioned, to specify the non-smoothness seen in initial data, we rely on the non-uniform knot vector. Note that it has nothing to do with adaptive FEM since this is natural by the properties of the splines. Throughout the parametric domain, splines are continuously differentiable, which is an advantage over other polynomial-based approaches. In our initial data, the kink is presented at strike price, therefore, one shall use a non-uniform knot vector which meant to be repeated knots at certain point.

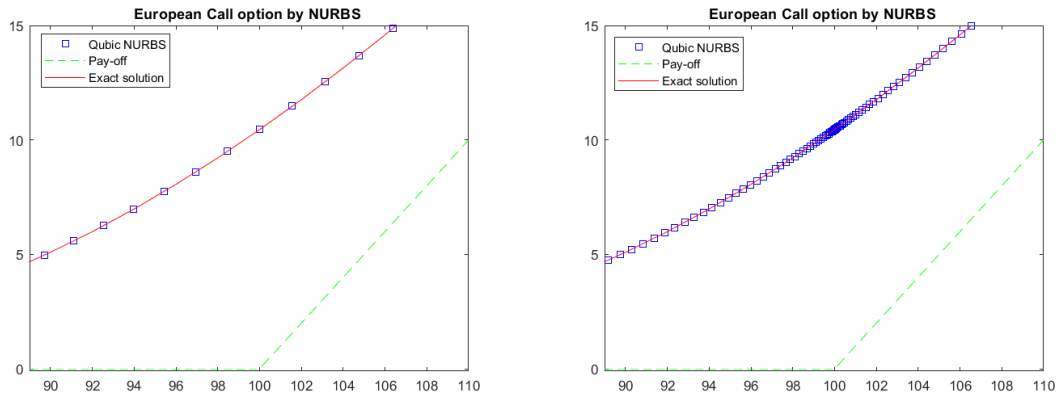

Figure 2.13: Solution of the European call option $t = 0$, $r = 0.05$, $\sigma = 0.2$, $\hat{K} = \$100$. Left figure: Uniform meshing with $nE = 2^8$, $n_\tau = 6 * 10^4$; Right figure: Non-uniform meshing with $nE = 2^8$, $n_\tau = 6 * 10^4$.

As an example, we considered the linear European call option with IGA non-uniform knot vector to see its effect on the solution at the linear level, aiming to apply it for the nonlinear convertible bond case. In Figure 2.12 and 2.13, we could observe how the grid points are distributed in uniform and non-uniform knot vector cases in large and small scales, respectively. In the case of a non-uniform knot vector, the grid points are concentrated in a dense way near the strike price. The kink position in initial data motivates the choice of repeating knot values. The original Black-Scholes problem involves a varying Peclet number throughout the space. However, using Landau transformation, the absence of varying Peclet numbers eases the range where non-uniform grids are distributed to capture the possible instability that could be caused by the non-smooth kink in the pay-off. The results of these modifications are reported in Table 2.1; using a few levels of refinement, one could see that Cubic-NURBS-IGA is converging to the exact solution away faster than its counterpart. n_τ is intentionally set to a large number to avoid the error contribution from the time dimension. Based on the evolution of errors for uniform mesh, the average cubic convergence using Cubic-NURBS is maintained. This result is one degree lower when compared to a priori error estimates from Bazilevs et al. (2006) for the elliptic problem, which agrees with the classical FEM result where the convergence order is $p+1$ under $h-$refinement. In the case of P2-FEM, one shall notice that the integration of element matrices is computed analytically, which suggests better convergence than Cubic-NURBS. However, the non-uniform knot vector by Cubic-NURBS deals with the linear European call option relatively satisfactorily since the FEM approximation by exactly calculated element matrices results in a better convergence using a lesser

degree of freedom (DOF). Nevertheless, the following results, presented only for linear Black Scholes, can not be expected for nonlinear cases with convertible bonds.

Table 2.1: European call option at $t = 0$ and $\hat{K} = \$100$ computed by NURBS. Exact price is \$10.4505. During the refinement $n_\tau = 6 * 10^4$ is fixed.

Unfitted NURBS							Fitted NURBS	
nE	P2-FEM	NURBS	NURBS_n	E_1	E_2	E_3	nE	NURBS_n^F
2^5	10.3792	12.2987	10.5256	1.8482	0.0751	0.0712	2^5	10.4505
2^6	10.4702	10.9524	10.4691	0.5019	0.0185	0.0197	2^6	10.4505
2^7	10.4513	10.5652	10.4544	0.1147	0.0025	0.0008	2^7	10.4505
2^8	10.4506	10.4835	10.4513	0.0330	0.0006	0.0001	2^8	10.4505
2^9	10.4505	10.4555	10.4507	0.0050	0.0002	0.0000		
2^{10}	10.4505	10.4519	10.4505	0.0014	0.0000	0.0000		
2^{11}	10.4505	10.4509	10.4505	0.0004	0.0000	0.0000		
2^{12}	10.4505	10.4507	10.4505	0.0002	0.0000	0.0000		

The weights used to define the role of the control point throughout the physical domain were equal by using unfitted weights, therefore, the role of the control points was equally distributed in the spatial domain having equal impact at each node. Nevertheless, this kind of configuration is motivated to produce a fair comparison with other techniques. It is a well-known fact that the NURBS is able to describe complex geometry because of its supreme flexibility Hughes et al. (2005). Furthermore, to realize the potential of the NURBS, we aim to use fitted weights Pospíšil and Švígler (2018) according to the initial data represented as a pay-off function. The kink at the strike price is the area where the gradient is dominant and can entail stronger changes during the refinement process. Essentially, the range around that kink is of interest to determine how the model behaves in time and space as we approach the exact solution, depending on the specific task.

In Table 2.1, the fitted NURBS with non-uniform knot vector results are noteworthy, compared to those by unfitted NURBS or other techniques, suggesting the numerical result which is consistent with an exact solution using a few DOFs. As we increase the DOFs, one can observe that they remain unchanged since 4 decimal place precision is achieved by just 32 elements. However, achieving such results is only possible in the presence of a closed-form or reference solution. This demands a reference to manually adjust the weights, resulting in exactly described geometry. For instance, in reference Pospíšil and Švígler (2018), authors have solved the optimization task to find the best fitting NURBS weights using a uniform knot vector in the presence of

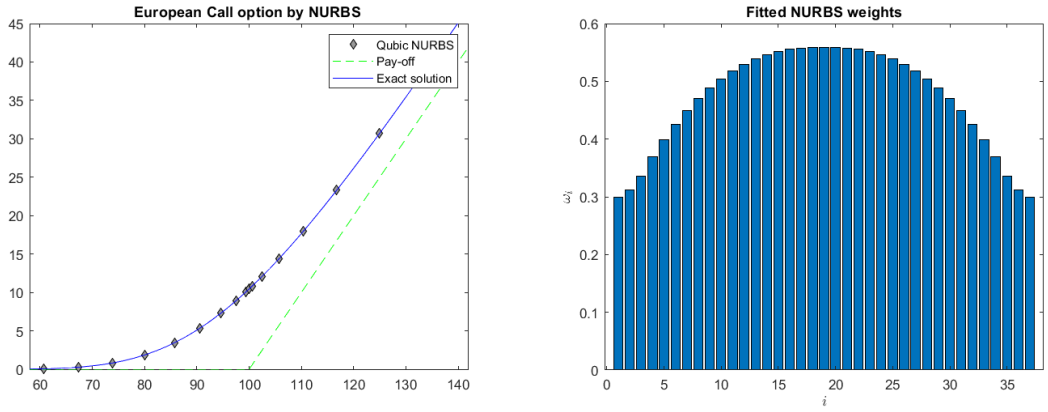

Figure 2.14: Solution of the European call option $t = 0$, $r = 0.05$, $\sigma = 0.2$, $\hat{K} = \$100$. Left figure: Non-uniform meshing with $nE = 2^5$, $n_\tau = 2 * 10^4$; Right figure: NURBS weights.

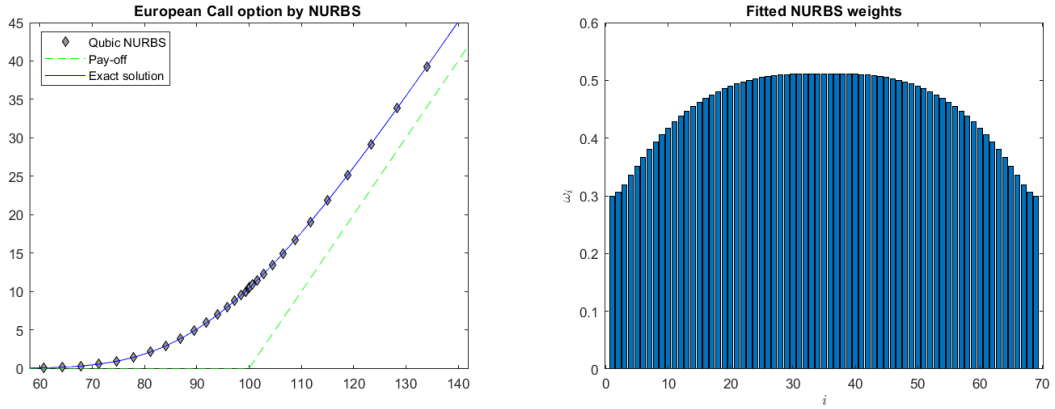

Figure 2.15: Solution of the European call option $t = 0$, $r = 0.05$, $\sigma = 0.2$, $\hat{K} = \$100$. Left figure: Non-uniform meshing with $nE = 2^6$, $n_\tau = 2 * 10^4$; Right figure: NURBS weights.

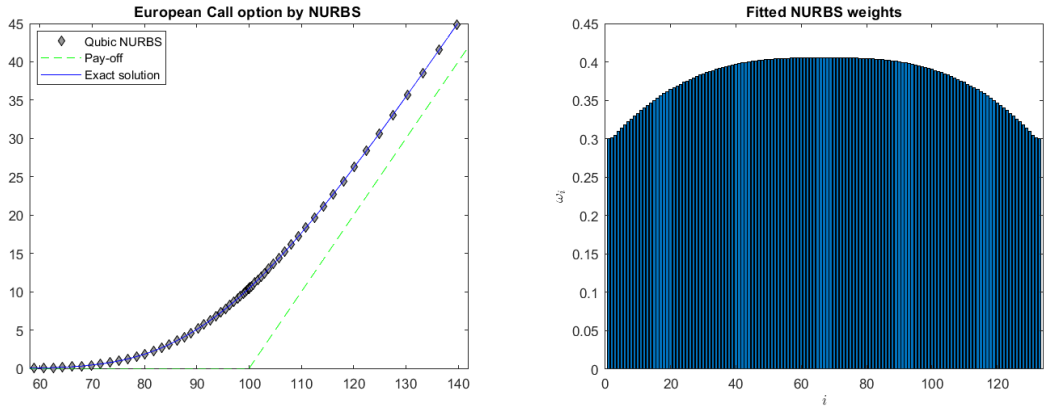

Figure 2.16: Solution of the European call option $t = 0$, $r = 0.05$, $\sigma = 0.2$, $\hat{K} = \$100$. Left figure: Non-uniform meshing with $nE = 2^7$, $n_\tau = 2 * 10^4$; Right figure: NURBS weights.

exact solutions. In contrast, we focus on the kink area using a non-uniform knot vector supplemented with experimentally obtained unequal weights. Firstly, the weights on both ends are assigned to be equal, secondly, we use a higher value of the weights at non-uniformly defined knot value at the kink. After several experiments with different weights, one could easily obtain the desired weight value, where the weights are adjusted manually at three points, as mentioned, to fit the benchmark range. As a result, in Figure 2.16, a few control points are depicted aligning with the exact solution. The weight distribution is higher in the middle of control points, implying that those near the strike price play a more crucial role in accurately representing the kink geometry. However, it is important to use this approach with great care, as inappropriate choice of weights can lead to numerical instability. While validated reference weights for specific higher-dimensional engineering problems are used in the research community Hughes et al. (2005). Selecting appropriate weights for a specific problem remains a variable challenge and the quest. For a universal tool that can optimally tune any geometry remains an open research gap in the literature.

Chapter 3

Leland model for option pricing with transactions

3.1 Introduction

A European call option without transaction costs or stock borrowing fees can be considered in a frictionless market, which does not align with real market conditions. Numerous models in the literature are designed to accurately represent transaction costs, such as those by Leland (1985); Frey and Stremme (1997); Barles and Soner (1998); Jandačka and Ševčovič (2005). Additionally, various numerical methods exist for solving PDE-based option pricing models that incorporate transaction costs Christara and Wu (2022); Wei et al. (2024). However, no studies have applied isogeometric analysis (IGA) to the Leland model for transaction option pricing. Furthermore, calculating post-processing Greek values is of significant interest, comparable to determining the option price itself. We apply IGA for a nonlinear European call option with transaction costs Wei et al. (2024); Leland (1985). Numerical results justify that IGA outperforms conventional P2-FEM regarding the accuracy and variation diminishing property for the benchmark problem Wei et al. (2024). A P2-FEM basis function is partially negative, and a description of the price using it can entail the so-called Gibbs phenomenon Cottrell et al. (2009). However, the spurious oscillations caused by P2-FEM are effectively mitigated by Non-Uniform Rational B-Splines (NURBS) for post-processing Greek values. Moreover, computed option prices generated by IGA reveal consistency with reference solutions. Although one could use traditional FDM to compute the Greeks from the IGA solution, this does not suggest any advancements. As NURBS basis functions are C^p continuous, Greeks can be captured by these basis functions. For example, P2-FEM exhibits spurious oscillations

in second-order Greek values, in contrast, IGA post-processing values obtain smooth second-order Greeks.

Within this chapter, we would like to propose several novelties that warrant the reader's attention:

- It is the first instance when IGA based on NURBS is applied to a nonlinear European contract.
- IGA performance has demonstrated the treatment of spurious oscillations previously encountered with P2-FEM.
- The Greeks are calculated by post-processing IGA-FEM and FEM algorithms rather than simply relying on FDM, which could create and change the nature of the solution by introducing another source of error.
- Computation of Greeks using IGA for nonlinear European contracts was handled smoothly, whereas P2-FEM ended up with oscillations in second-order Greek values.

3.1.1 Leland model as European contract

European call option price with transaction costs $V = V(S,t)$ can be calculated at any time t and asset value S using Leland's PDE:

$$\frac{\partial V}{\partial t} + \frac{1}{2}\sigma^2 S^2 \left(1 + Le\,\mathrm{sgn}\left(\frac{\partial^2 V}{\partial S^2}\right)\right)\frac{\partial^2 V}{\partial S^2} + rS\frac{\partial V}{\partial S} - rV = 0.$$

For European-style contracts, the option can not be exercised before terminal time T, the terminal and boundary conditions are:

$$V(S,T) = \max(S - \hat{K}, 0),$$

$$V(0,t) = 0 \quad \text{as } S \to 0,$$

$$V(S,t) \approx S \quad \text{as } S \to \infty,$$

where r is risk-free interest rate, S is the asset value and σ is volatility. The constant $Le = \sqrt{\frac{2}{\pi}}\frac{c}{\sigma\sqrt{\delta t}}$ is the Leland number where c is the round trip of transaction costs per currency limit and sgn is the sign function.

The Black-Scholes model in linear form suffers from being inconsistent with derivative market reality. Although the PDE is modified according to transaction costs

Leland (1985) does not promise to be a universal tool. More advanced financial flexibility can be delivered by introducing the American-style contract, where the option can be exercised at any time. This will introduce the nonlinearity into the PDE which is similar to the convertible bond task in 5. This modification allows portfolio rebalancing at δt with transaction costs proportional to the asset value.

3.1.2 Transformation

For the Leland model, based on previous work Wei et al. (2024), a different transformation is applied:

- $\tau = \frac{1}{2}\sigma^2(T-t)$ and hence $t = T - \frac{2\tau}{\sigma^2}$;
- $x = \ln(S) + k\tau$ and hence $S = e^{x-k\tau}$; and
- $\hat{u}(x,\tau) = e^{k\tau}V(S,t)$, and thus $V(S,t) = e^{-k\tau}\hat{u}(x,\tau)$.

Corresponding derivatives:

- $\frac{\partial V}{\partial t} = \frac{\sigma^2}{2}e^{-k\tau}(-k\frac{\partial \hat{u}}{\partial x} + k\hat{u} - \frac{\partial \hat{u}}{\partial \tau})$,
- $\frac{\partial V}{\partial S} = \frac{1}{S}e^{-k\tau}\frac{\partial \hat{u}}{\partial x}$, and
- $\frac{\partial^2 V}{\partial S^2} = \frac{1}{S^2}e^{-k\tau}(\frac{\partial^2 \hat{u}}{\partial x^2} - \frac{\partial \hat{u}}{\partial x})$.

A European call option with transaction costs:

$$\frac{\partial \hat{u}}{\partial \tau} = \frac{\partial^2 \hat{u}}{\partial x^2} - \frac{\partial \hat{u}}{\partial x} + Le\left|\frac{\partial^2 \hat{u}}{\partial x^2} - \frac{\partial \hat{u}}{\partial x}\right| = 0, \tag{3.1.1}$$

for convenience, it can be formulated in a different way, which will be later discretized as Differential-Algebraic System (DAE):

$$\begin{cases} \frac{\partial \hat{u}}{\partial \tau} = \tilde{u} + Le\,|\tilde{u}|\,, \\ \tilde{u} = \frac{\partial^2 \hat{u}}{\partial x^2} - \frac{\partial \hat{u}}{\partial x} \end{cases} \tag{3.1.2}$$

note that, $Le\,\mathrm{sgn}\left(\frac{\partial^2 \hat{u}}{\partial x^2} - \frac{\partial \hat{u}}{\partial x}\right)\left(\frac{\partial^2 \hat{u}}{\partial x^2} - \frac{\partial \hat{u}}{\partial x}\right) = Le\left|\frac{\partial^2 \hat{u}}{\partial x^2} - \frac{\partial \hat{u}}{\partial x}\right|$. The corresponding boundary and initial conditions:

$$\hat{u}(x,0) = \max(S_{int}e^x - \hat{K}, 0)$$

$$\hat{u}(x,\tau) = 0 \quad \text{as } x \to -\infty$$

$$\hat{u}(x,\tau) \approx S_{int}e^x \quad \text{as } x \to \infty.$$

From a mathematical perspective, the Leland model for transaction costs introduces nonlinearity via the diffusion term. The classical Black-Scholes PDE for a European call option is linear, allowing for a closed-form solution. However, in the Leland model, an analytical solution is not available in the literature, necessitating the use of numerical methods. After certain transformations, the nonlinearity extends to the convection term as well. As demonstrated in Section 3.4, the choice of spatial-temporal mesh sizes must adhere to a specific upper bound to prevent blow-up solutions near the right boundary and current time. We first separate the single PDE into a system of DAEs. The decoupled system is solved at each time step and then substituted back into the main governing equation. Moreover, we solve this system using a linearization technique (see Section 3.3), which is not an iterative scheme. As a result, the convergent solutions may lack precision beyond a certain level of decimal-place accuracy. Another approach involves considering penalty-like matrices Christara and Wu (2022) and solving the problem using more advanced iterative schemes, which we defer to future work.

3.2 Isogeometric analysis

3.2.1 Weak formulation for Leland model

For spatial discretization, the collection of trial solution

$$\hat{u}(x,\tau), \tilde{u}(x,\tau) \in \mathcal{S} = \left\{ f \,|\, f \in \mathcal{H}^1(\Omega), f\big|_{\Gamma_D} = g \right\}$$

and weighting functions are defined as

$$w, q \in \mathcal{V} = \left\{ \hat{f} \,\middle|\, \hat{f} \in \mathcal{H}^1(\Omega), \hat{f}\Big|_{\Gamma_D} = 0 \right\}.$$

The weak formulation:

$$\begin{aligned} \int_\Omega w \frac{\partial \hat{u}}{\partial \tau} h &= \int_\Omega w \tilde{u} h + Le \int_\Omega w |\tilde{u}| h, \\ \int_\Omega q \tilde{u} h &= \int_\Omega q \left(\frac{\partial^2 \hat{u}}{\partial x^2} - \frac{\partial \hat{u}}{\partial x} \right) h, \end{aligned} \tag{3.2.1}$$

using integration by parts, it has the following form:

$$\int_\Omega q \tilde{u} h = -\int_\Omega \frac{\partial q}{\partial x} \frac{\partial \hat{u}}{\partial x} - \int_\Omega q \frac{\partial \hat{u}}{\partial x} h. \tag{3.2.2}$$

Consider now the finite dimensional subspace $S_0^h \subset \mathcal{H}_0^1$, spanned by the basis $\{R_1, R_2, \ldots, R_n\}$. The IGA NURBS-based finite-element approximation to the solution U is the function

$$\hat{u}_h = \sum_{i=1}^{n} \hat{u}_i R_i + \sum_{i \in \mathcal{I}_\partial} \hat{u}_i R_i, \quad \hat{u}_i \in \mathbb{R},$$

where $R_{i \in \mathcal{I}_\partial}$ are additional functions needed to interpolate the given solutions at the boundaries. A similar form of approximation to $\tilde{u}$ but without boundary terms, namely

$$\tilde{u}_h = \sum_{i=0}^{n+1} \tilde{u}_i R_i, \quad \tilde{u}_i \in \mathbb{R}.$$

Then, (3.2.1) can be written as

$$\begin{aligned}
0 &= \frac{\partial}{\partial \tau} \int_\Omega w \left\{ \sum_{i=1}^{n} \hat{u}_i R_i + \sum_{i \in \mathcal{I}_\partial} \hat{u}_i R_i \right\} dx - \int_\Omega (w \sum_{i=1}^{n} \tilde{u}_i R_i + Le \cdot w | \sum_{i=0}^{n+1} \tilde{u}_i R_i |) h \\
&= \frac{\partial}{\partial \tau} \sum_{i=1}^{n} \hat{u}_i \int_\Omega w R_i h + \frac{\partial}{\partial \tau} \sum_{i \in \mathcal{I}_{\partial\Omega}} \hat{u}_i \int_\Omega w R_i h - \sum_{i=1}^{n} \tilde{u}_i \int_\Omega w R_i h \\
&- Le \int_\Omega w | \sum_{i=0}^{n+1} \tilde{u}_i R_i | h.
\end{aligned}$$

For (3.2.2), with $\tilde{u}_x = \sum_{i=1}^{n} \tilde{u}_i R_{i,x} + \sum_{i \in \mathcal{I}_{\partial\Omega}} \tilde{u}_i \tilde{u}_{i,x}$, we have

$$\begin{aligned}
0 &= \int_\Omega q \sum_{i=0}^{n+1} \tilde{u}_i R_i h + \int_\Omega q_x \left(\sum_{i=1}^{n} \hat{u}_i R_{i,x} + \sum_{i \in \mathcal{I}_{\partial\Omega}} \hat{u} R_{i,x} \right) h \\
&+ \int_\Omega q \left(\sum_{i=1}^{n} \hat{u} R_{i,x} + \sum_{i \in \mathcal{I}_{\partial\Omega}} \hat{u} R_{i,x} \right) h \\
&= \sum_{i=1}^{n} \tilde{u}_i \int_\Omega q R_i h + \sum_{i=1}^{n} \hat{u}_i \left\{ \int_\Omega q_x R_{i,x} h + \int_\Omega q R_{i,x} h \right\} \\
&+ \sum_{i \in \mathcal{I}_{\partial\Omega}} \hat{u}_i \left\{ \int_\Omega q_x R_{i,x} h + \int_\Omega q R_{i,x} h \right\}.
\end{aligned}$$

By enforcing the above equation to be satisfied by q_j, $j = 0, \ldots, n+1$ results in the system of n equations

$$\begin{aligned} 0 &= \sum_{i=0}^{n+1} v_i \int_\Omega z_j \phi_i h + \sum_{i=1}^{n} u_i \left\{ \int_\Omega z_{j,x} \psi_{i,x} h + \int_\Omega z_j \psi_{i,x} h \right\} \\ &+ \sum_{i \in \mathcal{I}_{\partial\Omega}} u_i \left\{ \int_\Omega z_{j,x} \psi_{i,x} h + \int_\Omega z_j \psi_{i,x} h \right\}. \end{aligned} \tag{3.2.3}$$

For our finite element models, we consider the Galerkin approach, where we set $w_i = q_i = R_i$. Equations (3.2.3) and (3.2.3) then become, for $j = 1, \ldots, n$

$$\begin{aligned} \frac{\partial}{\partial \tau} \sum_{i=1}^{n} \hat{u}_i \int_\Omega R_j R_i h &+ \frac{\partial}{\partial \tau} \sum_{i \in \mathcal{I}_{\partial\Omega}} \hat{u}_i \int_\Omega R_j R_i h = \sum_{i=1}^{n} \tilde{u}_i \int_\Omega R_j R_i h + Le \int_\Omega R_j | \sum_{i=0}^{n+1} \tilde{u}_i R_i | h. \\ \sum_{i=0}^{n+1} \tilde{u}_i \int_\Omega R_j R_i h &= -\sum_{i=1}^{n} \hat{u}_i \left\{ \int_\Omega R_{j,x} R_{i,x} h + \int_\Omega R_j R_{i,x} h \right\} \\ &- \sum_{i \in \mathcal{I}_{\partial\Omega}} \hat{u}_i \left\{ \int_\Omega R_{j,x} R_{i,x} h + \int_\Omega R_j R_{i,x} h \right\}. \end{aligned}$$

Once we accumulate the last stage of weak formulation, one shall apply the Gauss-Legendre rule to approximate the integrals. Afterward, the element matrices will proceed through *assembling process* to obtain the global IGA system, to which later, the θ-scheme is supposed to be applied.

3.3 Time integration scheme

Based on (3.2.1) and (3.2.2), the system of differential-algebraic equations can be written as:

$$\frac{\partial}{\partial \tau}(M\hat{\mathbf{u}} + \mathbf{b}_M) = M\tilde{\mathbf{u}} + LeM|\tilde{\mathbf{u}}| := \mathbf{F}, \tag{3.3.1}$$

where $\tilde{\mathbf{u}} = M^{-1}(-K\hat{\mathbf{u}} - N\hat{\mathbf{u}} - \mathbf{b}_K - \mathbf{b}_N)$,

$$\frac{1}{\Delta\tau}(M\hat{\mathbf{u}}^{n+1} + \mathbf{b}_M^{n+1} - (M\hat{\mathbf{u}}^n + \mathbf{b}_M^n)) = \theta\mathbf{F}^{n+1} + (1-\theta)\mathbf{F}^n,$$

with $\theta \in [0, 1]$. $\theta = 0$ and 1 correspond to the explicit forward and implicit backward Euler method, respectively. Rearranging

$$M\hat{\mathbf{u}}^{n+1} - \theta\Delta\tau(M\tilde{\mathbf{u}}^{n+1} + LeM|\tilde{\mathbf{u}}^{\mathbf{n+1}}|) = M\hat{\mathbf{u}}^n + (1-\theta)\Delta\tau\mathbf{F}^n - \mathbf{b}_M^{n+1} + \mathbf{b}_M^n.$$

With $\mathbf{v}^{n+1} = M^{-1}(-K\mathbf{u}^{n+1} - N\mathbf{u}^{n+1} - \mathbf{b}_K^{n+1} - \mathbf{b}_N^{n+1})$, we have

$$\begin{aligned} M\hat{\mathbf{u}}^{n+1} - \theta\Delta\tau(-K\hat{\mathbf{u}}^{n+1} - N\hat{\mathbf{u}}^{n+1} + LeM|\tilde{\mathbf{u}}^{\mathbf{n+1}}|) &= M\hat{\mathbf{u}}^n + (1-\theta)\Delta\tau\mathbf{F}^n - \mathbf{b}_M^{n+1} + \mathbf{b}_M^n \\ &+ \theta\Delta\tau(-\mathbf{b}_K^{n+1} - \mathbf{b}_N^{n+1}) \end{aligned} \tag{3.3.2}$$

linearization using $|\tilde{\mathbf{u}}^{\mathbf{n+1}}| = |\tilde{\mathbf{u}}^n|$ gives

$$A\hat{\mathbf{u}}^{n+1} = M\hat{\mathbf{u}}^n + (1-\theta)\Delta\tau\mathbf{F}^n + \theta\Delta\tau LeM|\tilde{\mathbf{u}}^{\mathbf{n}}| - \mathbf{b}_M^{n+1} + \mathbf{b}_M^n + \theta\Delta\tau(-\mathbf{b}_K^{n+1} - \mathbf{b}_N^{n+1})$$

with

$$\begin{aligned} A &= M - \theta\Delta\tau(-K - P), \\ \mathbf{F}^n &= M\tilde{\mathbf{u}}^n + LeM|\tilde{\mathbf{u}}^n|, \\ \tilde{\mathbf{u}}^n &= M^{-1}(-K\hat{\mathbf{u}}^n - N\hat{\mathbf{u}}^n - \mathbf{b}_K^n - \mathbf{b}_N^n) \end{aligned}$$

The Crank-Nicolson method is modified with variable time-stepping such as the Rannacher approach Rannacher (1984), in which the iterant is replaced by the n_R backward implicit Euler steps with modified time steps (e.g., $\Delta\tau_R = \Delta\tau/n_R$), where n_R is the number of backward Euler time steps. Since the boundary conditions for the Leland model are fixed, it eases the time integration process. Therefore, the solutions are computed using Crank-Nicolson scheme except the first time step, when Rannacher start shall be used. In Yousuf et al. (2012), Leland model is reformulated in terms of min function, which is called Penalty-like matrix Christara and Wu (2022) and can in principle be solved by incorporating the Newton's method.

3.4 Numerical results

After the transformation technique used for the Leland model, the semi-infinite problem in space is now truncated for numerical methods' convenience as $x \in [-6, 6]$. The system of DAEs has been solved using Cubic-NURBS based on IGA in space and utilizing the Rannacher start in time combined with the modified Crank-Nicolson method. To compare two different methods fairly, the choice of $\Delta\tau/h^2$ is adopted from Wei et al. (2024). First test, when $Le \approx 0.8$, a surface solution of the Leland model demonstrates that Cubic-NURBS produces smooth and stable results for different choices of temporal-spatial parameters, as shown in Figure 3.3. The numerical results for the ill-posed problem with extreme $Le \geq 1$ are considered, even though they lack meaning due to blow-up behavior. Indeed, the extreme case could be solved,

but the presence of instability makes it useless. For comparison purposes, the extreme values of Le are considered in Figure 3.4 to validate our numerical technique, as referenced in the literature Wei et al. (2024).

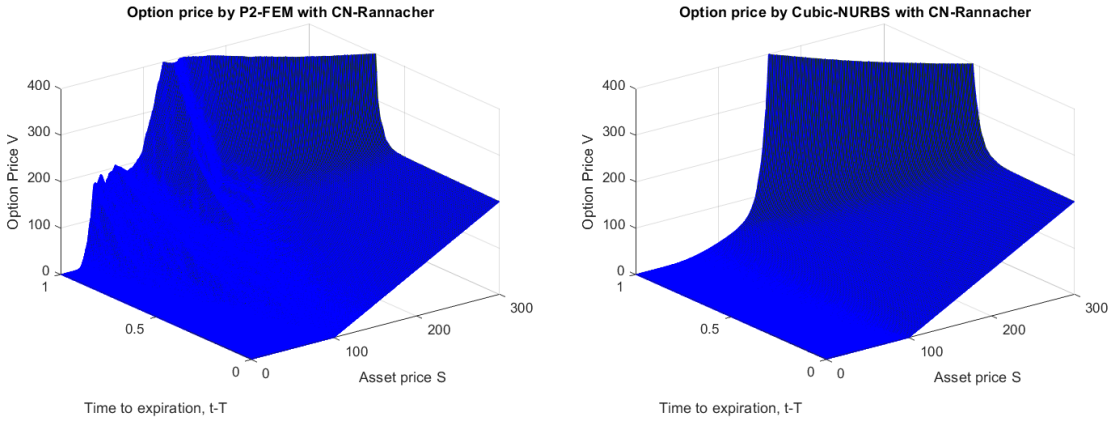

Figure 3.1: Solution of the Leland's model $t = 0$, $r = 0.1$, $\sigma = 0.2$, $\hat{K} = \$100$, $Le \approx 0.8$. Left figure by Cubic-NURBS: $\Delta\tau/h = 0.02$, $\Delta\tau/h^2 = 0.8$; Right figure by Cubic-NURBS: $\Delta\tau/h = 0.05$, $\Delta\tau/h^2 = 0.1$.

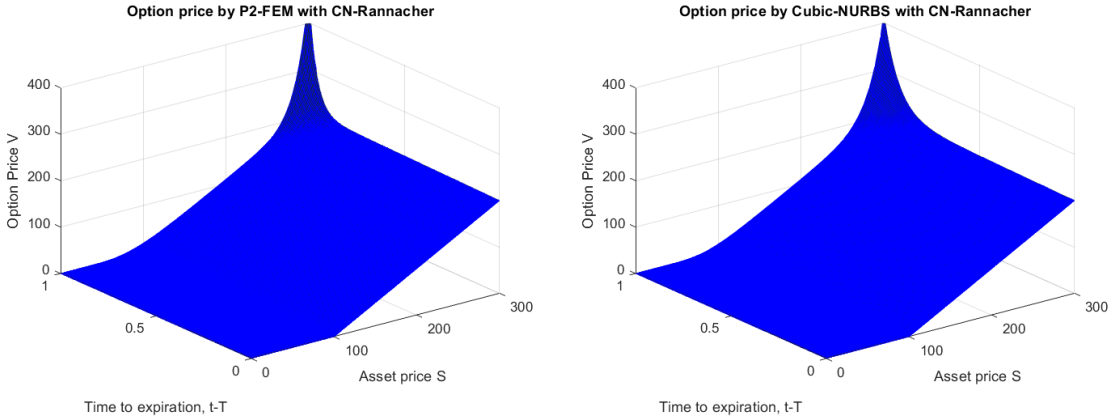

Figure 3.2: Solution of the Leland's model $t = 0$, $r = 0.1$, $\sigma = 0.2$, $\hat{K} = \$100$, $Le \approx 0.8$. Left figure by Cubic-NURBS: $\Delta\tau/h = 0.02$, $\Delta\tau/h^2 = 0.8$; Right figure by Cubic-NURBS: $\Delta\tau/h = 0.05$, $\Delta\tau/h^2 = 0.1$.

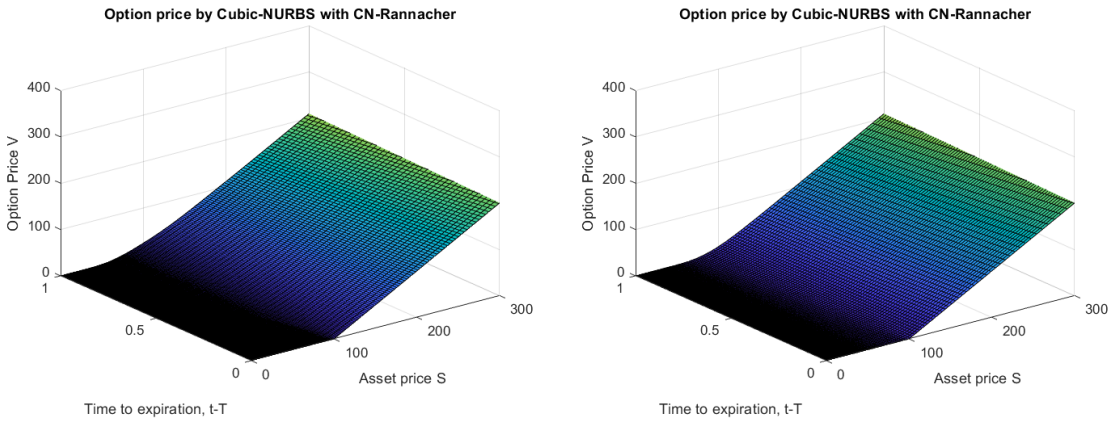

Figure 3.3: Solution of the Leland's model $t = 0$, $r = 0.1$, $\sigma = 0.2$, $\hat{K} = \$100$, $Le \approx 0.8$. Left figure by Cubic-NURBS: $\Delta\tau/h = 0.02$, $\Delta\tau/h^2 = 0.8$; Right figure by Cubic-NURBS: $\Delta\tau/h = 0.05$, $\Delta\tau/h^2 = 0.1$.

In Figure 3.4, Cubic-NURBS describes the solution compared to P1-P2-FEM. P1-FEM is a solution that is adopted as a reference solution. Cubic-NURBS converges to P1-FEM solution, and FDM converges in Wei et al. (2024). When $Le = 0.8 \leq 1$, the problem is well-posed, and the level of nonlinearity is milder compared to the second test for extreme $Le = 1.33 \geq 1$ value when the problem is ill-posed. In the extreme case, one could observe that the solution's stability is controlled by proper temporal-spatial ratio choices. Originally in Wei et al. (2024), the P2-FEM solution tends to deviate from those by P1-FEM. However, this can be attributed to the nature of partially negative basis functions of P2-FEM. P2-FEM(version-2) is a modified basis function that is described in great detail Wei et al. (2024). While P1-FEM does not suffer from being negative, it is comparable with the FDM reference solution. Therefore, in Table 3.1, it can be easily seen how the L^2 error estimates Amanbek and Wheeler (2019); Amanbek et al. (2020) approaches zero as the ratio is maintained during the refinement. Moreover, the convergence rate of Cubic-NURBS close to cubic convergence is promising for nonlinear cases when $Le = 0.8$; this phenomenon was expected since for linear problem Cubic-NURBS has converged with average cubic convergence in Table 2.1. The framework under IGA-FEM is valid to be used for nonlinear Black-Scholes PDEs, which has numerically justified to be consistent or better in specific settings to conventional FEM or FDM approaches. Moreover, the convergence result for the nonlinear model is highly remarkable since it has almost inherited the results from the linear one. The difference of $\| \hat{u}_{P1} - \hat{u}_{NU} \|_{L^2}$ error estimates at each refinement level is noted as, Δ_{NURBS} and its ratio is noted as Ratio.

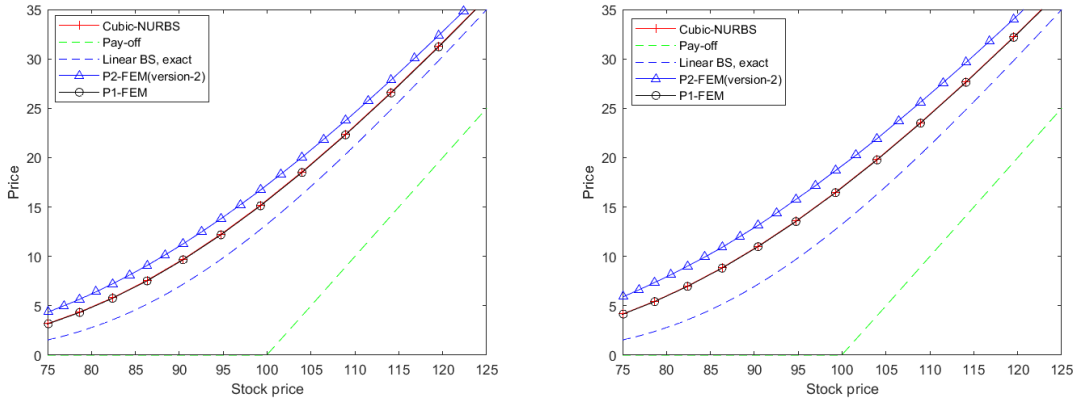

Figure 3.4: Solution of the Leland's model $t = 0$, $r = 0.1$, $\sigma = 0.2$, $\hat{K} = \$100$. Left figure: $Le \approx 0.8$, $h = 0.0017$, $\Delta\tau = 0.0000007$, therefore, $\Delta\tau/h = 0.0004$, $\Delta\tau/h^2 = 0.2$; Right figure: $Le \approx 1.33$, $h = 0.05$, $\Delta\tau = 0.00025$, therefore, $\Delta\tau/h = 0.005$,$\Delta\tau/h^2 = 0.1$.

3.4.1 Absolute stability region

Absolute stability region details are given in the Section 2.6. Based on accumulated information, one can derive the absolute stability region and check if eigenvalues meet the region's requirement. For the Crank-Nicolson time-stepping methods for nonlinear European call option problem with transaction costs, we have presented the eigenvalues in Figire 3.5, which are crucial for the determination of the absolute stability region. Moreover, one could see that for linear problems, there are no instability issues that can be posed based on the absolute stability region for the time integrator and depicted eigenvalues that belong to the same stability range. One might observe that the eigenvalues are almost identical to the linear BS cases. This might be justified by the tricky moment with the linearization, which requires the equality of two consecutive time steps as in the section 3.3. It is important to note that based on realistic parameters of the model, such as r, h, σ, θ, $\Delta\tau$, and Le the eigenvalues meet the requirement of the absolute stability region, however, employing an impractical set of parameters the instability may occur.

3.5 Greeks

In Figure 3.7, the nonlinear Leland case when $Le = 0.8$, all three Greek values are computed at $t = 0$ and compared with $Le = 0$. The evolution of Greek values deviates from those by linear call options, highlighting the effect of transaction costs. It can be seen that Cubic-NURBS and P2-FEM exhibit smooth Delta values for nonlinear

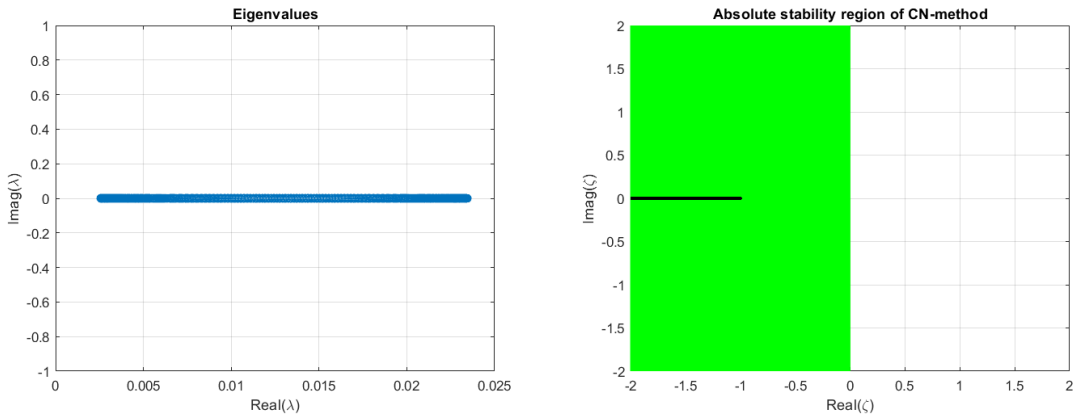

Figure 3.5: Absolute stability region of the time integration scheme for Crank-Nicolson method, when $\theta = 1/2$

Table 3.1: Solution of the Leland's model $t = 0$, $r = 0.1$, $\sigma = 0.2$, $\hat{K} = \$100$, $Le \approx 0.8$ and $\Delta\tau/h^2 = 0.1$ throughout the refinement (with Rannacher start).

nE	n_τ	$\| \hat{u}_{P1} - \hat{u}_{P2} \|_{L^2}$	$\| \hat{u}_{P1} - \hat{u}_{NU} \|_{L^2}$	Δ_{NU}	Ratio
2^8	80	5.424767	0.451445	-	-
2^9	320	7.749684	0.157192	0.294253	2.87
2^{10}	1280	10.932378	0.050986	0.106206	3.08
2^{11}	5120	15.831059	0.017970	0.033016	2.83
2^{12}	20480	22.569910	0.006319	0.011651	2.84

cases. Even though the perfect similarity can not be expected as the price of P2-FEM deviates from the reference P1-FEM and Cubic-NURBS solutions as it was shown in Figure 3.4. However, the case with Delta is way clearer and simpler for P2-FEM than second-order Gamma values. Gamma has precisely shown how P2-FEM can produce shocks around the strike price $\hat{K} = 100\$$, which could not be avoided even for really fine temporal-spatial grid size.

The most common practice for the computation of Greek alphabets is FDM. Indeed, FDM serves as a fast and robust computation for pricing problems and Greeks. Since numerical results were generated by IGA-NURBS, the usage of FDM will create another source of error as the nature of the two methodologies is totally different. To maintain the consistency, corresponding Greek values are calculated by IGA-NURBS and P2-FEM for comparison. Once the solutions are generated by IGA-NURBS, one could apply the post-processing algorithm to investigate the character of the contract value according to variable quantities. Note that the cubic-NURBS is at least twice

differentiable, which suffices to compute the Gamma by twice differentiable basis functions. Initially, our IGA-NURBS approximation is given as:

$$U_h = \sum_{i=1}^{n} u_i R_i,$$

corresponding derivatives:

$$\frac{\partial U_h}{\partial x} = \sum_{i=1}^{n} u_i \frac{\partial R_i}{\partial x}$$

$$\frac{\partial^2 U_h}{\partial x^2} = \sum_{i=1}^{n} u_i \frac{\partial^2 R_i}{\partial x^2}$$

The first step is to compute the NURBS basis functions and their derivatives at Gaussian points. Secondly, we do use the above expressions to compute the corresponding first and second-order derivatives, utilizing the same *assembling process* approach as the one used for assembling the local to global element matrices.

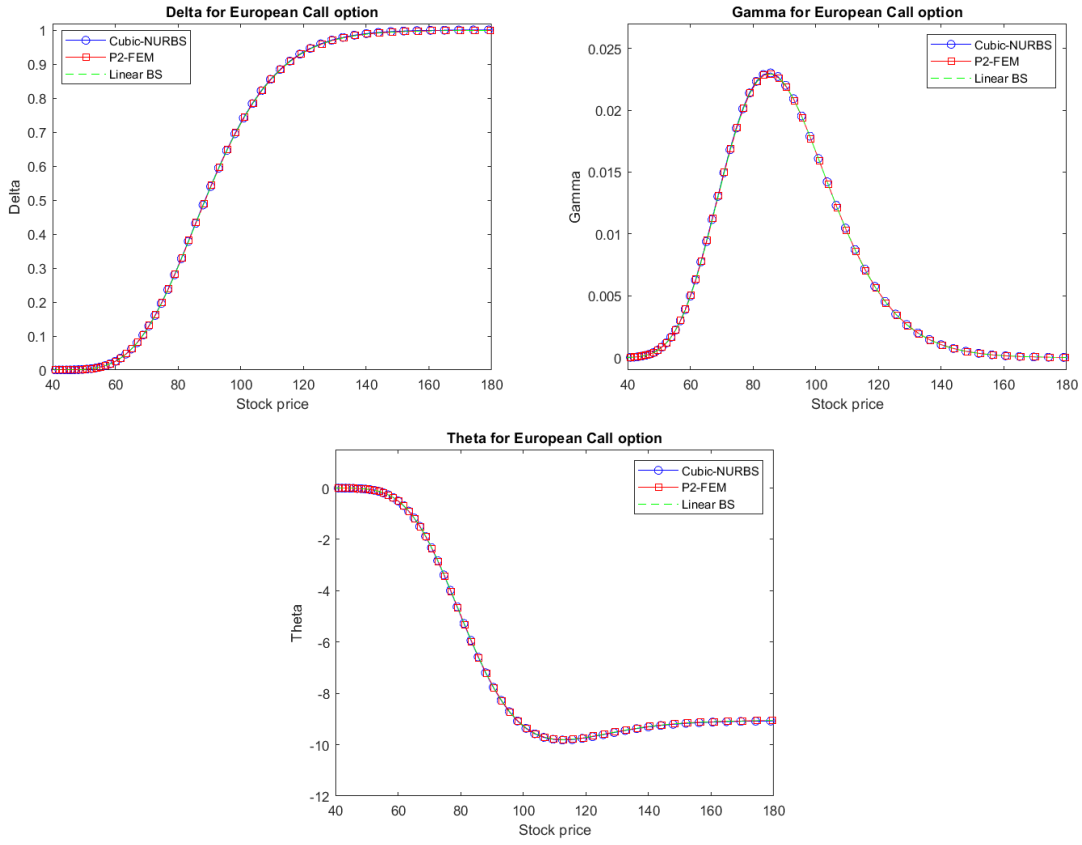

Figure 3.6: Greeks for European call option with the parameters $t = 0$, $r = 0.1$, $r_c = 0.02$, $\sigma = 0.2$, $\hat{K} = \$100$. For Cubic-NURBS: $n_E = 2^{12}$, $n_\tau = 20000$; For P2-FEM: $n_E = 2^{11}$, $n_\tau = 20000$; Left figure: Delta Δ; Right figure: Gamma Γ; Middle figure: Theta Θ.

For each particular quantity, a corresponding back-transformation shall be applied to obtain $\Delta = \dfrac{\partial U}{\partial S}$ and $\Gamma = \dfrac{\partial^2 U}{\partial S^2}$. Theta $\Theta = \dfrac{\partial U}{\partial t}$ values could be computed via FDM, however, to maintain the consistency, we retrieved its values from governing Black-Scholes PDEs for each contract, since the numerical solution, Delta and Gamma are known at current stage. Note that the Greeks by P2-FEM are calculated through derived explicit formulas in the previous work Kazbek et al. (2024).

For example, the linear European call option case ($Le = 0$) is considered to track the character of IGA-NURBS and P2-FEM versus available exact valued Greeks. In Figure 3.6, the exact values for the linear call option are comparable with those by Cubic-NURBS or P2-FEM, without having any spikes or shocks in all three cases.

In Figure 3.7, the nonlinear Leland case when $Le = 0.8$, all three Greek values are computed at $t = 0$ and compared with $Le = 0$. The evolution of Greek values deviates from those of linear call options, highlighting the effect of transaction costs. It can be seen that Cubic-NURBS and P2-FEM exhibit smooth Delta values for nonlinear cases. Even though almost identical sameness can not be expected as the price of P2-FEM deviates from the reference P1-FEM and Cubic-NURBS solutions as it was shown in Figure 3.4. However, the case with Delta is way clearer and simpler for P2-FEM than second-order Gamma values. In Gamma, it has precisely shown how P2-FEM can produce shocks around the strike price $\hat{K} = 100\$$, which could not be avoided even for really fine temporal-spatial grid size.

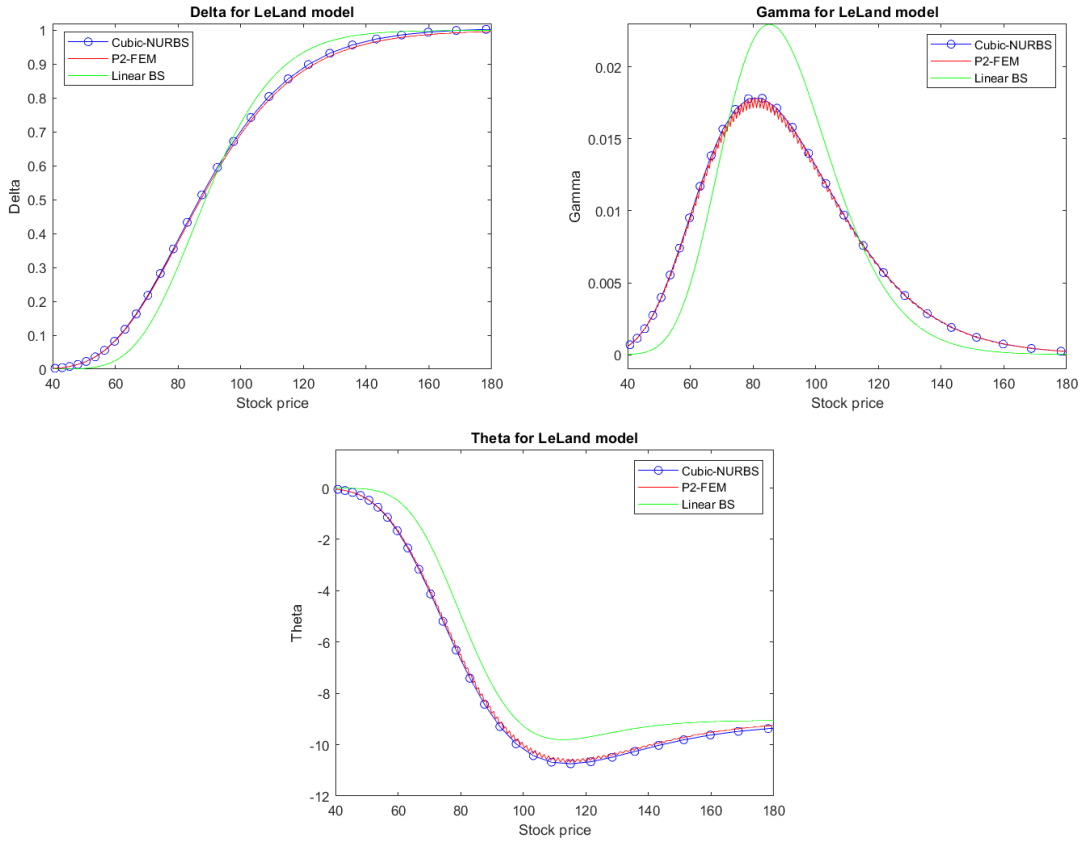

Figure 3.7: Greeks for Leland model with $t = 0$, $r = 0.1$, $\sigma = 0.2$, $\hat{K} = \$100$, $Le \approx 0.8$. For NURBS: $h = 0.005$, $\Delta\tau = 10^{-6}$, therefore, $\Delta\tau/h = 0.0001$, $\Delta\tau/h^2 = 0.02$; For P2-FEM: $h = 0.013$, $\Delta\tau = 5 * 10^{-7}$, therefore, $\Delta\tau/h = 3.6 * 10^{-5}$, $\Delta\tau/h^2 = 0.02$. Left figure: Delta Δ; Right figure: Gamma Γ; Middle figure: Theta Θ.

Whereas, Cubic-NURBS results for Gamma led to a smoother curve with no shocks. Theta inherits the behavior of Gamma for P2-FEM, and Cubic-NURBS performed a smoother curve again. As it can be concluded from numerical tests, the quality of Cubic-NURBS approximation is demonstrated via simulations superior to higher-order Greeks.

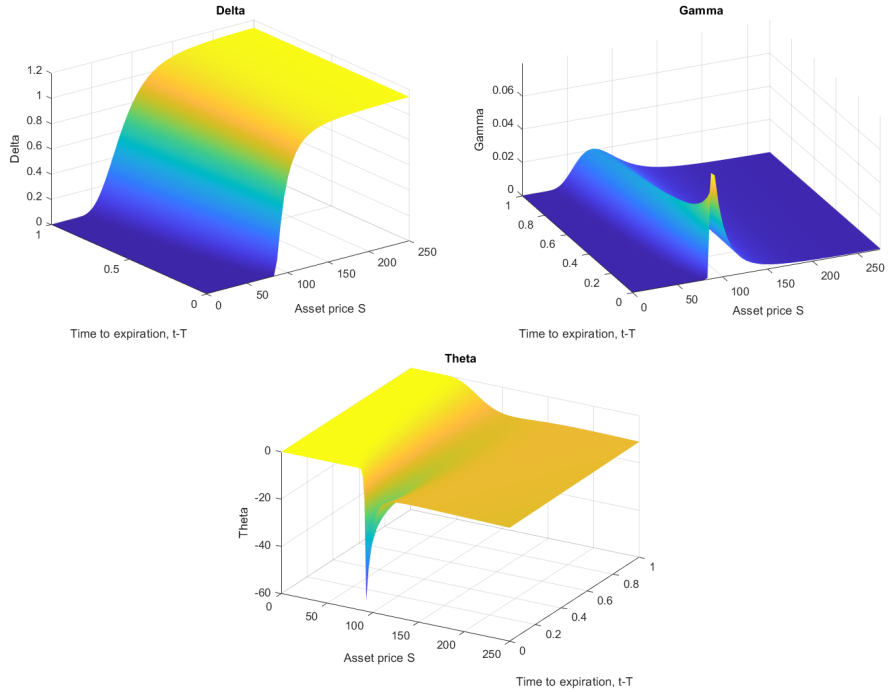

Figure 3.8: Greeks for Leland model with $t = 0$, $r = 0.1$, $\sigma = 0.2$, $\hat{K} = \$100$, $Le \approx 0.8$, $h = 0.0017$, $\Delta\tau = 0.0000007$, therefore, $\Delta\tau/h = 0.0004$, $\Delta\tau/h^2 = 0.2$. Left figure: Delta Δ; Right figure: Gamma Γ; Middle figure: Theta Θ.

Chapter 4

TF model for Convertible bonds

4.1 Introduction

A convertible bond (CB) is one of the first generations of financial derivatives; it originates from the 19th century, today, the role of convertible bonds is crucial in the derivative market Hull (2014); Jan De Spiegeleer (2011).

CB is a financial security mostly associated with fixed-income instruments as it suggests the holder has lower risk by provides coupon payments, dividends, and more profit if the exercise time is chosen correctly. CB contract normally involves three inequality constraints such as callability, puttability, and conversion, note that CB is an American-style contract since it can be exercised at any time. Callability gives a right the issuer to call the bond back under prescribed conditions in the contract; puttability offers flexibility to the holder to put it back to the issuing company depending on the behavior of the underlying asset. By conversion the holder decides to convert the bond to the stock. Puttability and callability are quite specific types of action if compared with more traditional options. Nevertheless, it inherits conversion possibility, which is analog to the call option. Pricing CBs is a sophisticated task because of its always varying time-dependent parameters, such as three constraints and their components. In literature, convertible bond pricing papers are not widely developed. However, one of them is tree methods (e.g., in Milanov and Kounchev (2012)), Monte-Carlo simulation (e.g., Ammann et al. (2008)) for the expected value of the stochastic differential equation, and partial differential equations approach are among the widely used techniques in the literature.

One of the pioneering work using PDE modelling for CB pricing is due to Ingersoll Ingersoll (1977), who developed a method for the determination of the optimal conversion and call policies for convertible securities using Black-Scholes Black and Scholes (1973) methodology. Brennan and Schwartz Brennan and Schwartz (1977)

extended Ingersoll's model to incorporate callability and dividend payments. They later improved by using stochastic interest rate, resulting in a two-factor model for CB pricing with callability and conversion strategies Brennan and Schwartz (1980). In the late 1990s, Tsiveriotis and Fernandes Tsiveriotis (1998) proposed an innovative model based on the system of two PDEs for pricing CBs under callability, puttability and conversion provisions with *hypothetical* cash-only convertible bond (COCB) part, known as the TF model. Another model for pricing CBs with credit risk and default strategy was developed by Ayache et al. Ayache et al. (2003) based on a system of triple PDEs. Barone-Adesi et al. are used characteristics/finite elements to handle multi-factors with stochastic interest rate based on Hull and White framework oriented for practical usage Barone-Adesi et al. (2003). Two-dimensional problems was solved and analyzed using bilinear finite element methods for pricing CBs by De Frutos de Frutos (2005). The pricing model with stochastic interest rate is handled by ADI FDM in Lin and Zhu (2020), are adjusted pricing CB by stochastic stock price, volatility, and interest rate. Default density using finite element method Kovalov and Linetsky (2008) with adaptive time integrator, so-called SUNDIALS that involves solving partial differential equations with inequality constraints and varying parameters. In Zhu et al. (2018), authors have implemented an integral approach for solving the puttable convertible bonds.

Because of their complexity, the TF and AFV models must be solved numerically. Due to their simplicity, FDM have become a popular numerical method in computational finance. In computational bond pricing, the authors of Brennan and Schwartz (1977, 1980); Tsiveriotis (1998) use FDM to solve their proposed model. It was noted that FEM performed comparably to FDM and suggested using it for nonlinear Black-Scholes problems. To improve the accuracy in the finite difference method, the order of approximation has to be increased, which entails trouble by exceeding left and right boundaries; therefore, corresponding exceeding nodes can not be evaluated. The accuracy can be improved in the finite element method by choosing higher-order approximation in the form of polynomials. However, the motivation for using the FEM comes from its advantage to converge using lesser DOFs and the capability of conducting the adaptive mesh generation, which in FDM has to be done by smooth-mapping functions Christara and Wu (2022).

In this chapter, we discuss the numerical solutions of the TF model for CB pricing with credit risk and without dividends by implementing the finite element method with penalty and P1 and P2 elements, respectively. In our previous work by Kazbek

et al. (2024), pricing the convertible bonds by TF model Tsiveriotis (1998) was numerically solved by P1-P2 finite elements. This chapter based on Kazbek et al. (2024) presents the following contributions:

1. To the best of our knowledge, we presented and expanded the existing literature on the numerical solution of the TF model by FEM subject to credit spread paying coupon payments.

2. The methodology presented by FEM can easily be extended to other American type of contracts.

3. nonlinear PDE consisting of two penalty terms was discretized by employing P1 and P2 FEM utilizing the *group* FEM.

4. We present the technique of handling the nonlinear doubled penalty terms by FEM, which entailed the advantage of faster convergence than FDM.

5. Post-processing Greek values using FE basis functions are compared with standard FDM values.

The TF model for convertible bond pricing is based on the system of partial differential equations (PDEs)

$$\frac{\partial U}{\partial t} + \frac{\sigma^2}{2} S^2 \frac{\partial^2 U}{\partial S^2} + r_g S \frac{\partial U}{\partial S} - r(U - V) - (r + r_c)V = 0, \tag{4.1.1}$$

$$\frac{\partial V}{\partial t} + \frac{\sigma^2}{2} S^2 \frac{\partial^2 V}{\partial S^2} + r_g S \frac{\partial V}{\partial S} - (r + r_c)V = 0, \tag{4.1.2}$$

for the time $t \in (0, T)$ and the underlying stock price $S \in (0, \infty)$, with U being the value of the CB, V the value of hypothetical COCB, r the risk-free rate, r_g the growth rate, which can be counted as risk-free rate r (see Hull (2014)), r_c the credit spread reflecting payoff default risk, σ be volatility, and T the maturity time.

The terminal condition at the maturity time T means that no one can call or put it back once the CB expires. The holder of the CB will get as much as possible, depending on the conversion ratio k and stock price. There is, however a minimum based on the face value F and the coupon payment K, yielding the terminal condition:

$$U(S, T) = \begin{cases} F + K, & \text{if } F + K \geq kS, \\ kS, & \text{otherwise,} \end{cases} \tag{4.1.3}$$

and

$$V(S, T) = \begin{cases} F + K, & \text{if } F + K \geq kS, \\ 0, & \text{otherwise.} \end{cases} \tag{4.1.4}$$

Throughout its lifetime, however, the CB can be converted to the underlying stock at the value kS, and the issuer should pay the principal value $F+K$ to the holder if the issuer has not converted until maturity time. These rights lead to three conditions that constrain the CB price:

1. Upside constraint due to conversion of bonds: for $t \in [0, T]$,

$$U(S,t) \geq kS, \tag{4.1.5}$$
$$V(S,t) = 0 \text{ if } U(S,t) \leq kS; \tag{4.1.6}$$

2. Upside constraint due to callability with the call price B_{call}: for $t \in [T_{call}, T]$, with T_{call} the earliest time the bond issuer is allowed to call back the bond,

$$U(S,t) \leq \max(B_{call}(t), kS), \tag{4.1.7}$$
$$V(S,t) = 0 \text{ if } U(S,t) \geq B_{call}(t); \tag{4.1.8}$$

3. Downside constraint due to puttability with the put price B_{put}: for $t \in [T_{put}, T]$, with T_{put} the earliest time the investor is allowed to put the bond back,

$$U(S,t) \geq B_{put}(t), \tag{4.1.9}$$
$$V(S,t) = B_{put}(t) \text{ if } U(S,t) \leq B_{put}(t). \tag{4.1.10}$$

Following Ayache et al. (2003), the call and put price in the callability and puttability constraints include the effect of future coupon payment and the underlying interest as follows. Let $\mathcal{T}_{\text{coupon}} = \{t_i\}$, the set of the coupon payment time, with $0 < t_{i-1} < t_i \leq T$. Then,

$$B_{put,call}(t) = B^{cl}_{put,call} + AccI(t), \tag{4.1.11}$$

where

$$AccI(t) = K_i \frac{t - t_{i-1}}{t_i - t_{i-1}}, \tag{4.1.12}$$

the accrued interest at any time t between the time of the last coupon payment t_{i-1} and the time of the next (pending) coupon payment t_i. Note that the constraints (4.1.5) and (4.1.9) can be combined to $U(S,t) \geq \max\{B_{put}, kS\}$. In this way, the constraints for U can be rewritten as

$$U(S,t) \leq \max(B_{call}(t), kS), \tag{4.1.13}$$
$$U(S,t) \geq \max(B_{put}(t), kS), \tag{4.1.14}$$

with

$$B_{call}(t) = \begin{cases} B_{call}^{cl} + AccI(t), & \text{if } t \in [T_{call}, T], \\ +\infty, & \text{otherwise,} \end{cases} \tag{4.1.15}$$

$$B_{put}(t) = \begin{cases} B_{put}^{cl} + AccI(t), & \text{if } t \in [T_{put}, T], \\ 0, & \text{otherwise.} \end{cases} \tag{4.1.16}$$

Two boundary conditions need to be supplemented to the PDEs (5.1.19) and (4.1.2). At $S = 0$, the PDEs are reduced to

$$\frac{\partial U(0,t)}{\partial t} = rU(0,t) + r_c V(0,t), \tag{4.1.17}$$

and

$$\frac{\partial V(0,t)}{\partial t} = (r + r_c)V(0,t), \tag{4.1.18}$$

with the terminal conditions $U(0,T) = V(0,T) = F + K$ (see Eqs. (5.1.22) and (5.1.23)). The other boundary condition is associated with the situation when the stock price S increases unboundedly, under which the CB is converted into stock. Therefore,

$$\lim_{S\to\infty} \begin{cases} U(S,t) = kS, \\ V(S,t) = 0. \end{cases} \tag{4.1.19}$$

After spatial discretization using, for instance, FDM or FEM, the initial-boundary value problems (IBVP) with constraints given by (5.1.19)–(5.1.50) can be solved by using a time-integration method, such as Crank-Nicolson, in combination with projected SSOR (PSSOR) method to tackle the nonlinearity. However, we shall consider a formulation of the above-stated IBVP in a penalty PDE to explicitly include some constraints in the PDEs and apply FEM and Crank-Nicolson method on the resulting penalty PDE.

4.2 The transformed TF model

The standard procedure for solving the Black-Scholes-type PDEs requires a transformation of the terminal-boundary value problem to an initial-boundary value problem, for which many numerical methods can be devised. Let $\tau = T - t$ and $x = \ln(S/S_{\text{int}})$, where S_{int} is the stock price at the initial time $t = 0$. With this change of variables,

it can be shown that the PDEs (5.1.19)–(4.1.2) are transformed to

$$\frac{\partial U}{\partial \tau} = \frac{\sigma^2}{2}\frac{\partial^2 U}{\partial x^2} + \left(r - \frac{\sigma^2}{2}\right)\frac{\partial U}{\partial x} - r(U - V) - (r + r_c)V, \tag{4.2.1}$$

$$\frac{\partial V}{\partial \tau} = \frac{\sigma^2}{2}\frac{\partial^2 V}{\partial x^2} + \left(r - \frac{\sigma^2}{2}\right)\frac{\partial V}{\partial x} - (r + r_c)V, \tag{4.2.2}$$

with $(\tau, x) \in (0, T) \times (-\infty, \infty)$. The terminal conditions at $t = T$ now become initial conditions at $\tau = 0$, given by

$$U(x, 0) = \begin{cases} F + K, & \text{if } F + K \geq kS_{\text{int}}e^x, \\ kS_{\text{int}}e^x\ , & \text{otherwise,} \end{cases} \tag{4.2.3}$$

and

$$V(x, 0) = \begin{cases} F + K, & \text{if } F + K \geq kS_{\text{int}}e^x, \\ 0, & \text{otherwise.} \end{cases} \tag{4.2.4}$$

Furthermore, the constraints for U are transformed into

$$U(x, \tau) \geq \max\{B_{put}(\tau), kS_{\text{int}}e^x\} =: U^{\star}_{put}(\tau), \tag{4.2.5}$$

$$U(x, \tau) \leq \max\{B_{call}(\tau), kS_{\text{int}}e^x\} =: U^{\star}_{call}(\tau), \tag{4.2.6}$$

where

$$B_{call}(\tau) = \begin{cases} B^{cl}_{call} + AccI(\tau), & \text{if } t \in [0, \tau_{call}], \\ +\infty, & \text{otherwise,} \end{cases} \tag{4.2.7}$$

and

$$B_{put}(\tau) = \begin{cases} B^{cl}_{put} + AccI(\tau), & \text{if } t \in [0, \tau_{put}], \\ 0, & \text{otherwise,} \end{cases} \tag{4.2.8}$$

with $\tau_{put,call} = T - T_{put,call}$ and, for $\tau_i \in \mathcal{T}_{\tau,\text{coupon}} = \mathcal{T}_{\text{coupon}}$,

$$B_{put,call}(\tau) = B^{cl}_{put,call} + K_i\frac{\tau - \tau_{i-1}}{\tau_i - \tau_{i-1}}. \tag{4.2.9}$$

The constraints for V now read

1. for $\tau \in [0, T]$,

$$V(x, \tau) = 0, \text{ if } U(\tau) \leq kS_{\text{int}}e^x, \tag{4.2.10}$$

2. for $\tau \in [0, \tau_{call}]$,

$$V(x, \tau) = 0, \text{ if } U(\tau) \geq B_{call}(\tau) \tag{4.2.11}$$

3. for $\tau \in [0, \tau_{put}]$,

$$V(x,\tau) = B_{put}, \text{ if } U(\tau) \leq B_{put}(\tau). \tag{4.2.12}$$

We note here that x is not defined at $S = 0$ for the boundary conditions. As in the actual numerical computation, we set S as close as possible to 0; we assume that (5.1.49) also holds at the proximity of $S = 0$, which corresponds to $x_{\min} \to -\infty$ in the x-space. This results in the boundary conditions at $x_{\min}$

$$\frac{\partial U(x_{\min},\tau)}{\partial \tau} = -rU(x_{\min},\tau) - r_c V(x_{\min},\tau), \tag{4.2.13}$$

$$\frac{\partial V(x_{\min},\tau)}{\partial t} = -(r + r_c)V(x_{\min},\tau). \tag{4.2.14}$$

Transformation of the boundary conditions at $S \to +\infty$ is: at $x_{\max} \to +\infty$,

$$U(x_{\max},\tau) = kS_{int}e^{x_{\max}}, \tag{4.2.15}$$

$$V(x_{\max},\tau) = 0. \tag{4.2.16}$$

As stated in Section 4.1, we focus on the penalty TF model. We, therefore, need to reformulate the model into a PDE model with penalty terms associated with some constraints. In particular, as in practice, we are mainly concerned with the CB price U, not V, we shall reformulate the CB PDE (5.1.35) with the associated constraints (4.2.5) and (4.2.6) into a penalty PDE. To this end, note that the linear complementarity problem (LCP) for (5.1.35) with constraints (4.2.5) and (4.2.6) is given by (Ayache et al., 2003)

$$\begin{pmatrix} \mathcal{L}U - r_c V = 0 \\ U \geq \max(B_p, \kappa S_{\text{int}} e^x) \\ U \leq \max(B_c, \kappa S_{\text{int}} e^x) \end{pmatrix} \vee \begin{pmatrix} \mathcal{L}U - r_c V \leq 0 \\ U = \max(B_p, \kappa S_{\text{int}} e^x) \\ U \leq \max(B_c, \kappa S_{\text{int}} e^x) \end{pmatrix} \vee \begin{pmatrix} \mathcal{L}U - r_c V \geq 0 \\ U \geq \max(B_p, \kappa S_{\text{int}} e^x) \\ U = \max(B_c, \kappa S_{\text{int}} e^x) \end{pmatrix}, \tag{4.2.17}$$

where $\mathcal{L} = -\dfrac{\partial}{\partial \tau} + \dfrac{\sigma^2}{2}\dfrac{\partial^2}{\partial x^2} + \left(r - \dfrac{\sigma^2}{2}\right)\dfrac{\partial}{\partial x} - r.$

The penalty PDE Forsyth and Vetzal (2002) for the bond valuation can be constructed from the LCP (4.2.17):

$$\frac{\partial U}{\partial \tau} = \frac{\sigma^2}{2}\frac{\partial^2 U}{\partial x^2} + \left(r - \frac{\sigma^2}{2}\right)\frac{\partial U}{\partial x} - rU - r_c V + \rho \max(U - U^\star_{call}, 0) + \rho \max(U^\star_{put} - U, 0),$$

where $\rho > 0$ is the penalty parameter, typically set very large. By rewriting $\max(U - U^\star_{call}, 0) = \alpha_{call}(U - U^\star_{call})$ and $\max(U^\star_{put} - U, 0) = \alpha_{put}(U - U^\star_{put})$, with

$$\alpha_{call} = \begin{cases} 1, & \text{if } U - U^\star_{call} \geq 0, \\ 0, & \text{otherwise,} \end{cases} \quad \text{and} \quad \alpha_{put} = \begin{cases} 1, & \text{if } U^\star_{put} - U \geq 0, \\ 0, & \text{otherwise,} \end{cases} \tag{4.2.18}$$

the CB PDE can be reformulated into

$$\frac{\partial U}{\partial \tau} = \frac{\sigma^2}{2}\frac{\partial^2 U}{\partial x^2} + (r - \frac{\sigma^2}{2})\frac{\partial U}{\partial x} - rU - r_c V \\ + \rho\alpha_{call}(U - U^\star_{call}) + \rho\alpha_{put}(U^\star_{put} - U). \tag{4.2.19}$$

4.3 Finite element method

In this section, we construct finite-element methods to approximately discretize the penalty CB PDE (5.1.51) and the COCB PDE (5.1.36) in the transformed TF model. To apply finite element spatial discretization to the PDEs, the domain $(0, \infty)$ is approximated by the bounded domain $\Omega = (x_{\min}, x_{\max})$ in the following:

Suppose that the solution of the bond PDEs are functions of the following class:

$$U(x,\tau), V(x,\tau) \in \mathcal{S} = \left\{ f \,\middle|\, f \in \mathcal{H}^1(\Omega), f\big|_{\Gamma_D} = g \right\}.$$

Consider two test functions $w, z \in \mathcal{V} = \left\{ \hat{f} \,\middle|\, \hat{f} \in \mathcal{H}^1(\Omega), \hat{f}\Big|_{\Gamma_D} = 0 \right\}$. The weak formulation of the penalty PDE (5.1.51) and (5.1.36) reads

$$\int_\Omega w\frac{\partial U}{\partial \tau} = \frac{\sigma^2}{2}\int_\Omega w\frac{\partial^2 U}{\partial x^2} + \left(r - \frac{\sigma^2}{2}\right)\int_\Omega w\frac{\partial U}{\partial x} - r\int_\Omega wU - r_c\int_\Omega wV \\ - \rho\int_\Omega \alpha_{call} w(U - U^\star_{call}) + \rho\int_\Omega \alpha_{put} w(U^\star_{put} - U),$$

$$\int_\Omega z\frac{\partial V}{\partial \tau} = \frac{\sigma^2}{2}\int_\Omega z\frac{\partial^2 V}{\partial x^2} + \left(r - \frac{\sigma^2}{2}\right)\int_\Omega z\frac{\partial V}{\partial x} - (r + r_c)\int_\Omega zV,$$

where the integration is carried out along the x-direction (dx is not indicated to save space). Integration by parts and applying the vanishing property of the function w and z at the boundary results in the weak formulation

$$\frac{\partial}{\partial \tau}\int_\Omega wU = -\frac{\sigma^2}{2}\int_\Omega \frac{\partial w}{\partial x}\frac{\partial U}{\partial x} - \left(r - \frac{\sigma^2}{2}\right)\int_\Omega \frac{\partial w}{\partial x}U - r\int_\Omega wU - r_c\int_\Omega wV \\ - \rho\int_\Omega \alpha_{call} w(U - U^\star_{call}) + \rho\int_\Omega \alpha_{put} w(U^\star_{put} - U),$$

$$\frac{\partial}{\partial \tau}\int_\Omega zV = -\frac{\sigma^2}{2}\int_\Omega \frac{\partial z}{\partial x}\frac{\partial V}{\partial x} - \left(r - \frac{\sigma^2}{2}\right)\int_\Omega \frac{\partial z}{\partial x}V - (r + r_c)\int_\Omega zV.$$

To build our finite-element approximation, we consider the finite-dimensional subspace $S_0^h \subset \mathcal{H}_0^1$, spanned by the basis $\{\psi_1, \psi_2, \ldots, \psi_n\}$. The finite-element approximation to the solution U is the function

$$U_h = \sum_{i=1}^{n} u_i \psi_i + \sum_{i \in \mathcal{I}_\partial} u_i \psi_i \simeq U, \quad u_i \in \mathbb{R},$$

where $\psi_{i \in \mathcal{I}_\partial}$ are additional functions needed to interpolate the given solutions at the boundaries. A similar form of approximation to V is devised, namely

$$V_h = \sum_{i=1}^{n} v_i \psi_i + \sum_{i \in \mathcal{I}_\partial} v_i \psi_i \simeq V, \quad v_i \in \mathbb{R}.$$

The use of the above approximations results in the weak formulation in the finite-dimensional space:

$$\begin{aligned}
\frac{\partial}{\partial \tau}\left(\sum_{i=1}^{n} u_i \int_\Omega w\psi_i + \sum_{i \in \mathcal{I}_\partial} u_i \int_\Omega w\psi_i\right) &= -\frac{\sigma^2}{2}\left(\sum_{i=1}^{n} u_i \int_\Omega \frac{\partial w}{\partial x}\frac{\partial \psi_i}{\partial x} + \sum_{i \in \mathcal{I}_\partial} u_i \int_\Omega \frac{\partial w}{\partial x}\frac{\partial \psi_i}{\partial x}\right) \\
&\quad - \left(r - \frac{\sigma^2}{2}\right)\left(\sum_{i=1}^{n} u_i \int_\Omega \frac{\partial w}{\partial x}\psi_i + \sum_{i \in \mathcal{I}_\partial}^{n} u_i \int_\Omega \frac{\partial w}{\partial x}\psi_i\right) \\
&\quad - r\left(\sum_{i=1}^{n} u_i \int_\Omega w\psi_i + \sum_{i \in \mathcal{I}_\partial} u_i \int_\Omega w\psi_i\right) \\
&\quad - r_c\left(\sum_{i=1}^{n} v_i \int_\Omega w\psi_i + \sum_{i \in \mathcal{I}_\partial} v_i \int_\Omega w\psi_i\right) \\
&\quad - \mathcal{P}_{call} + \mathcal{P}_{put},
\end{aligned} \tag{4.3.1}$$

where $\mathcal{P}_{call} = \rho \int_\Omega \alpha_{call} w \left(U - U^\star_{call}\right) dx$ and $\mathcal{P}_{put} = \rho \int_\Omega \alpha_{put} w \left(U^\star_{put} - U\right) dx$, and

$$\begin{aligned}
\frac{\partial}{\partial \tau}\left(\sum_{i=1}^{n} v_i \int_\Omega z\psi_i + \sum_{i \in \mathcal{I}_\partial} v_i \int_\Omega z\psi_i\right) &= -\frac{\sigma^2}{2}\left(\sum_{i=1}^{n} v_i \int_\Omega \frac{\partial z}{\partial x}\frac{\partial \psi_i}{\partial x} + \sum_{i \in \mathcal{I}_\partial} v_i \int_\Omega \frac{\partial z}{\partial x}\frac{\partial \psi_i}{\partial x}\right) \\
&\quad - \left(r - \frac{\sigma^2}{2}\right)\left(\sum_{i=1}^{n} v_i \int_\Omega \frac{\partial z}{\partial x}\psi_i + \sum_{i \in \mathcal{I}_\partial}^{n} v_i \int_\Omega \frac{\partial z}{\partial x}\psi_i\right) \\
&\quad - (r + r_c)\left(\sum_{i=1}^{n} v_i \int_\Omega z\psi_i + \sum_{i \in \mathcal{I}_\partial} v_i \int_\Omega z\psi_i\right).
\end{aligned} \tag{4.3.2}$$

In the Galerkin method (Kythe and Wei, 2004), the test functions w and z are chosen to coincide with the basis function ψ_i. Imposing this condition for $w, z = \psi_j$, $j = 1, \ldots, n$ results in the system of equations

$$\begin{aligned}\frac{\partial}{\partial \tau}\left(\sum_{i=1}^{n} u_i \int_{\Omega} \psi_j \psi_i + \sum_{i \in \mathcal{I}_\partial} u_i \int_{\Omega} \psi_j \psi_i\right) &= -\frac{\sigma^2}{2}\left(\sum_{i=1}^{n} u_i \int_{\Omega} \frac{\partial \psi_j}{\partial x}\frac{\partial \psi_i}{\partial x} + \sum_{i \in \mathcal{I}_\partial} u_i \int_{\Omega} \frac{\partial \psi_j}{\partial x}\frac{\partial \psi_i}{\partial x}\right) \\ &\quad - \left(r - \frac{\sigma^2}{2}\right)\left(\sum_{i=1}^{n} u_i \int_{\Omega} \frac{\partial \psi_j}{\partial x}\psi_i + \sum_{i \in \mathcal{I}_\partial}^{n} u_i \int_{\Omega} \frac{\partial \psi_j}{\partial x}\psi_i\right) \\ &\quad - r\left(\sum_{i=1}^{n} u_i \int_{\Omega} \psi_j \psi_i + \sum_{i \in \mathcal{I}_\partial} u_i \int_{\Omega} \psi_j \psi_i\right) \\ &\quad - r_c\left(\sum_{i=1}^{n} v_i \int_{\Omega} \psi_j \psi_i + \sum_{i \in \mathcal{I}_\partial} v_i \int_{\Omega} \psi_j \psi_i\right) \\ &\quad - \mathcal{P}_{call,j} + \mathcal{P}_{put,j},\end{aligned} \tag{4.3.3}$$

where $\mathcal{P}_{call,j}$ is $\mathcal{P}_{call}$ with w be replaced by ψ_j and similarly for $\mathcal{P}_{put,j}$, and

$$\begin{aligned}\frac{\partial}{\partial \tau}\left(\sum_{i=1}^{n} v_i \int_{\Omega} \psi_j \psi_i + \sum_{i \in \mathcal{I}_\partial} v_i \int_{\Omega} \psi_j \psi_i\right) &= -\frac{\sigma^2}{2}\left(\sum_{i=1}^{n} v_i \int_{\Omega} \frac{\partial \psi_j}{\partial x}\frac{\partial \psi_i}{\partial x} + \sum_{i \in \mathcal{I}_\partial} v_i \int_{\Omega} \frac{\partial \psi_j}{\partial x}\frac{\partial \psi_i}{\partial x}\right) \\ &\quad - \left(r - \frac{\sigma^2}{2}\right)\left(\sum_{i=1}^{n} v_i \int_{\Omega} \frac{\partial \psi_j}{\partial x}\psi_i + \sum_{i \in \mathcal{I}_\partial}^{n} v_i \int_{\Omega} \frac{\partial \psi_j}{\partial x}\psi_i\right) \\ &\quad - (r + r_c)\left(\sum_{i=1}^{n} v_i \int_{\Omega} \psi_j \psi_i + \sum_{i \in \mathcal{I}_\partial} v_i \int_{\Omega} \psi_j \psi_i\right).\end{aligned} \tag{4.3.4}$$

In practice, systems of equations (5.2.4) and (5.2.6) are constructed via an assembly process using (local) element matrices, whose structures depend on the choice of the basis functions ψ_i. The common choice for the basis functions is a class of functions satisfying the nodal condition,

$$\psi_i(x_j) = \begin{cases} 1, & i = j, \\ 0, & \text{otherwise}, \end{cases} \tag{4.3.5}$$

where x_j is the nodal point. This choice leads to global systems of linear equations with sparse and banded coefficient matrices.

4.3.1 Treating the constraints by Penalty method

We now turn to the two nonlinear penalty terms in (5.1.51) and construct a finite-element approximation to them. We, in particular, apply *group* finite element (Fletcher, 1983) to deal with the nonlinearity. We shall discuss the construction for $\mathcal{P}_{call,j}$; construction of finite element approximation for $\mathcal{P}_{put,j}$ is done in the same way.

We assume that the term $\zeta_{call} := \alpha_{call}(U - U^{\star}_{call})$ is approximated by

$$\zeta_{call} = \sum_{i=1}^{n} \zeta_i \psi_i + \sum_{\mathcal{I}_\partial} \zeta_i \psi_i,$$

where $\zeta_{call,i} = \alpha_{call}(x_i)(U(x_i) - U^{\star}_{call}(x_i)) =: \alpha_{call,i}(u_i - u^{\star}_{call,i})$. Therefore, for $w = \psi_j$, $j = 1, \ldots, n$, we have

$$\begin{aligned}\mathcal{P}_{call,j} &= \rho \int_\Omega \psi_j \left(\sum_{i=1}^{n} \zeta_i \psi_i + \sum_{\mathcal{I}_\partial} \zeta_i \psi_i \right) dx = \rho \left(\sum_{i=1}^{n} \zeta_i \int_\Omega \psi_j \psi_i dx + \sum_{\mathcal{I}_\partial} \zeta_i \int_\Omega \psi_j \psi_i dx \right) \\ &= \rho \left(\sum_{i=1}^{n} \alpha_{call,i}(u_i - u^{\star}_{call,i}) \int_\Omega \psi_j \psi_i dx + \sum_{\mathcal{I}_\partial} \alpha_{call,i}(u_i - u^{\star}_{call,i}) \int_\Omega \psi_j \psi_i dx \right).\end{aligned} \tag{4.3.6}$$

Each integral in the above equation is evaluated element-wise, resulting in the local element matrices M_j, K_j, and N_j, given in Sections 3.1 and 3.2.

By using the same argument,

$$\mathcal{P}_{put,j} = \rho \left(\sum_{i=1}^{n} \alpha_{put,i}(u_i - u^{\star}_{put,i}) \int_\Omega \psi_j \psi_i dx + \sum_{\mathcal{I}_\partial} \alpha_{put,i}(u_i - u^{\star}_{put,i}) \int_\Omega \psi_j \psi_i dx \right). \tag{4.3.7}$$

4.4 Time integration scheme

The global finite-element system obtained from assembling the local finite-element matrices can be represented by the differential algebraic equations (DAEs):

$$\begin{aligned}\frac{\partial}{\partial \tau}(M\boldsymbol{u} + \hat{\boldsymbol{b}}_{M,u}) &= -\frac{\sigma^2}{2} K\boldsymbol{u} - \left(r - \frac{\sigma^2}{2} \right) N\boldsymbol{u} - rM\boldsymbol{u} - r_c M\boldsymbol{v} - \boldsymbol{\beta}_1(\boldsymbol{u}, \boldsymbol{v}) \\ &\quad + \rho M P_{put}(\boldsymbol{u}^{\star}_{put} - \boldsymbol{u}) - \rho M P_{call}(\boldsymbol{u} - \boldsymbol{u}^{\star}_{call}) \\ &\quad + \rho \boldsymbol{b}_{put} - \rho \boldsymbol{b}_{call} := F_1(\boldsymbol{u}, \boldsymbol{v}),\end{aligned} \tag{4.4.1}$$

$$\frac{\partial}{\partial \tau}(M\boldsymbol{v} + \hat{\boldsymbol{b}}_{M,v}) = -\frac{\sigma^2}{2} K\boldsymbol{v} - \left(r - \frac{\sigma^2}{2} \right) N\boldsymbol{v} - (r + r_c) M\boldsymbol{v} - \boldsymbol{\beta}_2(\boldsymbol{v}) := F_2(\boldsymbol{v}), \tag{4.4.2}$$

where $P_{put} = \mathrm{diag}(\alpha_{put,j})$, $P_{call} = \mathrm{diag}(\alpha_{call,j})$, and

$$\boldsymbol{\beta_1}(\boldsymbol{u},\boldsymbol{v}) = \frac{\sigma^2}{2}\boldsymbol{b}_{K,u} + \left(r - \frac{\sigma^2}{2}\right)\boldsymbol{b}_{N,u} + r\boldsymbol{b}_{M,u} + r_c\boldsymbol{b}_{M,v}, \tag{4.4.3}$$

$$\boldsymbol{\beta}_2(\boldsymbol{v}) = \frac{\sigma^2}{2}\boldsymbol{b}_{K,v} + \left(r - \frac{\sigma^2}{2}\right)\boldsymbol{b}_{N,v} + (r + r_c)\boldsymbol{b}_{M,v}, \tag{4.4.4}$$

are the boundary condition vectors.

Time integration of the DAEs (5.3.1) and (5.3.2) is carried out by applying the θ-scheme on both equations, which results in the systems, with $\theta \in [0,1]$, $\Delta\tau = T/n_\tau$, and n_τ the number of time steps,

$$\begin{aligned} M\boldsymbol{u}^{m+1} + \hat{\boldsymbol{b}}_{M,u}^{m+1} - M\boldsymbol{u}^m - \hat{\boldsymbol{b}}_{M,u}^{m} &= \theta\Delta\tau F_1(\boldsymbol{u}^{m+1},\boldsymbol{v}^{m+1}) + (1-\theta)\Delta\tau F_1(\boldsymbol{u}^m,\boldsymbol{v}^m), \\ M\boldsymbol{v}^{m+1} + \hat{\boldsymbol{b}}_{M,v}^{m+1} - M\boldsymbol{v}^m - \hat{\boldsymbol{b}}_{M,v}^{m} &= \theta\Delta\tau F_2(\boldsymbol{v}^{m+1}) + (1-\theta)\Delta\tau F_2(\boldsymbol{v}^m), \end{aligned}$$

or

$$\begin{aligned} A_{11}\boldsymbol{u}^{m+1} + A_{12}\boldsymbol{v}^{m+1} &- \rho\theta\Delta\tau M\left(P_{put}^{m+1}(\boldsymbol{u}_{put}^{\star,m+1} - \boldsymbol{u}^{m+1}) - P_{call}^{m+1}(\boldsymbol{u}^{m+1} - \boldsymbol{u}_{call}^{\star,m+1})\right) \\ &= \widetilde{A}_{11}\boldsymbol{u}^m + \widetilde{A}_{12}\boldsymbol{v}^m + \rho(1-\theta)\Delta\tau M\left(P_{put}^{m}(\boldsymbol{u}_{put}^{\star,m} - \boldsymbol{u}^{m}) - P_{call}^{m}(\boldsymbol{u}^{m} - \boldsymbol{u}_{call}^{\star,m})\right) \\ &+ \theta\Delta\tau\boldsymbol{\beta}_1^{m+1} + (1-\theta)\Delta\tau\boldsymbol{\beta}_1^m + \hat{\boldsymbol{b}}_{M,u}^m - \hat{\boldsymbol{b}}_{M,u}^{m+1} + \theta\rho\Delta\tau(\boldsymbol{b}_{put}^{m+1} - \boldsymbol{b}_{call}^{m+1}) \\ &+ (1-\theta)\rho\Delta\tau(\boldsymbol{b}_{put}^{m} - \boldsymbol{b}_{call}^{m}), \end{aligned} \tag{4.4.5}$$

$$A_{22}\boldsymbol{v}^{m+1} = \widetilde{A}_{22}\boldsymbol{v}^m + \theta\Delta\tau\boldsymbol{\beta}_2^{m+1} + (1-\theta)\Delta\tau\boldsymbol{\beta}_2^m + \hat{\boldsymbol{b}}_{M,v}^m - \hat{\boldsymbol{b}}_{M,v}^{m+1}, \tag{4.4.6}$$

where

$$\begin{aligned} A_{11} &= M + \theta\Delta\tau\left(\frac{\sigma^2}{2}K + \left(r - \frac{\sigma^2}{2}\right)N + rM\right), \\ A_{12} &= \theta\Delta\tau r_c M, \\ A_{22} &= M + \theta\Delta\tau\left(\frac{\sigma^2}{2}K + \left(r - \frac{\sigma^2}{2}\right)N + (r+r_c)M\right) \\ \widetilde{A}_{11} &= M - (1-\theta)\Delta\tau\left(\frac{\sigma^2}{2}K + \left(r - \frac{\sigma^2}{2}\right)N + rM\right), \\ \widetilde{A}_{12} &= -(1-\theta)\Delta\tau r_c M, \\ \widetilde{A}_{22} &= M - (1-\theta)\Delta\tau\left(\frac{\sigma^2}{2}K + \left(r - \frac{\sigma^2}{2}\right)N + (r+r_c)M\right). \end{aligned}$$

Let the solutions $\boldsymbol{u}^m$ and $\boldsymbol{v}^m$ be known. The solutions at the next time level $m+1$ can, in principle, be computed by first solving (5.3.8) for $\boldsymbol{v}^{m+1}$. The solution $\boldsymbol{u}^{m+1}$ is then computed via (5.3.7) using the known $\boldsymbol{u}^m$, $\boldsymbol{v}^m$, and $\boldsymbol{v}^{m+1}$. This procedure, however, requires knowledge of the solutions at the boundaries at the time level $m+1$.

4.4.1 Boundary solutions

At $x_{\min}$, with $u_0(\tau) := U(x_{\min}, \tau)$, $v_0(\tau) := V(x_{\min}, \tau)$, etc, the boundary conditions with penalty in U can be written as follows:

$$\begin{cases} \dfrac{\partial u_0(\tau)}{\partial \tau} & = -ru_0(\tau) - r_c v_0(\tau) \\ & \quad -\rho \max\left(u_0(\tau) - u^\star_{call,0}(\tau), 0\right) + \rho \max\left(u^\star_{put,0}(\tau) - u_0(\tau), 0\right), \\ \dfrac{\partial v_0(\tau)}{\partial t} & = -(r + r_c)v_0(\tau). \end{cases} \tag{4.4.7}$$

Note that $\max\left(u_0(\tau) - u^\star_{call,0}(\tau), 0\right) = p_{call,0}(\tau)(u_0(\tau) - u^\star_{call,0}(\tau))$, with

$$p_{call,0} = \begin{cases} 1, & \text{if } u_0(\tau) > u^\star_{call,0}(\tau), \\ 0, & \text{otherwise,} \end{cases}$$

and $\max\left(u^\star_{put,0}(\tau) - u_0(\tau), 0\right) = p_{put,0}(\tau)(u^\star_{put,0}(\tau) - u_0(\tau))$, with

$$p_{put,0} = \begin{cases} 1, & \text{if } u_0(\tau) < u^\star_{put,0}(\tau), \\ 0, & \text{otherwise.} \end{cases}$$

Application of the θ-scheme on (5.3.10) leads to the discrete equations:

$$\begin{aligned} u_0^{m+1} + \theta\Delta\tau(ru_0^{m+1} + r_c v_0^{m+1} + \rho(p^{m+1}_{call,0}(u_0^{m+1} - u^{\star,m+1}_{call,0}) - p^{m+1}_{put}(u^{\star,m+1}_{put,0} - u_0^{m+1}))) \\ = u_0^m - (1-\theta)\Delta\tau(ru_0^m + r_c v_0^m \\ + \rho(p^m_{call,0}(u_0^m - u^{\star,m}_{call,0}) - p^m_{put}(u^{\star,m}_{put,0} - u_0^m))), \end{aligned} \tag{4.4.8}$$

$$[1 + \theta\Delta\tau(r + r_c)]\, v_0^{m+1} = [1 - (1-\theta)\Delta\tau(r + r_c)]v_0^m. \tag{4.4.9}$$

Let the boundary solution v_0^m be known. Then v_0^{m+1} can be computed from (5.3.12). With u_0^m, v_0^m, and v_0^{m+1} now known, (5.3.11) becomes a nonlinear function of u_0^{m+1}, which can be solved approximately using Newton's method. Assume that the penalty term in (5.3.11) is approximated in a fully implicit way at the new time level $m+1$. This results in the equation

$$\begin{aligned} 0 = (1 + \theta\Delta\tau r)u_0^{m+1} + \Delta\tau\rho(p^{m+1}_{call,0}(u_0^{m+1} - u^{\star,m+1}_{call,0}) - p^{m+1}_{put}(u^{\star,m+1}_{put,0} - u_0^{m+1})) \\ - \phi_0 =: f(u_0^{m+1}), \end{aligned} \tag{4.4.10}$$

where

$$\phi_0 = u_0^m - (1-\theta)\Delta\tau\left(ru_0^m + r_c v_0^m\right) - \theta\Delta\tau r_c v_0^{m+1}.$$

With

$$f'(u_0^{m+1}) = 1 + \theta\Delta\tau r + \Delta\tau\rho\left(p^{m+1}_{call,0} + p^{m+1}_{put,0}\right), \tag{4.4.11}$$

Newton's method for finding u_0^{m+1} satisfying (4.4.10) can be written as follows: with an initial guess $u_0^{m+1,0}$, compute $u_0^{m+1,k} = u_0^{m+1,k-1} - f(u_0^{m+1,k-1})/f'(u_0^{m+1,k-1})$, for $k = 1, 2, \ldots$.

$u_0^{m+1,0}$ is chosen to be the solution of the unconstrained boundary problem given by (5.1.49). Since we expect that $u_0^{m+1,0}$ computed in this way is a better approximation than, e.g., u_0^m, we can also use this value to evaluate the conditions to constraint v.

The complete algorithm for computing u_0^{m+1} and v_0^{m+1} is as follows:

Algorithm 1 Computing the boundary solutions

Input: input u_0^m, v_0^m;

compute $B_p(\tau^{m+1})$ and $B_c(\tau^{m+1})$;
compute v_0^{m+1} from (5.3.12);
compute u_0^{m+1} from (5.3.11) without penalty terms;
apply constraints on v_0^{m+1} using u_0^{m+1};
set $u_0^{m+1,0} \leftarrow u_0^{m+1}$;
for $k = 1, 2, \ldots$ until convergence **do**
    compute $f(u_0^{m+1,k-1})$ using (4.4.10);
    compute $f'(u_0^{m+1,k-1})$ using (4.4.11);
    $u_0^{m+1,k} \leftarrow u_0^{m+1,k-1} - f(u_0^{m+1,k-1})/f'(u_0^{m+1,k-1})$;
end for
apply constraints on v_0^{m+1} using $u_0^{m+1,k}$;
if $\tau^{m+1} \in \mathcal{T}_{\text{coupon}}$ **then**
    $u_0^{m+1} \leftarrow u_0^{m+1} + K$;
    $v_0^{m+1} \leftarrow v_0^{m+1} + K$;
end if

At $x_{\max}$ we need to compute $u_{n+1}^{m+1} := U(x_{\max}, \tau^{m+1})$ and $v_{n+1}^{m+1} := V(x_{\max}, \tau^{m+1})$ via (5.1.50), apply the constraints, and pay the coupon if $\tau^{m+1} \in \mathcal{T}_{\text{coupon}}$.

We remark here that the solution of Newton's method exists if the derivative $f'(u_0^m) \neq 0$. This condition, however, cannot be theoretically guaranteed. In this regard, for the tuple $(p_{call,0}^m, p_{put,0}^m) \in \{0,1\}^2$ and nonnegative θ, $\Delta\tau$, ρ, and r,

1. if $p_{call,0} = p_{put,0}$, then $f'(u_0^m) = 1 + \theta\Delta\tau r > 0$;
2. if $p_{call,0} \neq p_{put,0}$, we have two situations:
   (a) if $p_{call,0} = 1$ and $p_{put,0} = 0$, then $f'(u_0^m) = 1 + \Delta\tau(\theta r + \rho) > 0$;
   (b) if $p_{call,0} = 0$ and $p_{put,0} = 1$, then $f'(u_0^m) = 1 + \Delta\tau(\theta r - \rho) = 0$ if $\Delta\tau = 1/(\rho - \theta r)$.

Since the penalty parameter ρ is taken large (e.g., $\rho = 10^6$), vanishing f' is very unlikely to happen under a reasonable choice of the time step $\Delta\tau$. For instance, using the simulation parameters in Table 5.1 in Section 4.5, the vanishing f' situation outlined in Point 2(b) above may occur if $\Delta\tau$ is chosen to be in the order of $\rho^{-1} = 10^{-6}$, which makes the time-integration process extremely impractical.

4.4.2 Interior solutions

With solutions at the boundaries available at τ^m and τ^{m+1}, all related boundary vectors in (5.3.7) and (5.3.8) are known. We are thus now able to compute the solutions $\boldsymbol{u}^{m+1}$ and $\boldsymbol{v}^{m+1}$. $\boldsymbol{v}^{m+1}$ is readily computed from (5.3.8). With $\boldsymbol{v}^{m+1}$ known, (5.3.7) reduces to a nonlinear function of $\boldsymbol{u}^{m+1}$. As we do for the boundary equations, we assume that the penalty terms in (5.3.8) are approximated in a fully implicit way, resulting in the equation

$$\begin{aligned} 0 \;\; &= A_{11}\boldsymbol{u}^{m+1} - \rho\Delta\tau M\left(P_{put}^{m+1}(\boldsymbol{u}_{put}^{\star,m+1} - \boldsymbol{u}^{m+1}) + P_{call}^{m+1}(\boldsymbol{u}^{m+1} - \boldsymbol{u}_{call}^{\star,m+1})\right) \\ &\quad -\boldsymbol{\phi} := \boldsymbol{f}(\boldsymbol{u}^{m+1}), \end{aligned} \tag{4.4.12}$$

where

$$\begin{aligned} \boldsymbol{\phi} \;\; &= \widetilde{A}_{11}\boldsymbol{u}^m + \widetilde{A}_{12}\boldsymbol{v}^m - A_{12}\boldsymbol{v}^{m+1} + \theta\Delta\tau\boldsymbol{\beta}_1^{m+1} + (1-\theta)\Delta\tau\boldsymbol{\beta}_1^m + \hat{\boldsymbol{b}}_{M,u}^m - \hat{\boldsymbol{b}}_{M,u}^{m+1} \\ &\quad +\theta\Delta\tau(\boldsymbol{b}_{put}^{m+1} + \boldsymbol{b}_{call}^{m+1}). \end{aligned} \tag{4.4.13}$$

The nonlinear equation (5.3.14) is solved iteratively using Newton's method. Starting from an initial guess of the solution $\boldsymbol{u}^{m+1,0}$, the solution $\boldsymbol{u}^{m+1}$ is approximated using the iterands

$$\boldsymbol{u}^{m+1,k} \leftarrow \boldsymbol{u}^{m+1,k-1} - \left(\nabla\boldsymbol{f}(\boldsymbol{u}^{m+1,k-1})\right)^{-1}\boldsymbol{f}(\boldsymbol{u}^{m+1,k-1}), \quad k = 1, 2, \ldots$$

where $\nabla\boldsymbol{f}(\boldsymbol{u}^{m+1,k-1})$ is the Jacobian of $\boldsymbol{f}$, given by

$$\nabla\boldsymbol{f}(\boldsymbol{u}^{m+1,k-1}) = A_{11} + \rho\Delta\tau M\left(P_{call}^{m+1,k-1} - P_{put}^{m+1,k-1}\right). \tag{4.4.14}$$

The initial guess $\boldsymbol{u}^{m+1,0}$ is chosen such that it solves unconstrained CB PDE, which is equivalent to solving (5.3.7) without penalty terms. We shall also use this unconstrained solution $\boldsymbol{u}^{m+1,0}$ to constrain the initially computed $\boldsymbol{v}^{m+1}$ prior to the start of Newton's iterations. In the context of American-style derivatives, the convertible bond problem refers to the stopping criteria used to terminate computations to conserve computational resources. As in (Forsyth and Vetzal, 2002), the first typical criteria is the difference of two consecutive solution vectors $\| \boldsymbol{u}^{m+1,k} - \boldsymbol{u}^{m+1,k-1} \|_\infty \leq tol$,

which serves to guarantee the termination. The importance of the second criterion deserves attention since we are talking about gaps arising from the penalty matrices. Its equivalence (i.e. $P_{call}^{m+1,k-1} = P_{call}^{m+1,k}$) is crucial to facilitate the convergence of Newton's method using the less number of iterations per time step. The procedure for computing the solutions in the interior after one θ-scheme step is summarized in the following algorithm:

Algorithm 2 Computing the interior solutions

Input: input $\boldsymbol{u}^m$, $\boldsymbol{v}^m$;
compute $B_p(\tau^{m+1})$ and $B_c(\tau^{m+1})$;
compute $\boldsymbol{v}^{m+1}$ from (5.3.8);
compute $\boldsymbol{u}^{m+1}$ from (5.3.7) without penalty terms;
apply constraints on $\boldsymbol{v}^{m+1}$ using $\boldsymbol{u}^{m+1}$;
set $\boldsymbol{u}^{m+1,0} \leftarrow \boldsymbol{u}^{m+1}$;
for $k = 1, 2, \ldots$ until convergence **do**
    compute$\boldsymbol{f}(\boldsymbol{u}^{m+1,k-1})$ using (5.3.14);
    compute $\nabla \boldsymbol{f}(\boldsymbol{u}^{m+1,k-1})$ using (5.3.16);
    $\boldsymbol{u}^{m+1,k} \leftarrow \boldsymbol{u}^{m+1,k-1} - \left(\nabla \boldsymbol{f}(\boldsymbol{u}^{m+1,k-1})\right)^{-1} \boldsymbol{f}(\boldsymbol{u}^{m+1,k-1})$;
    if First stopping criteria OR Second stopping criteria is satisfied; **then**
        break
    end if
end for
apply constraints on $\boldsymbol{v}^{m+1}$ using $\boldsymbol{u}^{m+1,k}$;
if $\tau^{m+1} \in \mathcal{T}_{\text{coupon}}$ **then**
    $\boldsymbol{u}^{m+1} \leftarrow \boldsymbol{u}^{m+1} + K$;
    $\boldsymbol{v}^{m+1} \leftarrow \boldsymbol{v}^{m+1} + K$;
end if

The existence of a solution of Newton's method requires nonsingularity of the Jacobian ∇f. Like in the case of Newton's method for computing boundary solutions, there may exist values of parameters r, h, σ, θ, $\Delta\tau$, and ρ such that the Jacobian is singular. Quantification of such conditions requires some analysis. The following theorem serves as a guarantee of the existence of a solution in Newton's method.

Theorem 4.4.1. *The Jacobian matrix $J = \nabla \boldsymbol{f}(\boldsymbol{u}^{m+1,k-1})$ is diagonally dominant. Therefore, it is non-singular. For any penalty parameter, $\rho > 1$ the Crank-Nicolson scheme is stable if $\Delta\tau < \dfrac{h^2}{6\theta\sigma^2 - \theta h^2 r - 2\rho h^2(\alpha_c - \alpha_p)}$ or*
$\dfrac{h^2}{\Delta\tau(6\theta\sigma^2 - \theta h^2 r - 2\rho h^2(\alpha_c - \alpha_p))} < 1.$

Remark: This stability condition is consistent with the general stability condition for linear constant coefficient parabolic problems.

Proof. One can use diagonally dominance, also known as *Levy–Desplanques theorem* (Roger A. Horn, 2013) as a sufficient condition for non-singularity. Fix $\forall i \in [1, n]$

$$|J_{ii}| = \left| \frac{2h^2(1 + \theta\Delta\tau r) - 3\theta\Delta\tau\sigma^2 + 2\rho\Delta\tau h(\alpha_c - \alpha_p)}{3h} \right|,$$

and sum of the off-diagonal elements of the Jacobian:

$$\sum_{j \neq i} |J_{ij}| = \left| \frac{h}{3}(1 + \theta\Delta\tau r) + \theta\Delta\tau \frac{\sigma^2}{h} \right|.$$

To maintain the diagonal dominance of the Jacobian, there are some given constants: $\theta \in [0, 1]$, $r = 0.05$, $\sigma = 0.2$, and $\rho > 1$. To ensure the diagonal dominance of the Jacobian below inequality has to be true:

$$|J_{ii}| > \sum_{j \neq i} |J_{ij}|.$$

The J_{ii} can be zero if $\rho < \dfrac{3\theta\sigma^2}{2h}$, which is not true under the given parameters, hence J_{ii} is always non-zero. After some tedious algebraic manipulations, one can deduce the conditions. The right-hand side of the above inequality is positive, then to ensure that the left-hand side is positive as well, one can end up by following conditions: $h^2 > \dfrac{3\theta\Delta\tau\sigma^2}{2(1 + \theta\Delta\tau r + \rho\Delta\tau(\alpha_c - \alpha_p))}$ and $\Delta\tau < \dfrac{2h^2}{3\theta\sigma^2 - 2h^2\theta r - 2\rho h^2(\alpha_c - \alpha_p)}$. Therefore, we have the final condition: $\Delta\tau < \dfrac{h^2}{6\theta\sigma^2 - \theta h^2 r - 2\rho h^2(\alpha_c - \alpha_p)}$ which can be true if $\rho \neq \dfrac{\theta(h^2 r - 6\sigma^2)}{2h^2}$ is satisfied. Following the aforementioned conditions, the Jacobian is invertible, and its determinant is non-zero and, therefore, non-singular. ■

Numerical tests using various realistic values of parameters exhibit no convergence issues with the methods, suggesting nonsingularity of ∇f.

4.4.3 Summary of the time integration method

By including Algorithm 1 and 2 in the θ-scheme, the complete time stepping procedure to compute the solutions $\boldsymbol{u}(x, \tau)$ and $\boldsymbol{v}(x, \tau)$ is shown in Algorithm 3.

Algorithm 3 θ-scheme for time integration with constraints

Input: input the initial solution at $\tau^0 = 0$: $\boldsymbol{u}^0$, $\boldsymbol{v}^0$, u_0^0, u_{n+1}^0, v_0^0, and v_{n+1}^0;

1: **for** $m = 0, 1, \ldots, n_\tau - 1$ **do**
2: Compute $B_p(\tau^{m+1})$ and $B_c(\tau^{m+1})$;
3: Compute u_0^{m+1} and v_0^{m+1} by performing of Algorithm 1;
4: Compute $u_{n+1}^{m+1} = \kappa S_{\text{int}} e^{x_{max}}$ and $v_{n+1}^{m+1} = 0$;
5: Apply the conversion-callability-puttability constraints on u_{n+1}^{m+1} and v_{n+1}^{m+1}.
6: **if** $\tau^{m+1} \in \mathcal{T}_{coupon}$ **then**
7: $u_{n+1}^{m+1} \leftarrow u_{n+1}^{m+1} + K$;
8: $v_{n+1}^{m+1} \leftarrow v_{n+1}^{m+1} + K$;
9: **end if**
10: Compute $\boldsymbol{u}^{m+1}$ and $\boldsymbol{v}^{m+1}$ by performing of Algorithm 2;
11: **end for**

For increased stability, it is possible to initiate the time integration using Rannacher's step Rannacher (1984). In this case, for $m = 0$, the solutions $\boldsymbol{u}^1$, $\boldsymbol{v}^1$, u_0^1, u_{n+1}^1, v_0^1, and v_{n+1}^1 are computed using the initial conditions using Step 2.1–2.6 but with a smaller time step than $\Delta\tau$ (e.g, $\Delta\tau_{rann} = \Delta\tau/n_{rann}$, where $1 < n_{rann} \in \mathbb{N}$). Since we did not see stability issues when $\theta = 1/2$, we did not implement Rannacher's step to obtain numerical results.

4.5 Numerical solution of the TF model

4.5.1 Comparison with FDM

In this section, we present numerical results obtained from the FEM and time integration method discussed in Sections 4.3 and 5.3. The modeling and computational parameters are summarized in Table 5.1, taken from (Ayache et al., 2003; Forsyth and Vetzal, 2002). The numerical solution is computed for $x \in [-18, 2]$, so that the left boundary is sufficiently close to 0 in the S-space. We compare the numerical results with a second-order finite difference method (FDM), combined with the θ-scheme for time integration. To have a fair comparison, we set the number of unknowns in both methods to be equal. For instance, the same meshing can be used for P1-FEM and FDM. n_E and $n_t = n_\tau$ denote the number of elements and time steps, respectively. Thus, for P1-FEM, the number of unknowns (nodal points) is $n = n_E - 1$ and, for P2-FEM, $n = 2n_E - 1$. For the θ-scheme, we set $\theta = \frac{1}{2}$ (Crank-Nicolson).

Figures 4.1, 4.2, and 4.3 show surfaces of the CB price U for $40 \leq S \leq 160$, computed using $n_E = 100$ and 200 and with $n_t = 200$. We note here that the steps in the solution surfaces correspond to the coupon payment time. Qualitatively, the

Table 4.1: Modeling and computational parameters

Parameter	**Value**
Time to maturity T	5 years
Conversion	0 to 5 years into k shares
Conversion ratio k	1.0
Face Value F	\$100
Clean call price B_c	\$110, from Year 3 to Year 5
Clean put price B_p	\$105, during Year 3
Coupon payments K	\$4.0
Coupon dates	.5, 1.0, 1.5, ... ,5.0 (semiannual)
Risk-free interest rate r	5% or 0.05
Credit risk r_c	2% or 0.02
Volatility σ	20% or 0.2
Underlying stock price at $t = 0$, S_{int}	\$100
Penalty parameter ρ	10^6
Newton-Raphson's method tolerance *tol*	10^{-6}

surfaces indicate no noticeable difference between solutions of FDM and P1- or P2-FEM. That the FDM and FEM are qualitatively not distinguishable can be seen from Figure 4.4 and 4.5, where the solutions at $t = 0$ are plotted.

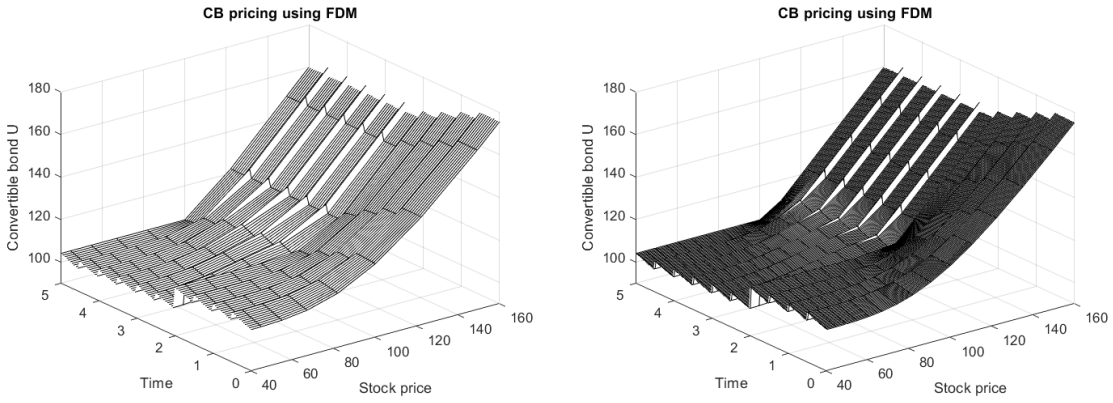

Figure 4.1: Finite difference solution of the penalty TF model over time $t \in [0, 5]$, with $r = 0.05$, $r_c = 0.02$, $\sigma = 0.2$, $F = \$100$, $K = \$4$, $\rho = 10^6$; Left figure: $n = 100$, $n_t = 100$; Right figure: $n = 200$, $n_t = 200$.

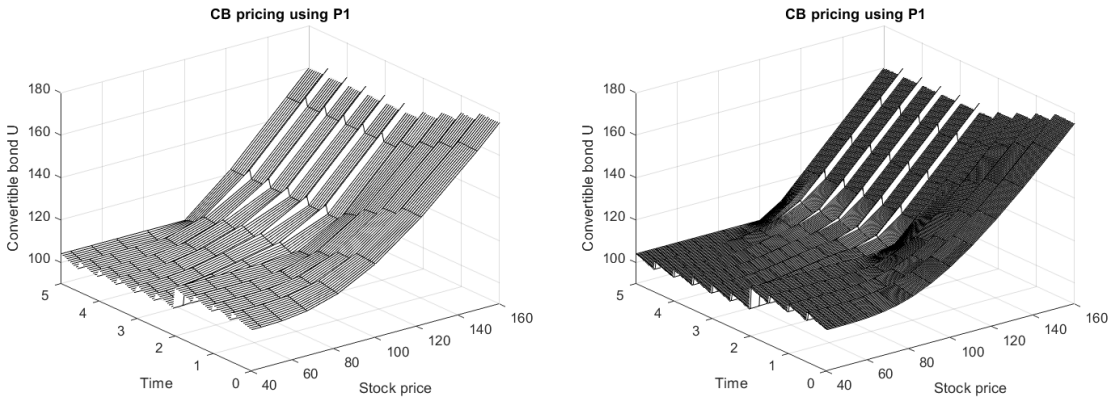

Figure 4.2: P1-FEM solution of the penalty TF model over time $t \in [0, 5]$, with $r = 0.05$, $r_c = 0.02$, $\sigma = 0.2$, $F = \$100$, $K = \$4$, $\rho = 10^6$; Left figure: $n_E = 100$, $n_t = 100$; Right figure: $n_E = 200$, $n_t = 200$.

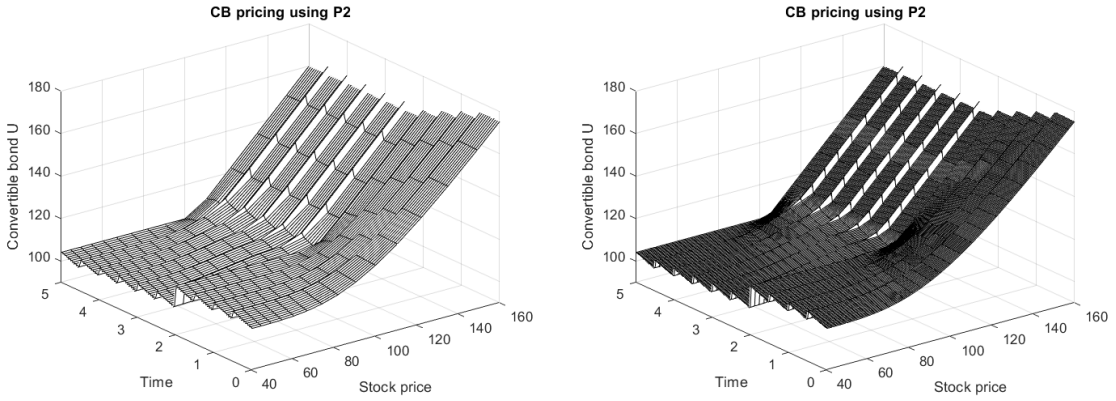

Figure 4.3: P2-FEM solution of the penalty TF model at $t \in [0, 5]$, with $r = 0.05$, $r_c = 0.02$, $\sigma = 0.2$, $F = \$100$, $K = \$4$, $\rho = 10^6$; Left figure: $n_E = 100$, $n_t = 100$; Right figure: $n_E = 200$, $n_t = 200$.

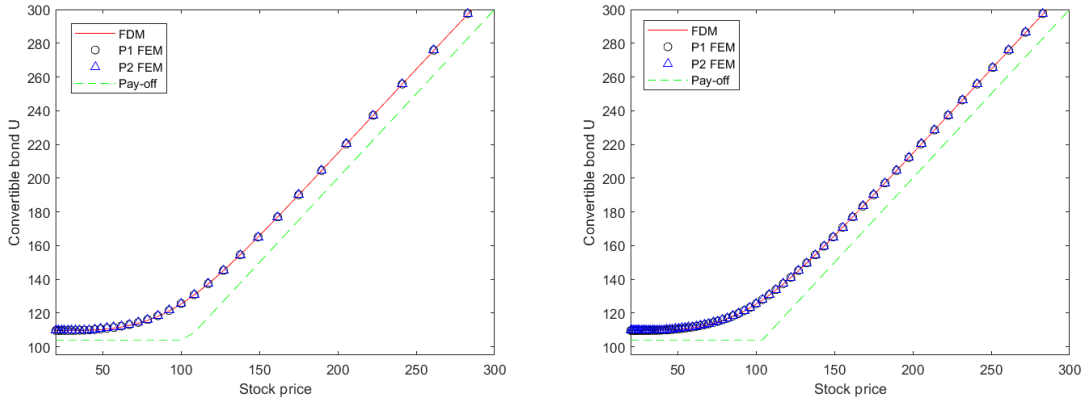

Figure 4.4: Solution of the TF model at $t = 0$, with $r = 0.05$,$r_c = 0.02$, $\sigma = 0.2$, $F = \$100$, $K = \$4$, $\rho = 10^6$; Left figure: for P1-FEM and P2-FEM, $n_E = 100$, $n_t = 100$, and for FDM $n = 200$; Right figure: for P1-FEM and P2-FEM, $n_E = 200$, $n_t = 200$, for FDM, $n = 400$.

In Figure 4.4, FEM and FDM solutions are having strong similarities at relatively coarser spatial-temporal grids. One can mention that using the above-mentioned parameters, a solution of P1 and P2 finite elements is comparable to FDM solution Ayache et al. (2003). The convergence of the solution based on P2 elements was indeed obtained using even coarser grids than with P1 or FDM, which is reasonable.

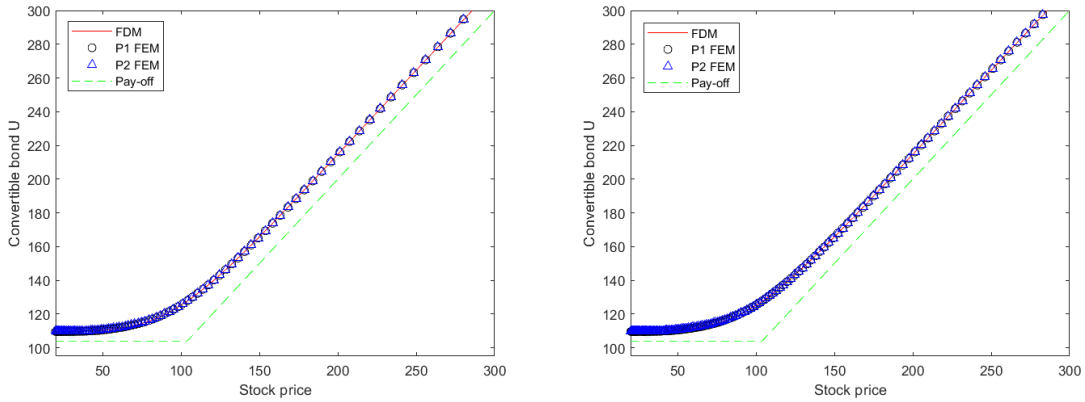

Figure 4.5: Solution of the TF model at $t = 0$, with $r = 0.05$,$r_c = 0.02$, $\sigma = 0.2$, $F = \$100$, $K = \$4$, $\rho = 10^6$; Left figure: for P1-FEM and P2-FEM, $n_E = 400$, $n_t = 400$, for FDM $n = 800$; Right figure: for P1-FEM and P2-FEM, $n_E = 800$, $n_t = 800$, for FDM $n = 1600$.

For convergence(mesh-independence) and comparison of the FE solutions with the FD solutions obtained using various spatial meshes, we present the bond price U at the initial time $t = 0$ and $S = 100$ in Table 4.2 computed using FDM, P1-FEM, and

P2-FEM, with $n_E = n_t$ to keep the ratio $\Delta\tau/h$ constant ($\Delta\tau/h = 0.25 < 1$). The standard stability condition for the convection-diffusion equation discretized by FDM with explicit scheme ($\theta = 0$) requires that

$$\Delta\tau \leq C_{\theta=0} \min\left(\frac{h}{|a|}, \frac{h^2}{2\epsilon}\right), \quad 0 < C_{\theta=0} \leq 1,$$

where, for the TF model, $a = r - \sigma^2/2$ and $\epsilon = \sigma^2/2$. With $n_E = n_t$, there exists, however, some constant n_E^* such that the above stability condition is violated for $n_E > n_E^*$. Instability was not observed in our numerical simulation with $\theta = 1/2$ and $C_{\theta=1/2} < 1$. Our results shown in Table 4.2 illustrated that both P1-FEM and P2-FEM solutions converge to a value around 123.96 at $S = 100$\$, agreeing with the solutions reported in (Ayache et al., 2003) for up to 2 decimal places as the time-spatial mesh is refined. The P1-FEM solution exhibits a similar convergence towards 123.96, but at a lower rate than P2-FEM. As can be observed, our FE solutions compared favorably with the FD solutions across these spatial meshes using half of the number of grid points. P2-FEM solution converges significantly faster than P1-FEM or FDM spending reduced grid points. Moreover, according to the error estimates in 4.6, P2-FEM is theoretically faster than P1-FEM, which has been validated in Table 4.2. In Table 4.2, we also compare the CPU time needed for P1/P2-FEM with the time needed for FDM. P2-FEM takes almost half the time of FDM while keeping the same accuracy with fewer points in the mesh. However, it's important to note that P2-FEM takes less time to converge compared to FDM ($t_{\text{FDM}} > t_{\text{P2-FEM}}$), even though P2-FEM is more computationally expensive than P1-FEM or FDM. Nevertheless, P2-FEM provides more accurate results at early refinement levels than P1-FEM and FDM. The CPU time of P2-FEM for the convergent result is decreased by factor 100 compared to FDM or P1-FEM. The results of Newton's iterations for P1/P2-FEM

Table 4.2: Convertible bond price at $t = 0$ and $S = 100$ computed by P1-FEM, P2-FEM, and FDM with $n, n_E = n_t$

Convertible bond price at $t = 0$ and $S = 100$						Relative execution time	
n	FDM	n_E	P1-FEM	n_E (DOF)	P2-FEM	$t_{\text{P1-FEM}}/t_{\text{FDM}}$	$t_{\text{P2-FEM}}/t_{\text{FDM}}$
400	124.01	400	123.69	100 (200)	123.40	0.87	0.65
800	124.03	800	123.86	200 (400)	124.02	0.71	0.94
1600	123.99	1600	123.90	800 (1600)	123.98	0.84	0.58
3200	123.97	3200	123.94	1200 (2400)	123.98	0.87	0.56
6400	123.97	6400	123.94	1600 (3200)	123.96	0.84	0.56
12800	123.96	12800	123.96	2000 (4000)	123.96	1.04	0.55

and FDM demonstrate a similar number of iterations required for convergence up to

two decimal places among all methods. Based on these observations, P2-FEM offers advantages over FDM or/and P1-FEM in terms of both time and convergence using a four times lesser grid points space and 8 times lesser in time. All methods employed to address the current problem are fully implemented in Matlab, adopting a vectorized style. The only exception is the loop designed to execute Newton's method.

Table 4.3: Number of Newton's iterations for the results in Table 4.2 with $n, n_E = n_t$

FDM				P1-FEM				P2-FEM			
n	max	min	avg	n_E	max	min	avg	n_E	max	min	avg
400	2	1	1.08	400	3	1	1.11	100	2	1	1.24
800	2	1	1.11	800	3	1	1.08	200	3	1	1.23
1600	3	1	1.15	1600	4	1	1.06	800	4	1	1.24
3200	4	1	1.18	3200	6	1	1.06	1200	5	1	1.25
6400	5	1	1.24	6400	12	1	1.10	1600	6	1	1.31
12800	6	1	1.33	12800	16	1	1.39	2000	9	1	1.33

Figure 4.5 presents the solution using a finer spatial-temporal grid. It was noted that P2 solutions are decreasing for very few decimal points compared to FDM but using finer grids. However, this phenomenon can be recognized in FDM as well. What is more, a choice of the penalty parameter ρ has no effect on the solution once we exceed the number 10^6. The optimal choice of this parameter was adopted from (Forsyth and Vetzal, 2002) for American exercises.

In Figure 4.2 and 4.3, one can see the semi-annual coupon payments in time direction, which is shown as jumps over the surface. Moreover, when callability and puttability occur simultaneously at year 3, it tends to a higher price than it was before. Finally, any instability for chosen spatial-temporal grids and ρ was undetected.

4.5.2 Absolute stability region

Absolute stability region details are given in the Section 2.6. Based on accumulated information, one can derive the absolute stability region and check if eigenvalues meet the region's requirement. For the Crank-Nicolson time-stepping methods for nonlinear convertible bond pricing problem based on the TF model, we have presented the eigenvalues in Figire 4.6, which are crucial for the determination of the absolute stability region. Moreover, one could see that for nonlinear problems, there are no instability issues that can be posed based on absolute stability region for the time integrator and depicted eigenvalues that belong to the same stability range. One might observe that the eigenvalues differ from those of the linear BS cases. This

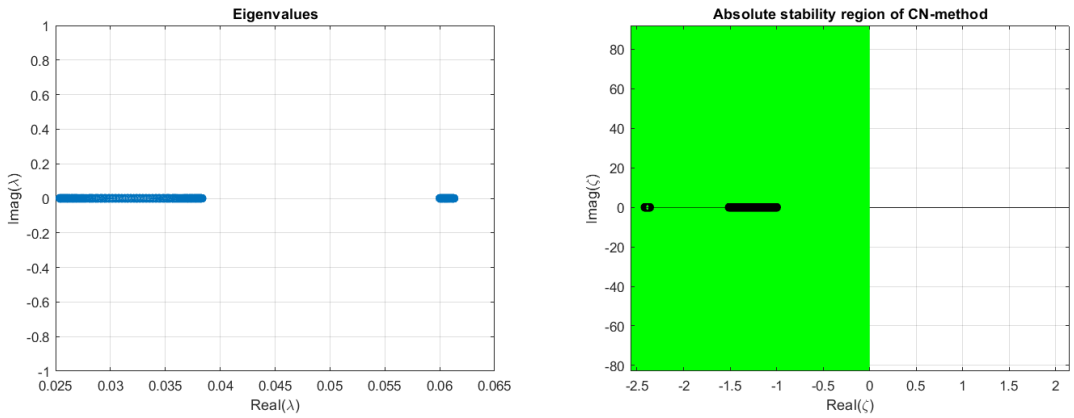

Figure 4.6: Absolute stability region of the time integration scheme for Crank-Nicolson method, when $\theta = 1/2$

might be justified by the nonlinearity introduced by penalty matrices, which are tridiagonal in nature. It is important to note that based on realistic parameters of the model such as r, h, σ, θ, $\Delta\tau$, B_c, B_p, and ρ, the eigenvalues meet the requirement of the absolute stability region, however, employing an impractical set of parameters the instability may occur.

4.5.3 The Greeks

For practical trading purposes, we also need to measure the sensitivity of the CBs with respect to the underlying price, time, volatility, risk-free interest rate, etc. (Wilmott, 1998; Higham, 2004), through the values of the Greeks. In the literature, because FDM is mostly used to compute the price of the options as solutions, the calculation of the Greeks is done approximately using finite differencing (Christara and Wu, 2022; Zvan et al., 1999) of the solutions at grid points. Finite difference approaches can also, in principle, be used to approximate the Greeks once the solutions are available via FEM. Although it will create additional error sources since FDM solutions and FEM solutions are different in their nature, therefore, to maintain consistency, we shall compute some of the Greeks, i.e., the Delta (Δ) and the Gamma (Γ), directly from the finite-element approximation functions. We note, however, that since the approximating P1 FE function is piece-wise continuous and non-differentiable at the element boundaries,we can, in this case, only compute the Greeks at any point inside the elements.

For P1-FEM, the approximating function is piece-wise linear continuous. Therefore, Δ can be explicitly computed by differentiating the finite element solution. In

the element Ω_j, the FEM solution is given by

$$U_h(x) = -u_{j-1}(x - x_j)/h + u_j(x - x_{j-1})/h, \quad x \in \Omega_j. \tag{4.5.1}$$

Therefore, at an instant time t,

$$\Delta(S_{j-1/2}) = \frac{\partial U_h}{\partial S}\bigg|_{S_{j-1/2}} = \frac{S_{\text{int}}}{S_{j-1/2}} \frac{\partial U_h}{\partial x}\bigg|_{x_{j-1/2}} = \frac{S_{\text{int}}}{hS_{j-1/2}}(u_j - u_{j-1})$$

after using the change of variables, $S_{j-1/2} = S_{\text{int}} e^{x_{j-1/2}}$, $x_{j-1/2} = (x_{j-1} + x_j)/2$.

The Greeks corresponding to higher-order derivatives, however, vanish. In this case, we have to resort to finite differencing using the FEM solutions at nodal points. For instance,

$$\frac{\partial^2 U_h}{\partial x^2}\bigg|_{x_{j-1}} \simeq (u_j - 2u_{j-1} + u_{j-2})/h^2.$$

Hence,

$$\Gamma(S_{j-1}) = \frac{\partial^2 U_h}{\partial S^2}\bigg|_{S_{j-1}} = \frac{S_{\text{int}}^2}{S^2} \frac{\partial^2 U_h}{\partial x^2}\bigg|_{x_{j-1}} = \frac{S_{\text{int}}^2}{h^2 S^2}(u_j - 2u_{j-1} + u_{j-2}). \tag{4.5.2}$$

For P2-FEM, the approximating FE function is differentiable, which in the element Ω_j reads

$$U_h(x) = 2u_{j-1}(x - x_{j-\frac{1}{2}})(x - x_j)/h^2 - 4u_{j-1/2}(x - x_{j-1})(x - x_j)/h^2 + 2u_j(x - x_{j-1})(x - x_{j-\frac{1}{2}})/h^2.$$

After differentiation at $x_{j-1/2}$, yields

$$\frac{\partial U_h}{\partial x}\bigg|_{x_{j-1/2}} = (u_j - u_{j-1})/h \text{ and } \frac{\partial^2 U_h}{\partial x^2}\bigg|_{x_{j-1/2}} = 4(u_j - 2u_{j-1/2} + u_{j-1})/h^2.$$

This in turn results in $\Delta(S_{j-1/2})$ in (4.5.1) and

$$\Gamma(S_{j-1/2}) = \frac{4S_{\text{int}}^2}{h^2 S^2}(u_j - 2u_{j-1/2} + u_{j-1}). \tag{4.5.3}$$

An example of the numerical results of the Greeks obtained by using derived formulas is shown in Figure 4.8 for Δ and Γ at $(t = 0)$. The corresponding Greeks are computed using P2-FEM for Δ and Γ at $S_{j-1/2}$. The FDM Greeks are performed by a central difference scheme evaluated at the same nodal points. As can be seen, the Delta and Gamma curves obtained by the two methods are smooth curves without spikes or peaks, highlighting their suitability for hedging purposes. It appears that

the the Greeks obtained by P2-FEM demonstrate the similarity with those obtained by FDM.

Visible peaks and spikes in the solution surfaces are due to the constraints and coupon payment; at this point, the solution is not differentiable. Delta and Gamma, however, are smooth at the locations where the inequality constraints are not imposed.

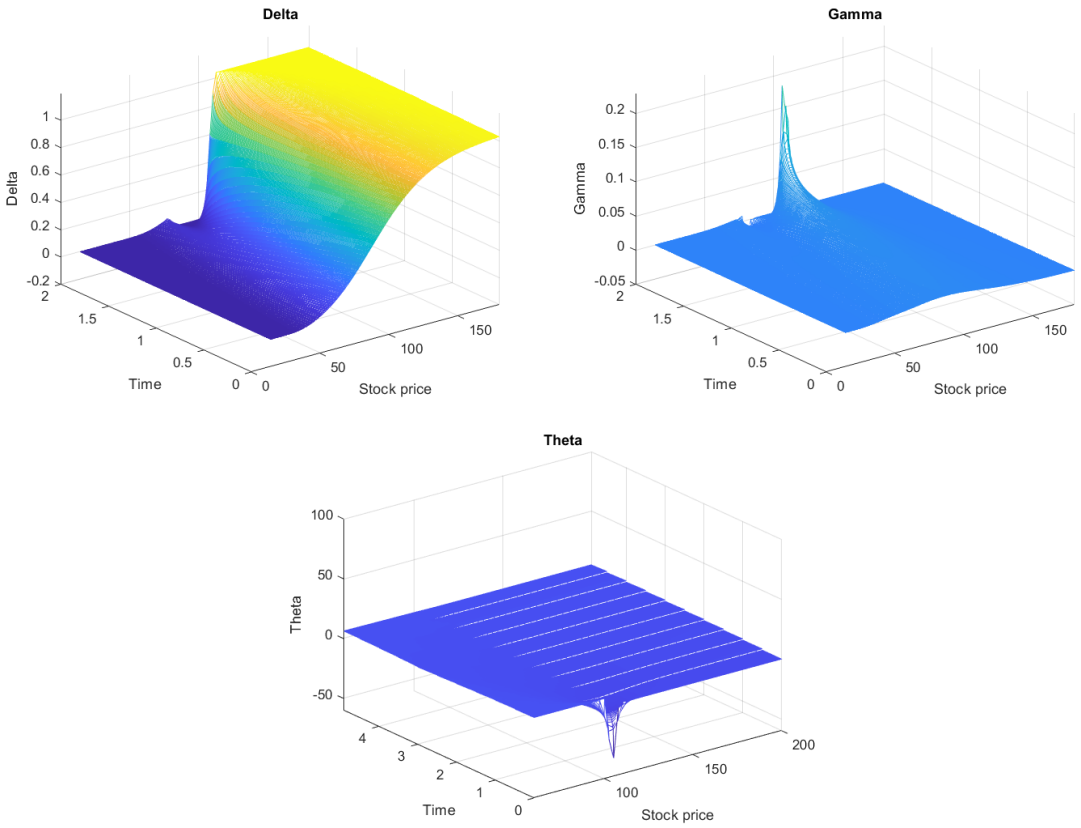

Figure 4.7: Greeks by with the parameters $t = 0$, $r = 0.05$, $r_c = 0.02$, $\sigma = 0.2$, $F = \$100$, $K = \$4$, $\rho = 10^6$, $n_E = 1600$, $n_t = 1000$ by P2-FEM; Left figure: Delta Δ; Right figure: Gamma Γ; Right figure: Theta Θ.

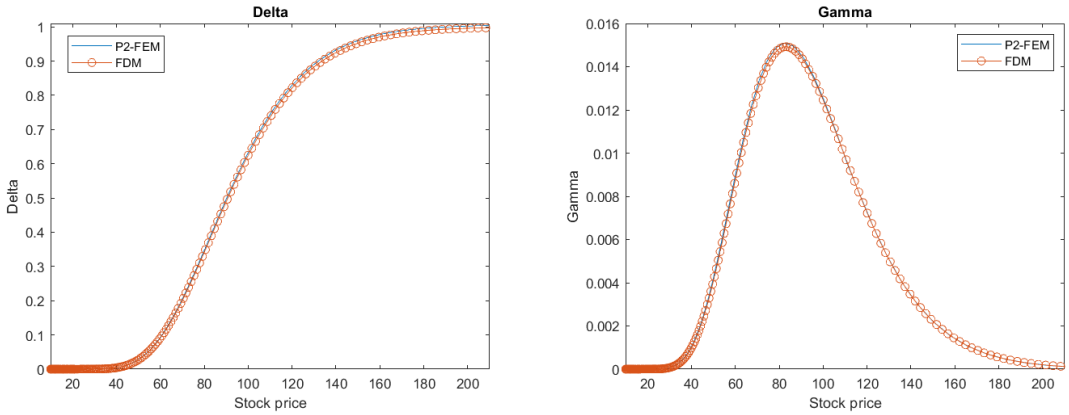

Figure 4.8: Greeks by with the parameters $t = 0$, $r = 0.05$, $r_c = 0.02$, $\sigma = 0.2$, $F = \$100$, $K = \$4$, $\rho = 10^6$, $n_E = 1600$, $n_t = 1000$ by P2-FEM; Left figure: Delta Δ; Right figure: Gamma Γ.

4.6 Accuracy of the approximations

To demonstrate that our FEM approach to the TF problem described above may obtain first order accuracy, we consider the following linear model problem (Roache, 2001), which keeps the left-hand side of the TF the system defined by (1) and (2), without constraints (and hence no penalty term), and coupon payment corresponding to the exact solution

$$\begin{aligned} U(x,\tau) &= S_{int}^2 e^{2x}\sqrt{S_{int}e^x} - Fe^{-r\tau}\sqrt{S_{int}e^x}, \\ V(x,\tau) &= S_{int}^2 e^{2x}\sqrt{S_{int}e^x} - Fe^{-r\tau}\sqrt{S_{int}e^x} + x^2\tau, \end{aligned}$$

where $\tau \in (0,1)$. This manufactured solution corresponds to the initial conditions

$$\begin{cases} U(x,0) = S_{int}^2 e^{2x}\sqrt{S_{int}e^x} - F\sqrt{S_{int}e^x}, \\ V(x,0) = S_{int}^2 e^{2x}\sqrt{S_{int}e^x} - F\sqrt{S_{int}e^x}, \end{cases}$$

the boundary conditions

$$\begin{cases} U(0,\tau) = S_{int}^2\sqrt{S_{int}} - Fe^{-r\tau}\sqrt{S_{int}}, \\ V(0,\tau) = S_{int}^2\sqrt{S_{int}} - Fe^{-r\tau}\sqrt{S_{int}}, \end{cases} \quad \begin{cases} U(1,\tau) = S_{int}^2 e^2\sqrt{S_{int}e} - Fe^{-r\tau}\sqrt{S_{int}e}, \\ V(1,\tau) = S_{int}^2 e^2\sqrt{S_{int}e} - Fe^{-r\tau}\sqrt{S_{int}e} + \tau, \end{cases}$$

and the non-homogeneous BS equations

$$\begin{aligned} f_1 &= U_\tau - \frac{\sigma^2}{2}U_{xx} - (r - \frac{\sigma^2}{2})U_x + rU + r_cV, \\ f_2 &= V_\tau - \frac{\sigma^2}{2}V_{xx} - (r - \frac{\sigma^2}{2})V_x + (r + r_c)V, \end{aligned}$$

in the CB and COCB PDE, respectively. Applying FEM and the θ-scheme leads to the numerical procedure

$$A_{11}\boldsymbol{u}^{m+1} = \widetilde{A}_{11}\boldsymbol{u}^{m} - A_{12}\boldsymbol{v}^{m+1} + \widetilde{A}_{12}\boldsymbol{v}^{m} + \theta\Delta\tau\boldsymbol{\beta}_1^{m+1} + (1-\theta)\Delta\tau\boldsymbol{\beta}_1^{m} + \hat{\boldsymbol{b}}_{M,u}^{m} - \hat{\boldsymbol{b}}_{M,u}^{m+1} + \theta\Delta\tau f_1 + (1-\theta)\Delta\tau f_1,$$

$$A_{22}\boldsymbol{v}^{m+1} = \widetilde{A}_{22}\boldsymbol{v}^{m} + \theta\Delta\tau\boldsymbol{\beta}_2^{m+1} + (1-\theta)\Delta\tau\boldsymbol{\beta}_2^{m} + \hat{\boldsymbol{b}}_{M,v}^{m} - \hat{\boldsymbol{b}}_{M,v}^{m+1} + \theta\Delta\tau f_2 + (1-\theta)\Delta\tau f_2.$$

Calculated errors are presented in Figure 4.9 and 4.10 using two measures (Amanbek and Wheeler, 2019; Amanbek et al., 2020):

$$\|Error\|_{L^2} = \|U(x,1) - \boldsymbol{u}^{n_t}\|_{L^2},$$
$$\|Error\|_{L^\infty(L^2)} = \max_{1\le m\le n_t} \left(\|U(x,m\Delta\tau) - \boldsymbol{u}^{m}\|_{L^2}\right),$$

where $\boldsymbol{u}^m$ is the solution of the model problem at $\tau = m\Delta\tau$, computed by P1-FEM or P2-FEM. In Figure 4.9, the errors are calculated for varying $\Delta\tau$ and a fixed value of h. The errors decrease as $\Delta\tau$ is reduced to 0, with a rate that is proportional to $\Delta\tau$ (first-order convergence).

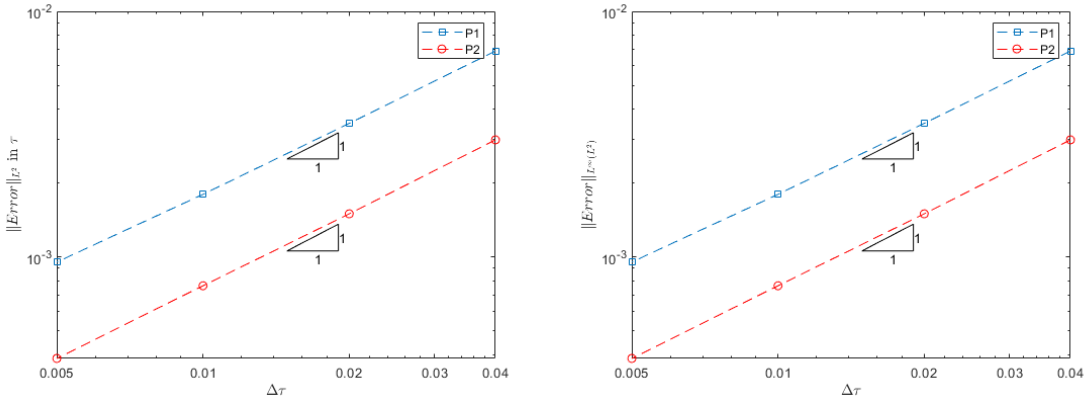

Figure 4.9: Error estimates of the model problem in $\tau \in [0,1]$, with $r = 0.05$,$r_c = 0.02$, $\sigma = 0.2$, $h_{P1} = 3\times10^{-4}$, and $h_{P2} = 10^{-3}$.

In Figure 4.10, the errors are calculated for varying h and fixed $\Delta\tau$. The plots suggest convergence of P1-FEM and P2-FEM at the rate proportional to h and h^2, respectively (Theoretically, e.g. for P1-FEM the convergence rate is given by the relation $\|Error\|_{L^\infty(L^2)} \le C(h+\Delta\tau)$) Amanbek and Wheeler (2019); Amanbek et al. (2020). This convergence rate is as expected for the linear model but cannot be expected when nonlinear (e.g., penalty) terms are added.

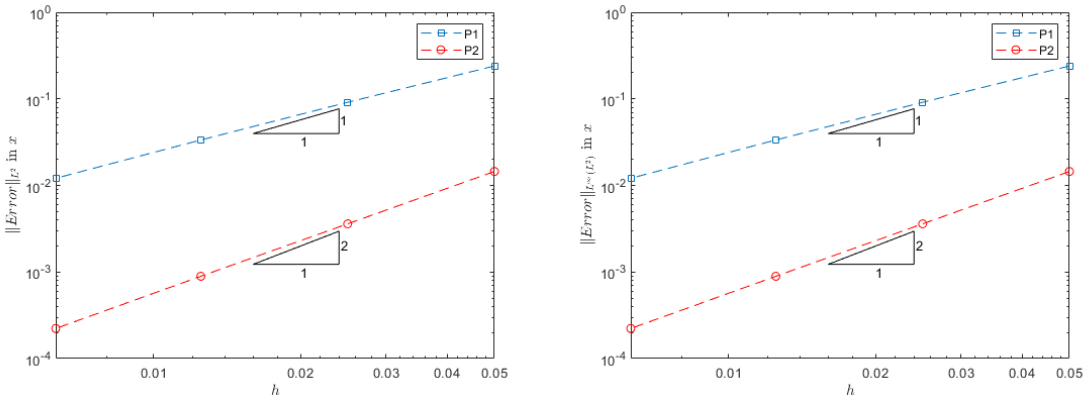

Figure 4.10: Error estimates of the MMS model in $x \in [0, 1]$, with $r = 0.05$,$r_c = 0.02$, $\sigma = 0.2$, and $\Delta\tau = 10^{-4}$.

Chapter 5

AFV model for Convertible bonds

5.1 Introduction

Convertible bonds subject to default strategies can be priced by the so called AFV model developed in Ayache et al. (2003). However, the TF model's modeling aspect is criticized and justified as inconsistent in Ayache et al. (2003) addressing why this model falls short of derivative market requirements. The intuitive continuation from the TF to the AFV model involves the development of partial and total default strategies. Numerical results by IGA present a comparable performance on the benchmark problem Forsyth and Vetzal (2002) by the Finite Volume Method (FVM). In the latter, the authors employed Van-leer flux limiters and Rannacher smoothing Zvan et al. (1999) technique, ensuring the high-resolution scheme with total variation diminishing properties, which guarantees monotonic convergence. The driving force behind applying these stabilization techniques is to avoid spurious oscillations caused by the convection-dominated term in the AFV model. Our approach incorporates the use of Landau transform Zhu and Zhang (2011) which reduces variable coefficients to constant coefficients, however, it can not avoid the convection-dominant nature of the problem. Nevertheless, the IGA framework successfully performed comparable solutions. Equally important, it maintained monotonic convergence during the refinement process, even in the presence of convection-dominance. Additionally, corresponding Greeks are calculated by IGA and P2-FEM with no peaks or shocks.

Pricing the American style of derivatives is a fundamental task in derivative pricing theory, especially the post-processing Greeks are of interest for hedging and trading strategies. For decades, the Finite Difference method (FDM) method has been a common choice among many scientists due to its computational speed and ease of implementation. The literature contains a vast amount of papers on FDM applied to Black-Scholes type of problems, such as smooth mapping functions for non-uniform

mesh Christara and Wu (2022) and predictor-corrector schemes for handling the nonlinear PDEs Lin and Zhu (2020). Another common choice is the conventional Finite Element Method (FEM) has produced superconvergence results in Golbabai et al. (2013) for barrier options. Authors in Wei et al. (2024) have shown that modified P2 basis functions under the FEM framework can effectively handle the nonlinear Leland model. Some rare numerical methods, like reduced basis functions, were utilized for jump-diffusion models by Cont et al. (2011), while the spectral element method is used by Zhu and Kopriva (2009). Additionally, articles have used the splines Christara and Leung (2016) and B-spline wavelets Ortiz-Gracia and Oosterlee (2013). There is only one paper that incorporates IGA for jump-diffusion models Pospíšil and Švígler (2018). Indeed, it is a well-known fact that FEM is a widespread tool among specialists, as it suggests mesh adaptivity and allows for error analysis conduction. Moreover, the FEM solution is superior to FDM in terms of convergence Andalaft-Chacur et al. (2011).

However, FEM basis functions become partially negative when higher-degree polynomials are used, leading to the so-called Gibbs phenomenon. Due to the specifics of the assembling process in FEM, basis functions with degrees higher than one require more computational resources. In contrast, IGA's element matrix size is independent of the polynomial degree, and the NURBS basis functions are always positive, with a variation diminishing property that avoids the Gibbs phenomenon. Since IGA directly relates to the FEM framework, it inherits the above-mentioned advantages of FEM. Another crucial point about IGA is that the complex geometries encountered in payoff functions in derivative pricing theory can be almost exactly described by NURBS Pospíšil and Švígler (2018), utilizing a non-uniform knot vector that entails the multiplicity of knots at points where it is less differentiable. Furthermore, the NURBS can offer greater flexibility by allowing control over the weights of control points, which is a feature not found in other methods.

Within this chapter, we present several novelties that warrant the reader's attention:

- IGA based on NURBS is applied to nonlinear American-style contracts for the first time.
- A fundamental framework for addressing the nonlinearities occurring in American contracts is established.
- IGA performance has showcased the suppression of spurious oscillations previously encountered with P2-FEM.

- The Greeks are calculated by post-processing IGA and FEM algorithms rather than simply relying on FDM, which could create and change the nature of the solution by adding another source of error.
- Monotonic convergence at the strike price is maintained without any stabilization techniques in the presence of Peclet number for nonlinear American contracts.
- The application of fitted NURBS to the AFV model suggests a solution with fewer degrees of freedom.
- Considerably consistent Greek results with no peaks or shocks are presented for nonlinear American contracts by IGA-FEM and P2-FEM.

5.1.1 Derivation of the AFV model

5.1.1.1 Convertible bond with no credit risk

One could start the modeling part with no default possibility. Suppose that interest rates are known functions of time, and that the stock price is described by Browninan motion.

$$dS = \mu S dt + \sigma S dz$$

where S is the stock price, μ is its drift rate, σ is its volatility, and dz is the increment of a Wiener process. Based on standard arguments of Ito's lemma and Delta hedging, the risk-neutral value of $V(S,t)$ of any claim contingent on S is given by

$$V_t + \left(\frac{\sigma^2}{2} S^2 V_{SS} + (r(t) - q) S V_S - r(t) V\right) = 0$$

where $r(t)$ is the known interest rate and q is the dividend rate. A convertible bond has the following contractual key properties, which distinguish among other derivatives:

- A continuous (time-dependent) puttability provision (with an exercise price of B_p).
- A continuous (time-dependent) conversion provision. At any time, the bond can be converted to K shares.
- A continuous (time-dependent) callability provision. At any time, the issuer can call the bond for price $B_c > B_p$. However, the holder can convert the bond if it is called.

The operator $\mathcal{L}V$ is defined as

$$\mathcal{L}V \equiv -V_t - \left(\frac{\sigma^2}{2} S^2 V_{SS} + (r(t) - q) S V_S - r(t) V \right)$$

The solution is defined in the domain where $\kappa S \geq B_C$ and $\kappa S < B_c$ separately:

- $B_C > \kappa S$. In this case, the problem is formulated as a linear complementarity problem (LCP)

$$\begin{pmatrix} \mathcal{L}V = 0 \\ (V - \max(B_p,\ \mathrm{K}S)) \geq 0 \\ (V - B_c) \leq 0 \end{pmatrix} \vee \begin{pmatrix} \mathcal{L}V \geq 0 \\ (V - \max(B_p,\ \mathrm{K}S)) = 0 \\ (V - B_c) \leq 0 \end{pmatrix} \vee \begin{pmatrix} \mathcal{L}V \leq 0 \\ (V - \max(B_p,\ \mathrm{K}S)) \geq 0 \\ (V - B_c) = 0 \end{pmatrix} \tag{5.1.1}$$

where the sign $\vee$ is standing to indicate that at least one of the three options is valid at each point in the solution domain.

- $B_c \leq \kappa S$. The convertible value is,

$$V = \kappa S$$

since the holder is likely to convert it swiftly. Equation (5.1.1) is an intuitive formulation of the problem $\mathcal{LV} = 0$ subject to simplified inequality constraints:

$$V \geq \max(B_p,\ \mathrm{K}S)$$
$$V \leq \max(B_c,\ \mathrm{K}S)\,.$$

The solution is associated with the continuous region where $\mathcal{LV} = 0$ and neither the callability nor the puttability provisions are obligated (left side term in (5.1.1)), or the puttability constraint is obligated (middle term in (5.1.1)), or the callability provision is obligated (right side term in (5.1.1)).

One shall take care of boundary conditions to cover the model's well-posedness. The operator $\mathcal{L}V$ at $S = 0$ and as $S \to \infty$. At $S = 0$, $\mathcal{L}V$ becomes

$$\mathcal{L}V \equiv -(V_t - r(t)V)\,; \quad S \to 0$$

5.1.1.2 Risky bond

The discussion of credit risk can sometimes be complicated due to uncertainty, where the risk might be capricious. One could start with the valuation of coupon-bearing bonds, where the issuer has some default risk. This idea can have a commonality with the paper Duffie and Singleton (1999). Therefore, we claim that the risk-free rate is a function. Moreover, the default risk is diversifiable, which implies that the probability of real-world and risk-neutral default are equal. Based on these assumptions, one could define the probability of default in the time increment $t + dt$ by $p(S, t)$, which is called the hazard rate.

Construct the hedging portfolio, where B is a risky bond.

$$\Pi = B - \Delta S.$$

If there is no default, the choice is $\Delta = B_S$, then the Ito lemma provides

$$d\Pi = \left[B_t + \frac{\sigma^2 S^2}{2} B_{SS} \right] dt + o(dt) \tag{5.1.2}$$

where $o(dt)$ denotes terms that go to zero faster than dt. The following assumptions are made:

- The probability of default in $t \to t + dt$ is pdt.
- The value of the bond immediately after default is RX where $0 \leq R \leq 1$ is the recovery factor.
- The stock price S remains unchanged on default case.

If the bond is coupon-bearing, then X is the face value. In contrast, X represents the accumulated value derived from the initial issue price, or one could assume that $X = B$ is the pre-default value. Then equation (5.1.2) is written as

$$\begin{aligned} d\Pi &= (1 - pdt) \left[B_t + \frac{\sigma^2 S^2}{2} B_{SS} \right] dt - pdt(B - RX) + o(dt) \\ &= \left[B_t + \frac{\sigma^2 S^2}{2} B_{SS} \right] dt - pdt(B - RX) + o(dt). \end{aligned} \tag{5.1.3}$$

The above-mentioned assumptions suggest

$$\mathrm{E}(d\Pi) = r(t)\Pi dt, \tag{5.1.4}$$

combining (5.1.3) and (5.1.4) gives

$$B_t + r(t)SB_S + \frac{\sigma^2 S^2}{2}B_{SS} - (r(t)+p)B + pRX = 0.$$

If a bond is not coupon bearing, then $X = B$, then the solution of bond with face value F is

$$B = F\exp\left[-\int_t^T (r(u)+p(u)(1-R))du\right].$$

Above assumptions might be adjusted to the stock price in the event of default. Adjustment is that the stock price S will jump to zero in the case of default, then equation (5.1.3) is reformulated as

$$\begin{aligned} d\Pi &= (1-pdt)\left[B_t + \frac{\sigma^2 S^2}{2}B_{SS}\right]dt - pdt(B - RX - \Delta S) + o(dt) \\ &= \left[B_t + \frac{\sigma^2 S^2}{2}B_{SS}\right]dt - pdt(B - RX - \Delta S) + o(dt) \end{aligned}$$

based on delta hedging arguments $\Delta = B_S$, one get

$$B_t + (r(t)+p)SB_S + \frac{\sigma^2 S^2}{2}B_{SS} - (r(t)+p)B + pRX = 0.$$

Now, p is shown in the drift term as well as in the discounting term. Notably, many bond valuation models do not incorporate the information about the stock dynamic behavior in the case of default.

5.1.1.3 The Hedge Model

In the previous section, the discussion of credit risk incorporation was revised in detail. For the sake of simplicity, one could use the put or call features, and that conversion is only allowed at the terminal time (as a European-style contract) or in the event of default. Let S^+ be the stock price immediately after default, and S^- be the stock price right before default. Suppose that

$$S^+ = S^-(1-\eta) \tag{5.1.5}$$

where $\eta \in [0,1]$. $\eta = 1$ is the "total default" case when the stock price becomes zero, and $\eta = 0$ is the "partial default" case when the issuing firm's status is defaulted, but the stock price remains unchanged. The usual portfolio is constructed as

$$\Pi = U - \Delta S.$$

If there was no credit risk, i.e. $p = 0$, then choosing $\Delta = U_S$ and applying Ito lemma leads to

$$d\Pi = \left[U_t + \frac{\sigma^2 S^2}{2} U_{SS}\right] dt + o(dt)$$

However, the context of interest considers the non-zero hazard rate p. The following assumptions are made:

- Upon default, the stock price jumps according to equation (5.1.5).
- Upon default, the convertible bondholders have the option of receiving
  - the amount RX, where $0 \leq R \leq 1$ is the recovery factor (as in the case of a simple risky bond, there are several possible assumptions that can be made about X (e.g. face value, the pre-default value of the bond portion of the convertible, etc.), but for now, we will not make any specific assumptions), or:
  - shares worth $\kappa S(1 - \eta)$.

Following the above assumptions, the change in the value of the hedging portfolio when $t \to t + dt$ is

$$\begin{aligned} d\Pi &= (1 - pdt)\left[U_t + \frac{\sigma^2 S^2}{2} U_{SS}\right] dt - pdt(U - \Delta S\eta)\Big) + pdt \max(\kappa S(1-\eta), RX) + o(dt) \\ &= \left[U_t + \frac{\sigma^2 S^2}{2} U_{SS}\right] dt - pdt\,(U - U_S S\eta) + pdt \max(\kappa S(1-\eta), RX) + o(dt). \end{aligned} \tag{5.1.6}$$

The expected return on the portfolio is given by equation (5.1.4) and making the standard approach of equalization with the expectation of equation (5.1.6), one can get

$$r\,[U - SU_S]\,dt = \left[U_t + \frac{\sigma^2 S^2}{2} U_{SS}\right] dt - p\,[U - U_S S\eta]\,dt + p[\max(\kappa S(1-\eta), RX)]dt + o(dt)$$

which leads to

$$U_t + (r(t) + p\eta)SU_S + \frac{\sigma^2 S^2}{2} U_{SS} - (r(t) + p)U + p \max(\kappa S(1-\eta), RX) = 0 \tag{5.1.7}$$

note that $r(t) + p\eta$ is shown in the drift term and $r(t) + p$ is shown in the discounting term in equation (5.1.7). When $R = 0, \eta = 1$, default is present, but with no recovery, the consequence is that one solves the full convertible bond problem (2.4), with $r(t)$ changed to $r(t) + p$. Then, we can define

$$\mathcal{M}U \equiv -U_t - \left(\frac{\sigma^2}{2} S^2 U_{SS} + (r(t) + p\eta - q)SU_S - (r(t) + p)U\right)$$

where the equation (4.6) for the case where the stock pays a proportional dividend q as

$$\mathcal{M}U - p\max(\kappa S(1-\eta), RX) = 0 \tag{5.1.8}$$

The important moment of considering the complete problem with risk debt can be done by generalizing problem (5.1.1), by means of(5.1.8), which leads to LCP:

- $B_c > \kappa S$

$$\begin{array}{l} \left(\begin{array}{c} \mathcal{M}U - p\max(\kappa S(1-\eta), RX) = 0 \\ (U - \max(B_p, \kappa S)) \geq 0 \\ (U - B_c) \leq 0 \end{array}\right) \\ \vee \left(\begin{array}{c} \mathcal{M}U - p\max(\kappa S(1-\eta), RX) \geq 0 \\ (U - \max(B_p, \kappa S)) = 0 \\ (U - B_c) \leq 0 \end{array}\right) \\ \vee \left(\begin{array}{c} \mathcal{M}U - p\max(\kappa S(1-\eta), RX) \leq 0 \\ (U - \max(B_p, \kappa S) \geq 0 \\ (U - B_c) = 0 \end{array}\right) \end{array} \tag{5.1.9}$$

- $B_c \leq \kappa S$

$$U = \kappa S \tag{5.1.10}$$

The value of the convertible bond is rewritten as

$$\mathcal{M}U - p\max(\kappa S(1-\eta), RX) = 0, \tag{5.1.11}$$

subject to the callability and puttability constraints

$$\begin{array}{l} U \geq \max(B_p,\ \mathrm{K}S) \\ U \leq \max(B_c,\ \mathrm{K}S)\,. \end{array} \tag{5.1.12}$$

Actually, equation (5.1.9) simply states that either we are in the continuation region or one of the two constraints (call or put) is obligated.

Referring to previous assumptions on recovery factor RX, we say that the recovery factor on default is equalized to face value, therefore, the value of the convertible bond value U can be computed from a single equation (5.1.1). However, this decoupling won't be true if we suppose that X represents the bond component of the convertible. Therefore, put/call provisions shall be applied to the value of the bond component. Following this recovery assumption, one is in necessity of solving another equation for the bond component B, which will later construct the system of equations to find the value of U.

5.1.1.4 Equity component upon default

Upon default, recovered value RB, where, B is the pre-default bond component of the convertible bond. Let us devise a splitting of the convertible bond into two components, such that $U = B + C$, where B is the bond component and C is the equity component. The moment that deserves to be highlighted is that the splitting is true if, upon default, the holder recovers RB, with B being the bond component of the convertible and C, the equity component.

Then, in the case where the holder recovers RB on default, we suggest the following LCP for bond and equity components

$$\begin{aligned}
&\begin{pmatrix} \mathcal{M}C - p\max(\kappa S(1-\eta) - RB, 0) = 0 \\ (C - (\max(B_c,\ \mathrm{K}S) - B)) \leq 0 \\ (C - (\kappa S - B) \geq 0 \end{pmatrix} \\
\vee &\begin{pmatrix} \mathcal{M}C - p\max(\kappa S(1-\eta) - RB, 0) \leq 0 \\ C = \max(B_c,\ \mathrm{K}S) - B \end{pmatrix} \\
\vee &\begin{pmatrix} \mathcal{M}C - p\max(\kappa S(1-\eta) - RB, 0) \geq 0 \\ C = \kappa S - B \end{pmatrix},
\end{aligned} \tag{5.1.13}$$

$$\begin{pmatrix} \mathcal{M}B - RpB = 0 \\ B - B_c \leq 0 \\ B - (B_p - C) \geq 0 \end{pmatrix} \vee \begin{pmatrix} \mathcal{M}B - RpB \leq 0 \\ B = B_c \end{pmatrix} \vee \begin{pmatrix} \mathcal{M}B - RpB \geq 0 \\ B = B_p - C \end{pmatrix}. \tag{5.1.14}$$

Combination of two LCPs (5.1.13)-(5.1.14), and recalling that $U = B + C$, it can be seen that equations (5.1.9)-(5.1.10) are satisfied. Informally, the equations (5.1.13) can be rewritten as

$$\mathcal{M}C - p\max(\kappa S(1-\eta) - RB, 0) = 0 \tag{5.1.15}$$

subject to the constraints

$$\begin{aligned}
B + C &\leq \max(B_c,\ \mathrm{K}S) \\
B + C &\geq \kappa S.
\end{aligned} \tag{5.1.16}$$

In the same manner, the LCP (5.1.14) is written as

$$\mathcal{M}B - RpB = 0 \tag{5.1.17}$$

subject to the constraints

$$\begin{aligned}
B &\leq B_c \\
B + C &\geq B_p.
\end{aligned} \tag{5.1.18}$$

One shall mention that the constraints of bond and equity components preserve the fact that $U = B + C$ and $B \leq B_c$. The payoff functions of each component are suggested to have the following forms:

$$U(S,T) = F + \max(\kappa S - F, 0)$$
$$C(S,T) = \max(\kappa S - F, 0)$$
$$B(S,T) = F.$$

5.1.2 AFV model as American contract

For American contract, we have extended our previous work on pricing the convertible Bonds by TF model Kazbek et al. (2024), as a natural evolution to AFV model, since the model has more sophisticated default strategies comparing to TF model. Ayache et al. Ayache et al. (2003) came up with a system of partial differential equations for pricing convertible bonds subject to the default strategy of the underlying asset, as described in 5.1.1. The combined system of equations are constructed from (5.1.11), (5.1.15), and (5.1.17) as a coupled system of triple PDEs

$$\frac{\partial U}{\partial t} + \frac{1}{2}\sigma^2 S^2 \frac{\partial^2 U}{\partial S^2} + (r + p\eta)S\frac{\partial U}{\partial S} - (r+p)U + p\max(kS(1-\eta), RB) = 0, \tag{5.1.19}$$

$$\frac{\partial B}{\partial t} + \frac{1}{2}\sigma^2 S^2 \frac{\partial^2 B}{\partial S^2} + (r + p\eta)S\frac{\partial B}{\partial S} - (r+p)B + RpB = 0, \tag{5.1.20}$$

$$\frac{\partial C}{\partial t} + \frac{1}{2}\sigma^2 S^2 \frac{\partial^2 C}{\partial S^2} + (r + p\eta)S\frac{\partial C}{\partial S} - (r+p)C + p\max(kS(1-\eta) - RB, 0) = 0, \tag{5.1.21}$$

for the time $t \in (0,T)$ and the underlying stock price $S \in (0,\infty)$, with U be the value of the convertible bond, B be the bond component, C be the equity component, r be the risk-free rate, p be the hazard rate, η be the indicator of the partial or total default strategies, R be the recovery factor upon the default, k be the conversion rate and σ be volatility.

The terminal condition at the maturity time T:

$$U(S,T) = \begin{cases} F + K, & \text{if} \quad F + K \geq kS, \\ kS, & \text{otherwise}, \end{cases}, \tag{5.1.22}$$

$$B(S,T) = F + K, \tag{5.1.23}$$

and

$$C(S,T) = \begin{cases} kS - F - K, & \text{if} \quad kS - F - K \geq 0, \\ 0, & \text{otherwise}. \end{cases} \tag{5.1.24}$$

Once the convertible bond is issued, before its expiration date, the holder can convert if it is reasonable, and the issuer will pay the principal. Otherwise, the following inequalities hold:

1. Value of the convertible bond (5.1.19), subject to following constraints:

$$U(S,t) \geq \max(B_p, kS), \tag{5.1.25}$$

$$U(S,t) \leq \max(B_c, kS). \tag{5.1.26}$$

2. Value of the bond component (5.1.20), subject to following constraints:

$$B(S,t) \leq B_c, \tag{5.1.27}$$

$$B(S,t) + C(S,t) \geq B_p. \tag{5.1.28}$$

3. Value of the equity component (5.1.21), subject to following constraints:

$$B(S,t) + C(S,t) \leq \max(B_c, kS), \tag{5.1.29}$$

$$B(S,t) + C(S,t) \geq kS. \tag{5.1.30}$$

Dirty call and put prices depend on accrued interest, which will be paid when coupon payment dates on the pending stage, therefore:

$$B_{p,c}(t) = B_{p,c}^{clean} + AccI(t), \tag{5.1.31}$$

where

$$AccI(t) = K_i \frac{t - t_{i-1}}{t_i - t_{i-1}}, \tag{5.1.32}$$

the accrued interest at any time t between the time of the last coupon payment t_{i-1} and the time of the next coupon payment t_i.

At $S = 0$, the boundary condition is a system of time-dependent equations:

$$\begin{cases} \dfrac{\partial U(0,t)}{\partial t} = (r+p)U(0,t) - RpB(0,t), \\ \dfrac{\partial B(0,t)}{\partial t} = (r + (1-R)p)B(0,t), \\ \dfrac{\partial C(0,t)}{\partial t} = (r+p)C(0,t), \end{cases} \tag{5.1.33}$$

As $S \to \infty$, the boundary condition reveals to be converted into stock with a particular conversion ratio:

$$\lim_{S\to\infty} \begin{cases} U(S,t) = kS, \\ B(S,t) = 0, \\ C(S,t) = kS \end{cases} \tag{5.1.34}$$

Henceforth, in the rest of the chapter, we shall refer to the American contract as the "AFV model".

5.1.3 Transformation of the models

Classical Landau transformation Zhu and Zhang (2011) is going to be used to transform the AFV model,

- $\tau = T - t$, and
- $x = \ln\left(\frac{S}{S_{\text{int}}}\right)$,

where S_{int} is the stock price at the initial time $t = 0$. The terminal-boundary value problem is transformed into the initial-boundary value problem.

5.1.3.1 AFV model

Equations (5.1.19)–(5.1.21) are transformed in the same manner:

$$\frac{\partial U}{\partial \tau} = \frac{\sigma^2}{2}\frac{\partial^2 U}{\partial x^2} + (r + p\eta - \frac{\sigma^2}{2})\frac{\partial U}{\partial x} - (r+p)U + p\max(kS_{int}e^x(1-\eta), RB), \tag{5.1.35}$$

$$\frac{\partial B}{\partial \tau} = \frac{\sigma^2}{2}\frac{\partial^2 B}{\partial x^2} + (r + p\eta - \frac{\sigma^2}{2})\frac{\partial B}{\partial x} - (r+p)B + RpB, \tag{5.1.36}$$

$$\frac{\partial C}{\partial \tau} = \frac{\sigma^2}{2}\frac{\partial^2 C}{\partial x^2} + (r + p\eta - \frac{\sigma^2}{2})\frac{\partial C}{\partial x} - (r+p)C + p\max(kS_{int}e^x(1-\eta) - RB, 0), \tag{5.1.37}$$

with $(\tau, x) \in (0, T) \times (-\infty, \infty)$. The equity component PDE can be written as:

$$\frac{\partial C}{\partial \tau} = \frac{\sigma^2}{2}\frac{\partial^2 C}{\partial x^2} + (r + p\eta - \frac{\sigma^2}{2})\frac{\partial C}{\partial x} - (r+p)C + p\gamma, \tag{5.1.38}$$

where,

$$\gamma = \begin{cases} 0, & \text{if } kS_{\text{int}}e^x(1-\eta) - RB < 0, \\ kS_{\text{int}}e^x(1-\eta) - RB, & \text{otherwise.} \end{cases}$$

The initial conditions transformed from terminal conditions:

$$\begin{cases} U(x,0) = F + K, & \text{if} \quad F + K \geq kS_{\text{int}}e^x, \\ U(x,0) = kS_{\text{int}}e^x, & \text{otherwise}, \end{cases}, \tag{5.1.39}$$

$$B(x,0) = F + K, \tag{5.1.40}$$

and

$$\begin{cases} C(x,0) = kS_{\text{int}}e^x - F - K, & \text{if} \quad kS_{\text{int}}e^x - F - K \geq 0, \\ C(x,0) = 0, & \text{otherwise}. \end{cases} \tag{5.1.41}$$

The three constraints are transformed into the following:

1. Value of the convertible bond (5.1.19), subject to following constraints:

$$U(x,\tau) \geq \max(B_p, kS_{\text{int}}e^x), \tag{5.1.42}$$

$$U(x,\tau) \leq \max(B_c, kS_{\text{int}}e^x). \tag{5.1.43}$$

2. Value of the bond component (5.1.20), subject to following constraints:

$$B(x,\tau) \leq B_c, \tag{5.1.44}$$

$$B(x,\tau) + C(x,\tau) \geq B_p. \tag{5.1.45}$$

3. Value of the equity component (5.1.21), subject to following constraints:

$$B(x,\tau) + C(x,\tau) \leq \max(B_c, kS_{\text{int}}e^x), \tag{5.1.46}$$

$$B(x,\tau) + C(x,\tau) \geq kS_{\text{int}}e^x. \tag{5.1.47}$$

with

$$B_{p,c}(\tau) = B_{p,c}^{cl} + K_i \frac{\tau - \tau_{i-1}}{\tau_i - \tau_{i-1}}. \tag{5.1.48}$$

For the boundary conditions, we note here that x is not defined at $S = 0$. As we set S as close as possible to 0 in the actual numerical computation, we can assume that (5.1.49) also holds at the proximity of $S = 0$, which corresponds to $x_{\min} \to -\infty$ in the x-space. Using the change of variables, the boundary conditions at $x_{\min}$ reads

$$\begin{cases} \dfrac{\partial U(x_{\min},\tau)}{\partial t} = -(r+p)U(x_{\min},\tau) + RpB(x_{\min},\tau), \\ \dfrac{\partial B(x_{\min},\tau)}{\partial t} = -(r+(1-R)p)B(x_{\min},\tau), \\ \dfrac{\partial C(x_{\min},\tau)}{\partial t} = -(r+p)C(x_{\min},\tau), \end{cases} \tag{5.1.49}$$

Transformation of the boundary conditions at $S \to +\infty$ is straightforward:

$$\begin{cases} U(x_{\max}, \tau) = kS_{int}e^{x_{\max}}, \\ B(x_{\max}, \tau) = 0, \\ C(x_{\max}, \tau) = kS_{int}e^{x_{\max}}, \end{cases} \tag{5.1.50}$$

specified at $x = x_{\max} \to \infty$.

To construct the penalty PDEs for the convertible bond valuation, one can use reformulate the inequality constraints Forsyth and Vetzal (2002) into:

$$U(x,\tau) \geq \max(B_p, kS_{\text{int}}e^x) \;\Rightarrow\; \Pi_p := U_p^\star - U(x,\tau) \leq 0.$$

where $U_p^\star = \max(B_p, kS_{\text{int}}e^x)$. With $\Pi_c := U(x,\tau) - U_c^\star \leq 0$, where $U_c^\star = \max(B_c, kS_{\text{int}}e^x)$, the penalty PDEs for the bond valuation:

$$\begin{aligned} \frac{\partial U}{\partial \tau} &= \frac{\sigma^2}{2}\frac{\partial^2 U}{\partial x^2} + (r + p\eta - \frac{\sigma^2}{2})\frac{\partial U}{\partial x} - (r+p)U + p\max(kS_{int}exp(x)(1-\eta), RB) \\ &+ \rho\max(U - U_c^\star, 0) + \rho\max(U_p^\star - U, 0) \\ &= \frac{\sigma^2}{2}\frac{\partial^2 U}{\partial x^2} + (r + p\eta - \frac{\sigma^2}{2})\frac{\partial U}{\partial x} - (r+p)U + p\delta + \rho\alpha_c\Pi_c + \rho\alpha_p\Pi_p, \end{aligned} \tag{5.1.51}$$

where $\rho > 0$ is the penalty parameter and

$$\delta = \begin{cases} RB, & \text{if } RB > kS_{\text{int}}e^x(1-\eta), \\ kS_{\text{int}}e^x(1-\eta), & \text{otherwise,} \end{cases} \quad \alpha_c = \begin{cases} 1, & \text{if } U - U_c^\star \geq 0, \\ 0, & \text{otherwise,} \end{cases} \quad \alpha_p = \begin{cases} 1, & \text{if } U_p^\star - U \geq 0, \\ 0, & \text{otherwise.} \end{cases}$$

Note that this penalty PDE is not defined in the entire time domain $[0, T]$. Instead, the penalty term is only active when the right to call or put is active.

5.2 Isogeometric analysis

In this section, the weak formulation for the AFV model is described in detail to construct the system of algebraic differential equations. We shall refer the reader to the basic knowledge about the spaces and basis function details in section 2.3. Detailed information about the class of functions and spaces are presented there, moreover, integration details of IGA approach can be found as well.

5.2.1 Weak formulation for AFV model

For spatial discretization, the collection of trial solution

$$U(x,\tau), B(x,\tau), C(x,\tau) \in \mathcal{S} = \left\{ f \,|\, f \in \mathcal{H}^1(\Omega), f\big|_{\Gamma_D} = g \right\}$$

and weighting functions are defined as

$$w, q, z \in \mathcal{V} = \left\{ \hat{f} \,\middle|\, \hat{f} \in \mathcal{H}^1(\Omega), \hat{f}\Big|_{\Gamma_D} = 0 \right\}.$$

The weak formulation:

$$\int_\Omega w\frac{\partial U}{\partial \tau}dx = \frac{\sigma^2}{2}\int_\Omega w\frac{\partial^2 U}{\partial x^2}dx + \left(r + p\eta - \frac{\sigma^2}{2}\right)\int_\Omega w\frac{\partial U}{\partial x}dx - (r+p)\int_\Omega wUdx + p\int_\Omega w\delta dx$$
$$+ \rho\int_\Omega \alpha_c w\Pi_c dx + \rho\int_\Omega \alpha_p w\Pi_p dx,$$
$$\int_\Omega z\frac{\partial B}{\partial \tau}dx = \frac{\sigma^2}{2}\int_\Omega z\frac{\partial^2 B}{\partial x^2}dx + \left(r + p\eta - \frac{\sigma^2}{2}\right)\int_\Omega z\frac{\partial B}{\partial x}dx - (r+p)\int_\Omega zBdx + Rp\int_\Omega zBdx,$$
$$\int_\Omega q\frac{\partial C}{\partial \tau}dx = \frac{\sigma^2}{2}\int_\Omega q\frac{\partial^2 C}{\partial x^2}dx + \left(r + p\eta - \frac{\sigma^2}{2}\right)\int_\Omega q\frac{\partial C}{\partial x}dx - (r+p)\int_\Omega qCdx + p\int_\Omega q\gamma dx,$$

weak formulation after integration by parts can be written as:

$$\frac{\partial}{\partial \tau}\int_\Omega wUdx = -\frac{\sigma^2}{2}\int_\Omega \frac{\partial w}{\partial x}\frac{\partial U}{\partial x}dx - \left(r + p\eta - \frac{\sigma^2}{2}\right)\int_\Omega \frac{\partial w}{\partial x}Udx - (r+p)\int_\Omega wUdx + p\int_\Omega w\delta dx$$
$$+ \rho\int_\Omega \alpha_c w\Pi_c dx + \rho\int_\Omega \alpha_p w\Pi_p dx,$$
$$\frac{\partial}{\partial \tau}\int_\Omega zBdx = -\frac{\sigma^2}{2}\int_\Omega \frac{\partial z}{\partial x}\frac{\partial B}{\partial x}dx - \left(r + p\eta - \frac{\sigma^2}{2}\right)\int_\Omega \frac{\partial z}{\partial x}Bdx - (r+p)\int_\Omega zBdx + Rp\int_\Omega zBdx,$$
$$\frac{\partial}{\partial \tau}\int_\Omega qCdx = -\frac{\sigma^2}{2}\int_\Omega \frac{\partial q}{\partial x}\frac{\partial C}{\partial x}dx - \left(r + p\eta - \frac{\sigma^2}{2}\right)\int_\Omega \frac{\partial q}{\partial x}Cdx - (r+p)\int_\Omega qCdx + p\int_\Omega q\gamma dx.$$

Consider now the finite dimensional subspace $S_0^h \subset \mathcal{H}_0^1$, spanned by the basis $\{R_1, R_2, \ldots, R_n\}$. The IGA NURBS-based finite-element approximation to the solution U is the function

$$U_h = \sum_{i=1}^{n} u_i R_i + \sum_{i\in\mathcal{I}_\partial} u_i R_i, \quad u_i \in \mathbb{R},$$

where $R_{i\in\mathcal{I}_\partial}$ are additional functions needed to interpolate the given solutions at the boundaries. A similar form of approximation to V and C can be devised, namely

$$B_h = \sum_{i=1}^{n} v_i R_i + \sum_{i\in\mathcal{I}_\partial} v_i R_i, \quad v_i \in \mathbb{R}.$$

$$C_h = \sum_{i=1}^{n} c_i R_i + \sum_{i\in\mathcal{I}_\partial} c_i R_i, \quad c_i \in \mathbb{R}.$$

The use of the above approximations results in the weak formulation in the finite-dimensional space:

$$\begin{aligned}\frac{\partial}{\partial\tau}\left(\sum_{i=1}^{n}u_i\int\limits_{\Omega}wR_i+\sum_{i\in\mathcal{I}_\partial}u_i\int\limits_{\Omega}wR_i\right)&=-\frac{\sigma^2}{2}\left(\sum_{i=1}^{n}u_i\int\limits_{\Omega}\frac{\partial w}{\partial x}\frac{\partial R_i}{\partial x}+\sum_{i\in\mathcal{I}_\partial}u_i\int\limits_{\Omega}\frac{\partial w}{\partial x}\frac{\partial R_i}{\partial x}\right)\\&\quad-\left(r+p\eta-\frac{\sigma^2}{2}\right)\left(\sum_{i=1}^{n}u_i\int\limits_{\Omega}\frac{\partial w}{\partial x}R_i+\sum_{i\in\mathcal{I}_\partial}^{n}u_i\int\limits_{\Omega}\frac{\partial w}{\partial x}R_i\right)\\&\quad-(r+p)\left(\sum_{i=1}^{n}u_i\int\limits_{\Omega}wR_i+\sum_{i\in\mathcal{I}_\partial}u_i\int\limits_{\Omega}wR_i\right)\\&\quad+p\left(\sum_{i=1}^{n}\delta_i\int\limits_{\Omega}wR_i+\sum_{i\in\mathcal{I}_\partial}\delta_i\int\limits_{\Omega}wR_i\right)-\mathcal{P}_c\pm\mathcal{P}_p,\end{aligned}\tag{5.2.1}$$

where $\mathcal{P}_c=\rho\int\limits_{\Omega}\alpha_c w\left(U-U_c^\star\right)dx$ and $\mathcal{P}_p=\rho\int\limits_{\Omega}\alpha_p w\left(U_p^\star-U\right)dx$.

$$\begin{aligned}\frac{\partial}{\partial\tau}\left(\sum_{i=1}^{n}v_i\int\limits_{\Omega}zR_i+\sum_{i\in\mathcal{I}_\partial}v_i\int\limits_{\Omega}zR_i\right)&=-\frac{\sigma^2}{2}\left(\sum_{i=1}^{n}v_i\int\limits_{\Omega}\frac{\partial z}{\partial x}\frac{\partial R_i}{\partial x}+\sum_{i\in\mathcal{I}_\partial}v_i\int\limits_{\Omega}\frac{\partial z}{\partial x}\frac{\partial R_i}{\partial x}\right)\\&\quad-\left(r+p\eta-\frac{\sigma^2}{2}\right)\left(\sum_{i=1}^{n}v_i\int\limits_{\Omega}\frac{\partial z}{\partial x}R_i+\sum_{i\in\mathcal{I}_\partial}^{n}v_i\int\limits_{\Omega}\frac{\partial z}{\partial x}R_i\right)\\&\quad-(r+p)\left(\sum_{i=1}^{n}v_i\int\limits_{\Omega}zR_i+\sum_{i\in\mathcal{I}_\partial}v_i\int\limits_{\Omega}zR_i\right)\\&\quad+Rp\left(\sum_{i=1}^{n}v_i\int\limits_{\Omega}zR_i+\sum_{i\in\mathcal{I}_\partial}v_i\int\limits_{\Omega}zR_i\right),\end{aligned}\tag{5.2.2}$$

and

$$\frac{\partial}{\partial\tau}\left(\sum_{i=1}^{n} c_i \int_\Omega qR_i + \sum_{i\in\mathcal{I}_\partial} c_i \int_\Omega qR_i\right) = -\frac{\sigma^2}{2}\left(\sum_{i=1}^{n} c_i \int_\Omega \frac{\partial q}{\partial x}\frac{\partial R_i}{\partial x} + \sum_{i\in\mathcal{I}_\partial} c_i \int_\Omega \frac{\partial q}{\partial x}\frac{\partial R_i}{\partial x}\right)$$
$$-\left(r + p\eta - \frac{\sigma^2}{2}\right)\left(\sum_{i=1}^{n} c_i \int_\Omega \frac{\partial q}{\partial x}R_i + \sum_{i\in\mathcal{I}_\partial}^{n} c_i \int_\Omega \frac{\partial q}{\partial x}R_i\right)$$
$$-(r+p)\left(\sum_{i=1}^{n} c_i \int_\Omega qR_i + \sum_{i\in\mathcal{I}_\partial} c_i \int_\Omega qR_i\right)$$
$$+p\left(\sum_{i=1}^{n} \gamma_i \int_\Omega qR_i + \sum_{i\in\mathcal{I}_\partial} \gamma_i \int_\Omega qR_i\right). \tag{5.2.3}$$

In the Galerkin method Cottrell et al. (2009), the test functions w,z, and q are chosen to coincide with the basis function R_i. Imposing this condition for $w, z, q = R_j$, $j = 1, \ldots, n$ results in the system of equations

$$\frac{\partial}{\partial\tau}\left(\sum_{i=1}^{n} u_i \int_\Omega R_jR_i + \sum_{i\in\mathcal{I}_\partial} u_i \int_\Omega R_jR_i\right) = -\frac{\sigma^2}{2}\left(\sum_{i=1}^{n} u_i \int_\Omega \frac{\partial R_j}{\partial x}\frac{\partial R_i}{\partial x} + \sum_{i\in\mathcal{I}_\partial} u_i \int_\Omega \frac{\partial R_j}{\partial x}\frac{\partial R_i}{\partial x}\right)$$
$$-\left(r + p\eta - \frac{\sigma^2}{2}\right)\left(\sum_{i=1}^{n} u_i \int_\Omega \frac{\partial R_j}{\partial x}R_i + \sum_{i\in\mathcal{I}_\partial}^{n} u_i \int_\Omega \frac{\partial R_j}{\partial x}R_i\right)$$
$$-(r+p)\left(\sum_{i=1}^{n} u_i \int_\Omega R_jR_i + \sum_{i\in\mathcal{I}_\partial} u_i \int_\Omega wR_i\right)$$
$$+p\left(\sum_{i=1}^{n} \delta_i \int_\Omega R_jR_i + \sum_{i\in\mathcal{I}_\partial} \delta_i \int_\Omega R_jR_i\right) - \mathcal{P}_{c,j} \pm \mathcal{P}_{p,j}, \tag{5.2.4}$$

$$\frac{\partial}{\partial\tau}\left(\sum_{i=1}^{n} v_i \int_{\Omega} R_j R_i + \sum_{i\in\mathcal{I}_\partial} v_i \int_{\Omega} R_j R_i\right) = -\frac{\sigma^2}{2}\left(\sum_{i=1}^{n} v_i \int_{\Omega} \frac{\partial R_j}{\partial x}\frac{\partial R_i}{\partial x} + \sum_{i\in\mathcal{I}_\partial} v_i \int_{\Omega} \frac{\partial R_j}{\partial x}\frac{\partial R_i}{\partial x}\right)$$
$$-\left(r + p\eta - \frac{\sigma^2}{2}\right)\left(\sum_{i=1}^{n} v_i \int_{\Omega} \frac{\partial R_j}{\partial x} R_i + \sum_{i\in\mathcal{I}_\partial}^{n} v_i \int_{\Omega} \frac{\partial R_j}{\partial x} R_i\right)$$
$$-(r+p)\left(\sum_{i=1}^{n} v_i \int_{\Omega} R_j R_i + \sum_{i\in\mathcal{I}_\partial} v_i \int_{\Omega} R_j R_i\right)$$
$$+Rp\left(\sum_{i=1}^{n} v_i \int_{\Omega} R_j R_i + \sum_{i\in\mathcal{I}_\partial} v_i \int_{\Omega} R_j R_i\right) \tag{5.2.5}$$

and

$$\frac{\partial}{\partial\tau}\left(\sum_{i=1}^{n} c_i \int_{\Omega} R_j R_i + \sum_{i\in\mathcal{I}_\partial} c_i \int_{\Omega} R_j R_i\right) = -\frac{\sigma^2}{2}\left(\sum_{i=1}^{n} c_i \int_{\Omega} \frac{\partial R_j}{\partial x}\frac{\partial R_i}{\partial x} + \sum_{i\in\mathcal{I}_\partial} c_i \int_{\Omega} \frac{\partial R_j}{\partial x}\frac{\partial R_i}{\partial x}\right)$$
$$-\left(r + p\eta - \frac{\sigma^2}{2}\right)\left(\sum_{i=1}^{n} c_i \int_{\Omega} \frac{\partial R_j}{\partial x} R_i + \sum_{i\in\mathcal{I}_\partial}^{n} c_i \int_{\Omega} \frac{\partial R_j}{\partial x} R_i\right)$$
$$-(r+p)\left(\sum_{i=1}^{n} c_i \int_{\Omega} R_j R_i + \sum_{i\in\mathcal{I}_\partial} c_i \int_{\Omega} R_j R_i\right)$$
$$+p\left(\sum_{i=1}^{n} \gamma_i \int_{\Omega} R_j R_i + \sum_{i\in\mathcal{I}_\partial} \gamma_i \int_{\Omega} R_j R_i\right) \tag{5.2.6}$$

Since the complexity of the NURBS functions entails the inevitable recourse to numerical integration. The actual integration of the element matrices is carried by Gauss-Legendre quadrature rule Cottrell et al. (2009). To increase the accuracy of the element matrices, one could increase the Gaussian points n_{gp}, but as it was tested for a linear European call option, a large number of Gaussian n_{gp} are not necessary for accuracy for integration. The standard number of quadrature points is chosen to be $n_{gp} = p + 1$.

5.2.2 Treatment of nonlinear term by *group* FEM

One can proceed by addressing the pair of nonlinear penalty terms found in equation (5.1.51) using the *group* finite element technique as described in the work of Fletcher (1983) to handle the nonlinearity. In this discussion, we will focus on outlining the

construction process for $\mathcal{P}_{call,j}$; the procedure for constructing the finite element approximation for $\mathcal{P}_{put,j}$ is identical. For "max" terms in (5.1.19) and (5.1.21), δ and γ, numerical approximations were obtained by means of *group* finite element as in the below-mentioned way.

Assume that the term $\zeta_{call} := \alpha_{call}(U - U^{\star}_{call})$ is approximated by

$$\zeta_{call} = \sum_{i=1}^{n} \zeta_i \psi_i + \sum_{\mathcal{I}_\partial} \zeta_i \psi_i,$$

where $\zeta_{call,i} = \alpha_{call}(x_i)(U(x_i) - U^{\star}_{call}(x_i)) =: \alpha_{call,i}(u_i - u^{\star}_{call,i})$. Therefore, for $w = R_j$, $j = 1, \ldots, n$, we have

$$\begin{aligned}\mathcal{P}_{call,j} &= \rho \int_{\Omega} R_j \left(\sum_{i=1}^{n} \zeta_i R_i + \sum_{\mathcal{I}_\partial} \zeta_i R_i \right) dx = \rho \left(\sum_{i=1}^{n} \zeta_i \int_{\Omega} R_j R_i dx + \sum_{\mathcal{I}_\partial} \zeta_i \int_{\Omega} R_j R_i dx \right) \\ &= \rho \left(\sum_{i=1}^{n} \alpha_{call,i}(u_i - u^{\star}_{call,i}) \int_{\Omega} R_j R_i dx + \sum_{\mathcal{I}_\partial} \alpha_{call,i}(u_i - u^{\star}_{call,i}) \int_{\Omega} R_j R_i dx \right).\end{aligned} \tag{5.2.7}$$

Integrals above generate the following element matrices: M_j, K_j, and N_j.

5.3 Time integration scheme

The system of differential-algebraic equations can now be written utilizing global element matrices and boundary contributions:

$$\begin{aligned}\frac{\partial}{\partial \tau}(Mu + \hat{b}_{M,u}) = &-\frac{\sigma^2}{2} Ku - \left(r + p\eta - \frac{\sigma^2}{2} \right) Nu - (r+p)Mu + pM\delta - \boldsymbol{\beta}_1(u, v) \\ &+ \rho M P_{put}(u^{\star}_{put} - u) + \rho M P_{call}(u - u^{\star}_{call}) + \rho b_{put} + \rho b_{call} := F_1(u, v),\end{aligned} \tag{5.3.1}$$

$$\frac{\partial}{\partial \tau}(Mv + \hat{b}_{M,v}) = -\frac{\sigma^2}{2} Kv - \left(r + p\eta - \frac{\sigma^2}{2} \right) Nv - (r+p)Mv + RpMv - \boldsymbol{\beta}_2(v) := F_2(v), \tag{5.3.2}$$

$$\frac{\partial}{\partial \tau}(Mc + \hat{b}_{M,c}) = -\frac{\sigma^2}{2} Kc - \left(r + p\eta - \frac{\sigma^2}{2} \right) Nc - (r+p)Mc + pM\gamma - \boldsymbol{\beta}_3(v, c) := F_2(v, c), \tag{5.3.3}$$

where $P_{put} = \text{diag}(\alpha_{put,j})$, $P_{call} = \text{diag}(\alpha_{call,j})$, and

$$\boldsymbol{\beta_1}(u,v) = \frac{\sigma^2}{2} b_{K,u} + \left(r + p\eta - \frac{\sigma^2}{2} \right) \boldsymbol{b}_{N,u} + (r+p) b_{M,u} - p b_{M,\delta}, \tag{5.3.4}$$

$$\boldsymbol{\beta}_2(v) = \frac{\sigma^2}{2} b_{K,v} + \left(r + p\eta - \frac{\sigma^2}{2} \right) b_{N,v} + (r+p) b_{M,v} - Rp b_{M,v}, \tag{5.3.5}$$

$$\boldsymbol{\beta}_2(v,c) = \frac{\sigma^2}{2} b_{K,c} + \left(r + p\eta - \frac{\sigma^2}{2} \right) b_{N,c} + (r+p) b_{M,c} - p b_{M,\gamma}, \tag{5.3.6}$$

are the boundary condition vectors.

Time integration of the DAEs (5.3.1), (5.3.2) and (5.3.3) is carried out by applying the θ-scheme on both equations, which results in the systems, with $\theta \in [0,1]$, $\Delta\tau = T/n_\tau$, and n_τ the number of time steps,

$$\begin{aligned}
M u^{m+1} + \hat{b}_{M,u}^{m+1} - M u^m - \hat{b}_{M,u}^m &= \theta \Delta\tau F_1(u^{m+1}, v^{m+1}) + (1-\theta)\Delta\tau F_1(u^m, v^m), \\
M v^{m+1} + \hat{b}_{M,v}^{m+1} - M v^m - \hat{b}_{M,v}^m &= \theta \Delta\tau F_2(v^{m+1}) + (1-\theta)\Delta\tau F_2(v^m), \\
M c^{m+1} + \hat{b}_{M,c}^{m+1} - M c^m - \hat{b}_{M,c}^m &= \theta \Delta\tau F_3(v^{m+1}, c^{m+1}) + (1-\theta)\Delta\tau F_2(v^m, c^m),
\end{aligned}$$

or

$$\begin{aligned}
A_{11} u^{m+1} &- \rho\theta\Delta\tau M \left(P_{put}^{m+1}(u_{put}^{\star,m+1} - u^{m+1}) + P_{call}^{m+1}(u^{m+1} - u_{call}^{\star,m+1}) \right) \\
&= \widetilde{A}_{11} u^m - \theta\Delta\tau p M \delta^{m+1} - (1-\theta)\Delta\tau p M \delta^m \\
&\quad + \rho(1-\theta)\Delta\tau M \left(P_{put}^m (u_{put}^{\star,m} - u^m) + P_{call}^m (u^m - u_{call}^{\star,m}) \right) \\
&\quad + \theta\Delta\tau \boldsymbol{\beta}_1^{m+1} + (1-\theta)\Delta\tau \boldsymbol{\beta}_1^m + \hat{b}_{M,u}^m - \hat{b}_{M,u}^{m+1} + \theta\rho\Delta\tau (b_{put}^{m+1} + b_{call}^{m+1}) \\
&\quad + (1-\theta)\rho\Delta\tau (b_{put}^m + b_{call}^m),
\end{aligned} \tag{5.3.7}$$

$$A_{22} v^{m+1} = \widetilde{A}_{22} v^m + \theta\Delta\tau \boldsymbol{\beta}_2^{m+1} + (1-\theta)\Delta\tau \boldsymbol{\beta}_2^m + \hat{b}_{M,v}^m - \hat{b}_{M,v}^{m+1}, \tag{5.3.8}$$

$$\begin{aligned}
A_{33} c^{m+1} &= \widetilde{A}_{33} v^m - \theta\Delta\tau p M \gamma^{m+1} - (1-\theta)\Delta\tau p M \gamma^m + \theta\Delta\tau \boldsymbol{\beta}_3^{m+1} \\
&\quad + (1-\theta)\Delta\tau \boldsymbol{\beta}_3^m + \hat{b}_{M,c}^m - \hat{b}_{M,c}^{m+1},
\end{aligned} \tag{5.3.9}$$

where

$$
\begin{aligned}
A_{11} &= M + \theta\Delta\tau\left(\frac{\sigma^2}{2}K + \left(r + p\eta - \frac{\sigma^2}{2}\right)N + (r+p)M\right),\\
A_{22} &= M + \theta\Delta\tau\left(\frac{\sigma^2}{2}K + \left(r + p\eta - \frac{\sigma^2}{2}\right)N + (r+p)M + RpM\right)\\
A_{33} &= M + \theta\Delta\tau\left(\frac{\sigma^2}{2}K + \left(r + p\eta - \frac{\sigma^2}{2}\right)N + (r+p)M\right)\\
\widetilde{A}_{11} &= M - (1-\theta)\Delta\tau\left(\frac{\sigma^2}{2}K + \left(r + p\eta - \frac{\sigma^2}{2}\right)N + (r+p)M\right),\\
\widetilde{A}_{22} &= M - (1-\theta)\Delta\tau\left(\frac{\sigma^2}{2}K + \left(r + p\eta - \frac{\sigma^2}{2}\right)N + (r+p)M + RpM\right),\\
\widetilde{A}_{33} &= M + \theta\Delta\tau\left(\frac{\sigma^2}{2}K + \left(r + p\eta - \frac{\sigma^2}{2}\right)N + (r+p)M\right).
\end{aligned}
$$

Let the solutions u^m,v^m and c^m be known. The solutions at the next time level $m+1$ will be computed by solving (5.3.8) for v^{m+1}. Then c^{m+1} can be computed using v^{m+1} solving (5.3.9), however, by imposing the constraints. The solution u^{m+1} is then computed via (5.3.7) using the known u^m, v^m, and v^{m+1}. This procedure, however, requires knowledge of the solutions at the boundaries at the time level $m+1$.

5.3.1 Boundary solutions

At $x_{\min}$, with $u_0(\tau) := U(x_{\min},\tau)$, $v_0(\tau) := V(x_{\min},\tau)$, and $c_0(\tau) := C(x_{\min},\tau)$ etc, the boundary conditions can be written as follows:

$$
\begin{cases}
\dfrac{\partial u_0(\tau)}{\partial\tau} = -(r+p)u_0(\tau)pRv_0(\tau),\\
\dfrac{\partial v_0(\tau)}{\partial t} = -(r+(1-R)p)v_0(\tau),\\
\dfrac{\partial c_0(\tau)}{\partial t} = -(r+p)c_0(\tau).
\end{cases}
\tag{5.3.10}
$$

Application of the θ-scheme on (5.3.10) leads to the discrete equations:

$$
u_0^{m+1} + \theta\Delta\tau\left((r+p)u_0^{m+1} + Rpv_0^{m+1}\right) = u_0^m - (1-\theta)\Delta\tau\left((r+p)u_0^m + Rpv_0^m\right), \tag{5.3.11}
$$

$$
\left[1 + \theta\Delta\tau(r+(1-R)p)\right]v_0^{m+1} = \left[1 - (1-\theta)\Delta\tau(r+(1-R)p)\right]v_0^m, \tag{5.3.12}
$$

$$
\left[1 + \theta\Delta\tau(r+p)\right]c_0^{m+1} = \left[1 - (1-\theta)\Delta\tau(r+p)\right]v_0^m. \tag{5.3.13}
$$

Let the boundary solution v_0^m be known. Then v_0^{m+1} and c_0^{m+1}can be computed from (5.3.12) and (5.3.13), respectively. With u_0^m, v_0^m, and v_0^{m+1}, the moving boundaries can be solved at each time iteration as a system of equations.

5.3.2 Interior solutions

With solutions at the boundaries available at τ^m and τ^{m+1}, all related boundary vectors in (5.3.7) and (5.3.8) are known. We are thus now in the position to compute the solutions u^{m+1}, v^{m+1} and c^{m+1}. v^{m+1} is readily computed from (5.3.8). With v^{m+1} known, c^{m+1} can be computed from (5.3.9). Then, we apply the inequality constraints of v and c. With already adjusted v^{m+1} known, (5.3.7) reduces to a nonlinear function of u^{m+1}. We assume that the penalty terms in (5.3.7) are approximated in a fully implicit way, resulting in the equation

$$0 = A_{11}u^{m+1} - \rho\Delta\tau M\left(P_{put}^{m+1}(u_{put}^{\star,m+1} - u^{m+1}) + P_{call}^{m+1}(u^{m+1} - u_{call}^{\star,m+1})\right) - \boldsymbol{\phi} := \boldsymbol{f}(u^{m+1}), \tag{5.3.14}$$

where

$$\begin{aligned}\boldsymbol{\phi} &= \widetilde{A}_{11}u^m + \widetilde{A}_{12}v^m - A_{12}v^{m+1} + \theta\Delta\tau\boldsymbol{\beta}_1^{m+1} + (1-\theta)\Delta\tau\boldsymbol{\beta}_1^m + \hat{b}_{M,u}^m - \hat{b}_{M,u}^{m+1} \\ &+ \theta\Delta\tau(b_{put}^{m+1} + b_{call}^{m+1}) - \theta\Delta\tau pM\delta^{m+1} - (1-\theta)\Delta\tau pM\delta^m. \end{aligned} \tag{5.3.15}$$

The nonlinear equation (5.3.14) is solved iteratively using Newton's method. Starting from an initial guess of the solution $u^{m+1,0}$, the solution u^{m+1} is approximated using the iterands

$$u^{m+1,k} \leftarrow u^{m+1,k-1} - \left(\nabla f(u^{m+1,k-1})\right)^{-1} f(u^{m+1,k-1}), \quad k = 1, 2, \ldots$$

where $\nabla f(u^{m+1,k-1})$ is the Jacobian of f, given by

$$\nabla f(u^{m+1,k-1}) = A_{11} + \rho\Delta\tau M\left(P_{call}^{m+1,k-1} - P_{put}^{m+1,k-1}\right). \tag{5.3.16}$$

The initial guess $u^{m+1,0}$ is chosen such that it solves unconstrained CB PDE, which is equivalent to solving (5.3.7) without penalty terms. We shall also use this unconstrained solution $u^{m+1,0}$ to constrain the initially computed v^{m+1} prior to the start of Newton's iterations. In the context of American-style derivatives, the convertible bond problem refers to the stopping criteria used to terminate iteration to conserve computational resources. As in Forsyth and Vetzal (2002), the first typical criteria is the difference of two consecutive solution vectors $\| \boldsymbol{u}^{m+1,k} - \boldsymbol{u}^{m+1,k-1} \|_\infty \leq$ inf, which serves to guarantee the termination. The importance of the second criterion

deserves attention since we are talking about gaps arising from the penalty matrices. Its equivalence (i.e $P_{call}^{m+1,k-1} = P_{call}^{m+1,k}$) is crucial to facilitate the convergence of Newton's method using the less number of iterations per time step.

The convergence and existence of the solution of Newton's method depends on the invertibility of the Jacobian matrix. The value of the only U is computed from Newton's method, therefore, the main nonlinear terms are same as in TF model. The nonsingularity, hence the convergence of Newton's method, is proved in Theorem 4.4.1.

The procedure for computing the solutions in the interior after one θ-scheme step is summarized in the following algorithm:

Algorithm 4 Computing the interior solutions

Input: input $\boldsymbol{u}^m$, $\boldsymbol{v}^m$;

compute $B_p(\tau^{m+1})$ and $B_c(\tau^{m+1})$;
compute $\boldsymbol{v}^{m+1}$ from (5.3.8), ignoring any constraints;
compute γ and solve for $^{m+1}$ (5.3.9);
apply minimum-maximum value constraints on $\boldsymbol{v}^{m+1}$ using $^{m+1}$;
for $k = 1, 2, \ldots$ until convergence **do**
    compute$\boldsymbol{f}(\boldsymbol{u}^{m+1,k-1})$ using (5.3.14);
    compute $\nabla \boldsymbol{f}(\boldsymbol{u}^{m+1,k-1})$ using (5.3.16);
    $\boldsymbol{u}^{m+1,k} \leftarrow \boldsymbol{u}^{m+1,k-1} - \left(\nabla \boldsymbol{f}(\boldsymbol{u}^{m+1,k-1})\right)^{-1} \boldsymbol{f}(\boldsymbol{u}^{m+1,k-1})$;
    if First stopping criteria OR Second stopping criteria is satisfied; **then**
        break
    end if
end for
apply constraints on $\boldsymbol{v}^{m+1}$ using $\boldsymbol{u}^{m+1,k}$;
if $\tau^{m+1} \in \mathcal{T}_{\text{coupon}}$ **then**
    $\boldsymbol{u}^{m+1} \leftarrow \boldsymbol{u}^{m+1} + \hat{K}$;
    $\boldsymbol{v}^{m+1} \leftarrow \boldsymbol{v}^{m+1} + \hat{K}$;
end if

5.4 Numerical results

AFV model is discretized by IGA-FEM in space, and a modified Crank-Nicolson scheme is used for time integration. Newton-Raphson's iterative method has been utilized to handle the non-smooth functions raised by penalty terms at each step. Numerical parameters for the convertible Bond problem are adopted from Ayache et al. (2003) to make a comparison between two different methodologies. The truncated domain for the simulation is chosen to be $x \in [-6, 2]$. In Figure 5.1, the first experiment is to check the matter of stability, as it can be seen without maintaining

a specific temporal-spatial ratio, the solution of both methods tends to be stable. The jumps are natural for discrete coupon payments Tsiveriotis (1998), which occur semiannually in the time direction. Using the same nE(number of elements) and n_τ, in Figure 5.2 and 5.3, one could easily observe the similarity between all the methods, except P2-FEM, where the number of grid points is doubled due to the specifics of assembling process and the midpoint resulted as finer mesh on surface.

Table 5.1: Modeling and computational parameters.

Parameter	**Value**
Time to maturity T	5 years
Conversion	0 to 5 years into k shares
Conversion ratio k	1.0
Face Value F	\$100
Clean call price B_c	\$110, from Year 3 to Year 5 ($t \in (2, 5]$)
Clean put price B_p	\$105, during Year 3 ($t = 3$)
Coupon payments K	\$4.0
Coupon dates	.5, 1.0, 1.5, ... ,5.0 (semiannual)
Recovery factor R	0
Hazard rate p	0.02
Partial default η	0
Total default η	1
Volatility σ	20% or 0.2
Underlying stock price at $t = 0$, S_{int}	\$100
Penalty parameter ρ	10^6
Newton-Raphson's method tolerance tol	10^{-6}

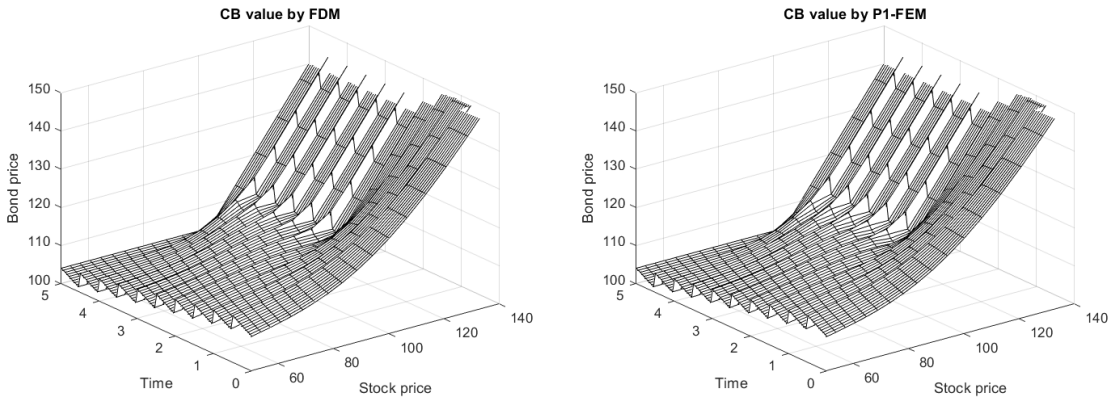

Figure 5.1: Solution of the AFV model $t = 0$, $r = 0.05$, $\sigma = 0.2$, $F = \$100$, $\rho = 10^6$. Left figure: $nE = 2^7$, $n_\tau = 100$, CB price by FDM; Right figure: $nE = 2^7$, $n_\tau = 100$, CB price by P1-FEM.

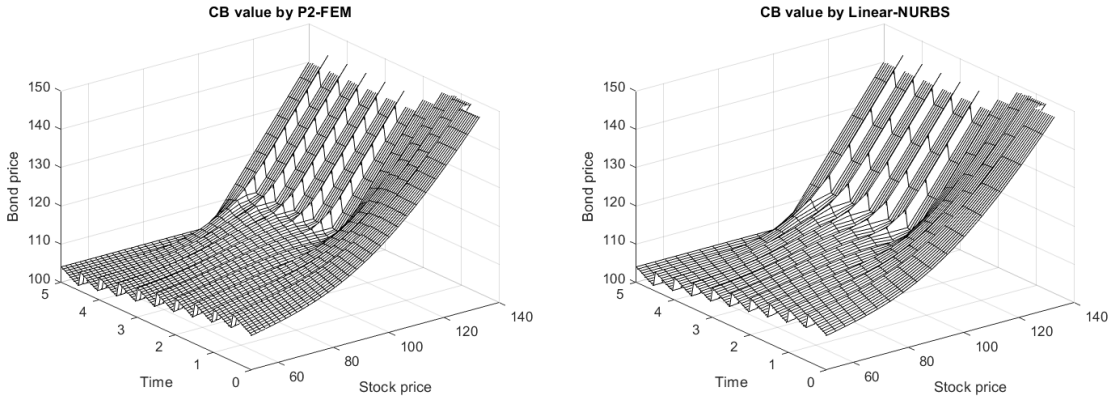

Figure 5.2: Solution of the AFV model $t = 0$, $r = 0.05$, $\sigma = 0.2$, $F = \$100$, $\rho = 10^6$. Left figure: $nE = 2^7$, $n_\tau = 100$, CB price by P2-FEM; Right figure: $nE = 2^7$, $n_\tau = 100$, CB price by Linear-NURBS.

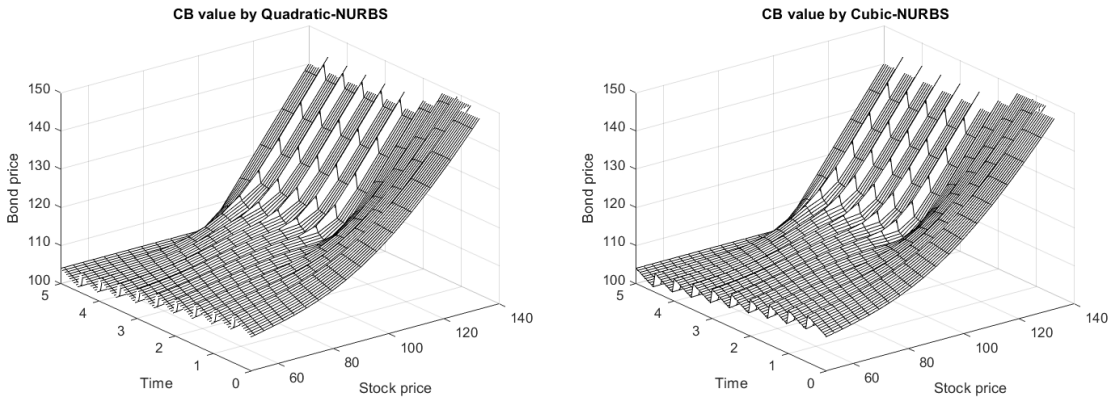

Figure 5.3: Solution of the AFV model $t = 0$, $r = 0.05$, $\sigma = 0.2$, $F = \$100$, $\rho = 10^6$. Left figure: $nE = 2^7$, $n_\tau = 100$, CB price by Quadratic-NURBS; Right figure: $nE = 2^7$, $n_\tau = 100$, CB price by Cubic-NURBS.

In Figure 5.4, the comparison between above-mentioned numerical tecnhiques are compared in the single graph, as we double the mesh size, in both experiments, instability issue is not observed. However, the comparison clearly reveals observable harmony among all the methods.

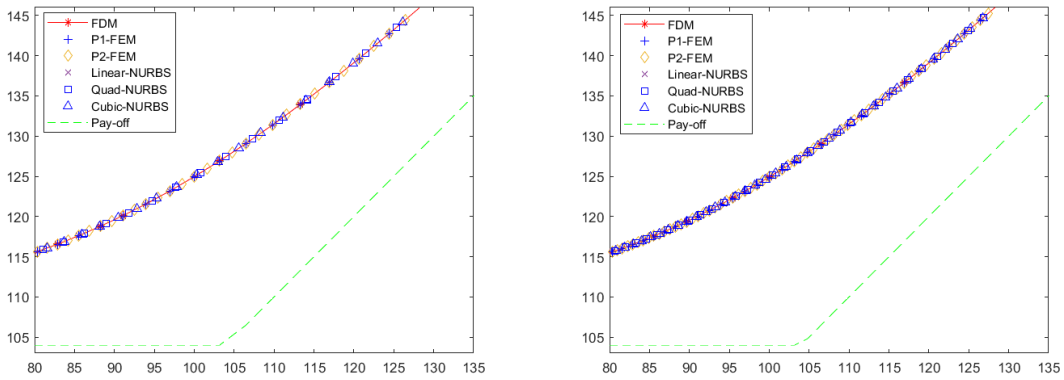

Figure 5.4: Solution of the AFV model $t = 0$, $r = 0.05$, $\sigma = 0.2$, $F = \$100$, $\rho = 10^6$. Left figure: $nE = 2^8$, $n_\tau = 200$; Right figure: $nE = 2^9$, $n_\tau = 400$.

In Table 5.2, Cubic-NURBS-based IGA-FEM is implemented to generate the price of convertible Bonds at face value $F = 100\$$. Once the refinement process started, the price evolution monotonically decreased and converged to the value 124.87\$, up to two decimal places, comparable with the results of the benchmark problem Ayache et al. (2003). However, the Peclet number $Pe = \frac{3}{2} \geq 1$ indicates the presence of convection dominance in the model and is expected to observe instabilities and spurious oscillations. Moreover, Cubic-NURBS yields consistent numerical results that

exhibit monotonic evolution, ultimately converging to values obtained by other techniques. It's worth noting that in Ayache et al. (2003), the methodology part refers to P. Forsyth's work Forsyth and Vetzal (2002), where they handled the American option problem using the Finite Volume Method (FVM) coupled with the nonlinear Van-Leer Flux Limiters and the Rannacher time-stepping approach. In contrast, our numerical experiments demonstrate that Cubic-NURBS can capture price dynamics monotonically without relying on these stabilization and smoothing techniques. We have to mention that the solutions produced by these methods exhibit a convergence to the viscosity solution using lesser DOFs compared to ours.

The fitted NURBS is now considered for the AFV model, and solutions were achieved by controlling the weights near the strike price. In reference Ayache et al. (2003), the viscosity solution for the same problem was achieved by 800 nodes and time steps by FVM, while the fitted NURBS obtained here has spent 32 elements and 100 time steps, shown in Table 5.2. In Figure 5.8, we could see that the same setting, which produced better results for linear cases, is able to deal with nonlinear problems as well by modifying the corresponding weight for each control point as it was described before. To be consistent with the reference solution, we experimentally obtain the weights that produce good matching results at each refinement. To maintain a fair comparison among other methods, the choice of time step is fixed to be 100. The corresponding choice of weights for each level is different but still produces the desired result. Consequently, varying weights at each level could be associated with the error introduced in the time dimension. To overcome this issue, the weights are needed to be adjusted. It is evident that the weights are higher for a reduced number of nodes, but the weights tend to be smaller for a higher number of nodes. As we keep the time step unchanged for an increasing number of nodes, the weights are affected by making the control points less engaged. These results highlight the efficiency of the proposed framework and its potential to deal with diverse types of problems.

Table 5.2: Convertible bond price based on the AFV model at $t = 0$ ans $S = 100$, computed using cubic NURBS. The numerical parameters are given in Table 5.1

					Unweighted NURBS		Weighted NURBS
nE	n_τ	FDM	P1-FEM	P2-FEM	Uniform	Nonuniform	$\omega_{non-optimal}$
2^6	50	125.1718	125.0198	124.6675	125.5205	125.2426	125.1409
2^7	100	125.0613	125.0557	125.0045	125.1139	125.0675	124.9433
2^8	200	124.9504	124.9210	124.9485	124.9676	124.9579	124.8542
2^9	400	124.9123	124.9000	124.9094	124.9154	124.9115	124.8120
2^{10}	800	124.8914	124.8867	124.8893	124.8895	124.8898	124.7915
2^{11}	1600	124.8805	124.8786	124.8789	124.8798	124.8795	
2^{12}	3200	124.8749	124.8739	124.8745	124.8746	124.8745	

Table 5.3: Convertible bond price based on the AFV model at $t = 0$ ans $S = 100$, computed using cubic NURBS with optimal weights.

		Weighted NURBS	
nE	n_τ	Nonuniform($\omega_{adjusted}$)	Nonuniform($\omega_{optimal}$)
2^6	50	124.8777	124.8745
2^7	100	124.6833	124.8745
2^8	200	124.5956	124.8745
2^9	400	124.5541	
2^{10}	800	124.5339	

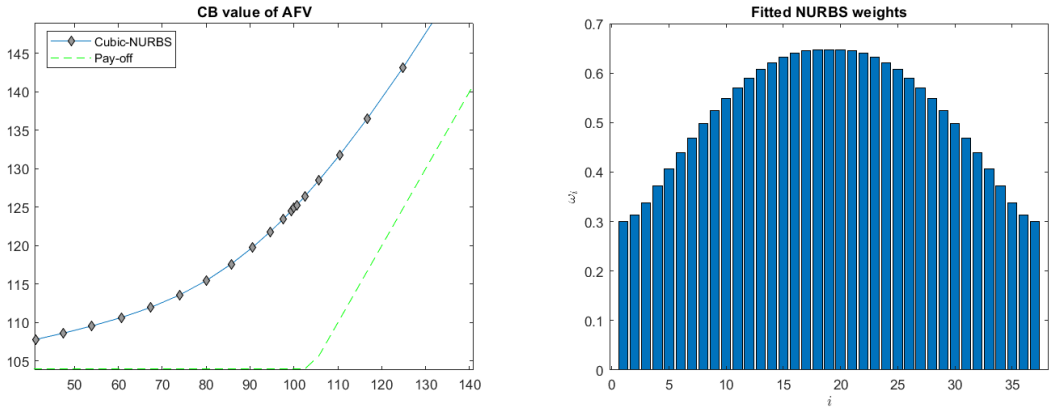

Figure 5.5: Solution of the AFV model $t = 0$, $r = 0.05$, $\sigma = 0.2$, $\hat{K} = \$100$. Left figure: Non-uniform meshing with $nE = 2^5$, $n_\tau = 100$; Right figure: NURBS weights.

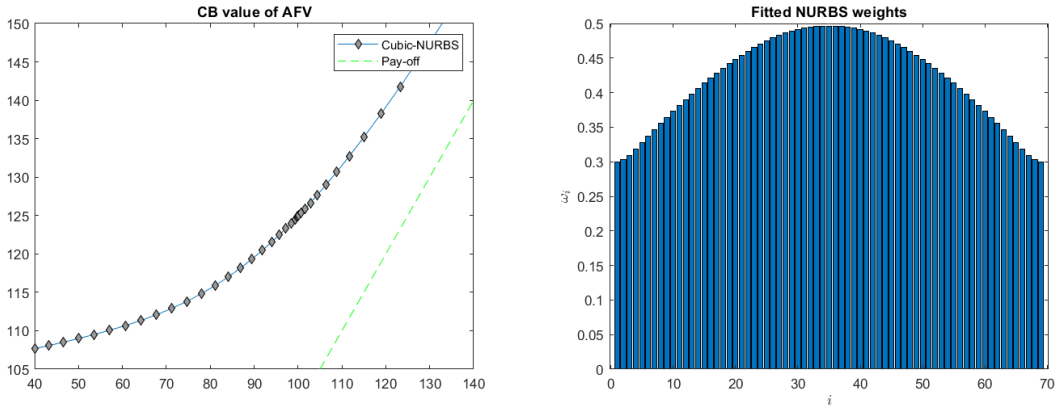

Figure 5.6: Solution of the AFV model $t = 0$, $r = 0.05$, $\sigma = 0.2$, $\hat{K} = \$100$. Left figure: Non-uniform meshing with $nE = 2^6$, $n_\tau = 100$; Right figure: NURBS weights.

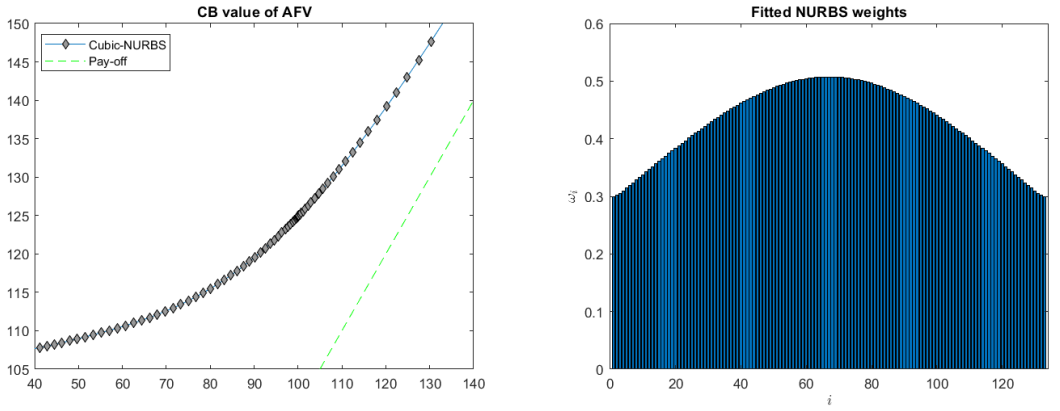

Figure 5.7: Solution of the AFV model $t = 0$, $r = 0.05$, $\sigma = 0.2$, $\hat{K} = \$100$. Left figure: Non-uniform meshing with $nE = 2^7$, $n_\tau = 100$; Right figure: NURBS weights.

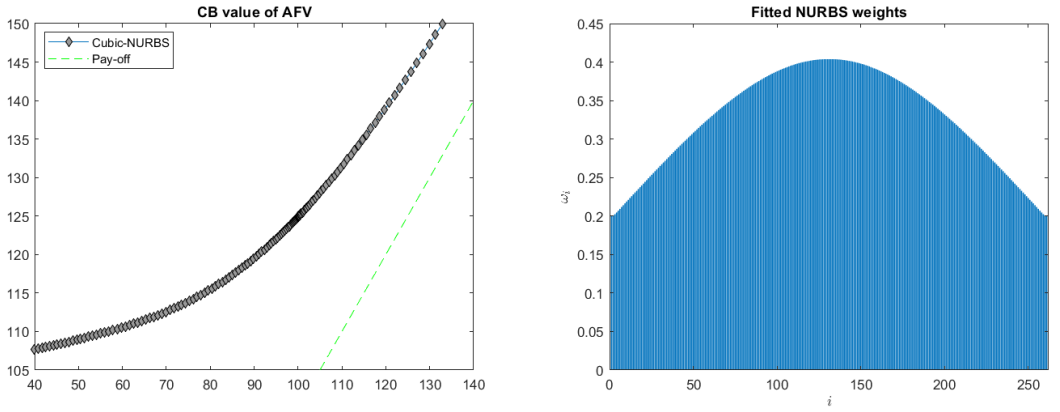

Figure 5.8: Solution of the AFV model $t = 0$, $r = 0.05$, $\sigma = 0.2$, $\hat{K} = \$100$. Left figure: Non-uniform meshing with $nE = 2^8$, $n_\tau = 100$; Right figure: NURBS weights.

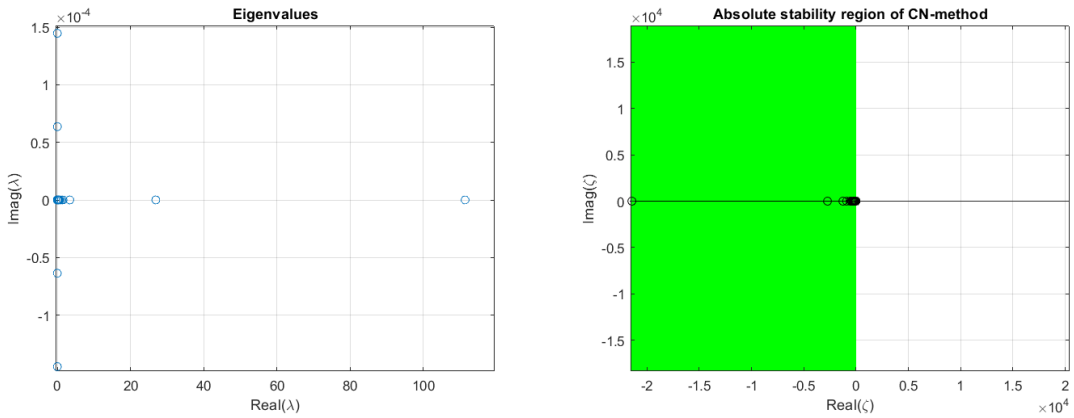

Figure 5.9: Absolute stability region of the time integration scheme for Crank-Nicolson method, when $\theta = 1/2$

5.4.1 Absolute stability region

Section 2.6 gives absolute stability region details. Based on accumulated information, one can derive the absolute stability region and check if eigenvalues meet the region's requirement. For the Crank-Nicolson time-stepping methods for the nonlinear convertible bond pricing problem under the AFV model, we have presented the eigenvalues in Figure 5.9, which are crucial for the determination of the absolute stability region. Moreover, one could see that for linear problems, there are no instability issues that can be posed based on absolute stability region for the time integrator and depicted eigenvalues that belong to the same stability range. One might observe that the eigenvalues differ from those of the linear BS cases. This might be justified by the nonlinearity introduced by penalty matrices, which are tridiagonal in nature. It is important to note that based on realistic parameters of the model, such as r, h, σ, θ, $\Delta\tau$, B_c, B_p, and ρ the eigenvalues meet the requirement of the absolute stability region, however, using an impractical set of parameters the instability may occur.

5.5 Greeks

For practitioners, the accuracy of the Greeks can lead to more precise and beneficial hedging and risk management scenarios Wilmott (1998), Higham (2004), Hull (2014). In Delta, one could observe how the contract value tends to change as the underlying asset increases. In Gamma, one could see the difference in Delta according to underlying asset movement. In Theta, it is possible to see how the contract value behaves as time approaches maturity.

A frequent problem of the Greeks, especially in nonlinear cases Forsyth and Vetzal (2002); Yousuf et al. (2012), is that the Greeks are suffering from spikes or shocks. This phenomenon creates trouble for hedging and controlling the risk in reality since the behavior of the Greeks is unreliable and can not be trusted due to spikes or shocks. Since the generated numerical solutions are weaker than exact from a mathematical and realistic point of view since it is an approximation. Consequently, one tries to value the Greeks claiming another sort of approximation using the already approximated solutions, therefore, in some nonlinear cases it is usual and expected to see instabilities in Greeks.

The most common practice for the computation of Greek alphabets is FDM. Indeed, FDM serves as fast and robust computations not only for pricing problems but also for Greeks. Since numerical results were generated by IGA-NURBS, the usage of FDM will create another source of error as the nature of the two methodologies is totally different. To remedy this, corresponding Greek values are calculated by IGA-NURBS and P2-FEM for comparison. Once the solutions are generated by IGA-NURBS, one could apply the post-processing algorithm to investigate the character of the contract value according to variable quantities. Note that the cubic-NURBS is at least twice differentiable, which suffices to deduce the second order Gamma. Initially, our IGA-NURBS approximation is given as:

$$U_h = \sum_{i=1}^{n} u_i R_i,$$

corresponding derivatives:

$$\frac{\partial U_h}{\partial x} = \sum_{i=1}^{n} u_i \frac{\partial R_i}{\partial x}$$

$$\frac{\partial^2 U_h}{\partial x^2} = \sum_{i=1}^{n} u_i \frac{\partial^2 R_i}{\partial x^2}$$

The first step is to compute the NURBS basis functions and their derivatives at Gaussian points. Secondly, we do use the above expressions to compute the corresponding first and second-order derivatives, utilizing the same *assembling process* approach as the one used for assembling the local to global element matrices.

For each particular quantity, a corresponding back-transformation shall be applied to obtain $\Delta = \dfrac{\partial U}{\partial S}$ and $\Gamma = \dfrac{\partial^2 U}{\partial S^2}$. Theta $\Theta = \dfrac{\partial U}{\partial t}$ values could be computed via FDM, however, to maintain the consistency, we retrieved its values from governing Black-Scholes PDEs for each contract, since the numerical solution, Delta and Gamma are

known at current stage. Note that the Greeks by P2-FEM are calculated using derived explicit formulas in the previous work Kazbek et al. (2024).

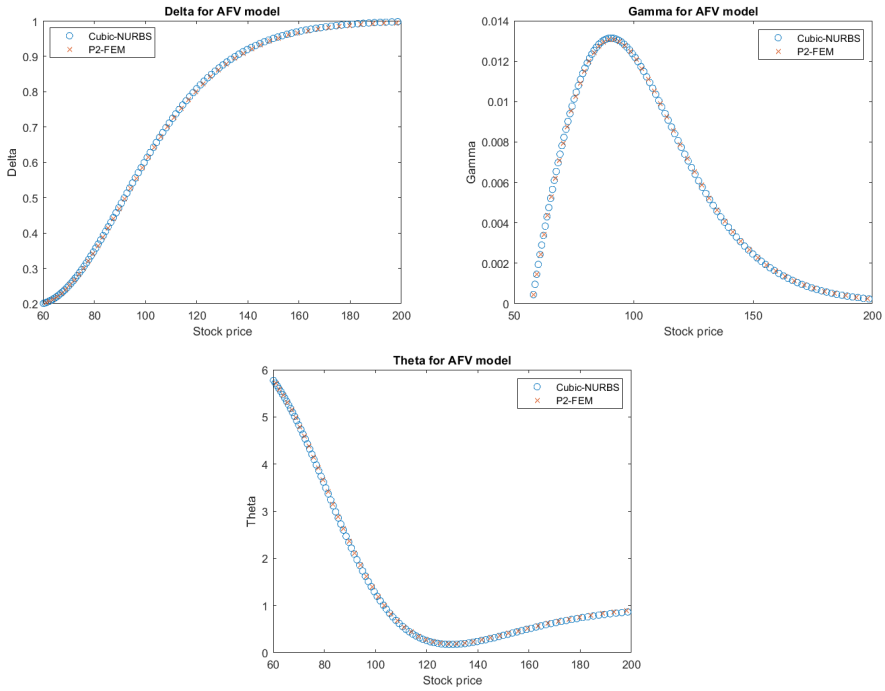

Figure 5.10: Greeks for AFV model with $t = 0$, $r = 0.05$, $\sigma = 0.2$, $F = \$100$. For NURBS: $nE = 2048$, $n_\tau = 2000$; For P2-FEM: $nE = 1000$, $d\tau = 2000$. Left figure: Delta Δ; Right figure: Gamma Γ; Middle figure: Theta Θ.

The surface of convertible bond values in Figure 5.3 is affected by discrete coupon payments and controlled by nonlinear term and inequality constraints. Therefore, the surface Greek values can not physically be smoothed since discontinuous jumps and angles can not be differentiated. Consequently, convertible Bonds in Figure 5.10 has produced smoother Greeks only at $t = 0$ but not the whole Greeks surfaces. In terms of stability, the numerical approximation tends to be more stable than the Leland model. The results of P2-FEM and Cubic-NURBS are almost identical, without any spikes or shocks.

Chapter 6

Conclusions

We have developed a framework for different types of American and European options based on FEM. The literature on PDE approaches for pricing tasks is versatile, encompassing various numerical methods that address specific nuances. FDM remains the mainstay for Black-Scholes-type problems in both industry and academic circles due to its robustness and simplicity. However, certain types of options may exhibit high non-linearity, and achieving a certain degree of accuracy and stability may not be possible with conventional FDM or FEM without serious modification of the original scheme.

This work aims to create efficient FEM-based algorithms to accurately tackle three fundamental nonlinear pricing problems encountered by financial institutions, such as European and American-style derivatives. Indeed, the methodology could be directly extended and applied to other types of problems, as the core engine is the BS operator whose derivatives remain unchanged while the nonlinear components are modified. Moreover, the treatment of various kinds of nonlinear terms is presented, further supporting the generality of the methodology. Therefore, the implementation strategy is based on an object-oriented approach, enabling users to apply it to various nonlinear tasks.

6.1 European contract: Call option

The point of departure is an example of the linear Black-Scholes equation used for pricing the European call option. For comparison, we opted to use the standard central difference scheme on uniform grids. However, considering that a non-uniform mesh in FDM is relatively straightforward, smooth-mapping functions are widely employed. FEM offers certain advantages over IGA in terms of rapid convergence in the original scheme without any modifications. Provided the linear European call option

has a closed-form solution, a set of FEM-based approaches were experimentally tested. Additionally, Von Neumann stability analysis was conducted, providing unconditional stability for the time integration scheme. Furthermore, the eigenvalues of the time integration scheme fall within the absolute stability region, as determined numerically. Conventional FEM based on Lagrange polynomials demonstrates superiority over standard NURBS basis functions with equally distributed weights. However, as observed in the linear case, using an unstructured grid near the exercise price region suggests better results without requiring additional grid points elsewhere in the domain. Naturally, B-Spline basis functions, and subsequently NURBS basis functions, do not interpolate the interior points but do it at boundaries, whereas Lagrangian basis functions are interpolatory across nodes. The potential of fitted NURBS is demonstrated through unequally distributed weights, resulting in convergence twenty times faster than that achieved by P1-P2 FEM or unfitted NURBS. However, the concept of fitted NURBS is mathematically feasible when a closed-form solution is present. Otherwise, particularly in highly nonlinear problems, it leads to a nonlinear optimization problem aimed at minimizing errors through optimal weight selection.

6.2 European contract: Call option with transaction costs by Leland

The European call option under the Leland model is considered to incorporate the effect of transaction costs into the fair price of the contract. This model includes a nonlinear term in the diffusion component, necessitating careful selection of spatial and temporal grid sizes to maintain an experimentally determined upper bound. In the literature, the model is solved using a linearization approach, wherein two consecutive solution vectors in time are treated as a single current vector. In order to assess the behavior of the IGA framework, we adopt the same approach, which has resulted in goodly matched prices. It is worth noting that the P2-FEM solution deviates from those obtained by P1-FEM and FDM. One possible explanation for this phenomenon could be the presence of negative basis functions in conventional FEM, leading to negative values in coefficient matrices. Particularly in convection-dominant or nonconservative convection-diffusion equations, this can result in spurious oscillations, necessitating fundamental modifications to the scheme to control diffusion and convection terms. In contrast, IGA NURBS-based technology consistently features positive basis functions with compact support, regardless of the polynomial degree. The accurate calculation of Greeks, which represent sensitivities of option prices to

various factors, is of great interest, as least as the fair price of the contract itself. The advantageous properties of NURBS technology enable us to obtain smoother Greeks compared to those generated by P2-FEM or FDM, which has produced shocks across the domain. Furthermore, numerical analysis reveals that the eigenvalues of the time integration scheme fall within the absolute stability region. To the best of the author's knowledge, this is the first instance of applying IGA technology to a nonlinear European option pricing task.

6.3 American contract: Convertible bonds by TF model

Pricing convertible bonds presents a formidable challenge due to their fluctuating parameters and the variational inequalities that serve to hedge risks from both above and below. While the TF model is a popular choice among practitioners, it has not gained as much traction among scientific groups. Therefore, the objective of this study is to present alternative FEM-based techniques to address this problem. P1-P2 FEM is applied to the TF model, demonstrating superior convergence properties compared to FDM. This is attributed to the fewer iterations required in Newton's method, which entails reduced computational time. As demonstrated, P2-FEM achieves accuracy in two decimal places using a relatively smaller number of points than P1-FEM and/or FDM. To the best of the author's knowledge, there have not been previous FEM solutions for the TF model and approximation results for the Greeks using FEM. Additionally, these results are favorably compared with those obtained using FDM.

6.4 American contract: Convertible bonds by AFV model

The assumptions of the TF model are shown to be inconsistent due to the default strategies of the underlying asset value. Consequently, the limitations of the TF model are addressed in the AFV model by incorporating partial and total default cases, thereby ensuring a recovery factor in the event of default. This modification results in a system of coupled triple PDEs and corresponding inequality constraints, which must be applied at each iteration. To approximate the contribution of the inequality constraints to the bond price, we adopt the approach proposed by P. Forsyth, utilizing a nonlinear penalty term where the constraints are implicitly imposed. The system is solved using Newton's method for non-smooth functions at each time step. Being

convection-dominated and nonconservative, the AFV model's benchmark solution is obtained using sophisticated FVM with flux limiters and Rannacher time-stepping methods. In contrast, our approach transforms physical coordinates into log coordinates to avoid variable coefficients. We then apply standard P1-P2 FEM along with IGA NURBS. This approach maintains monotonic convergence without the need for stabilization techniques to be used in benchmark solutions. Furthermore, using adjusted fitted NURBS based on reference solutions obtained with P1-P2 FEM enables convergence with almost thirty times lesser grids than those reported in the literature. Notably, there is no prior instance in the literature of using IGA NURBS for American-style contracts. Additionally, the fitting of NURBS is performed by optimizing weights according to reference solutions. The Greeks calculated using NURBS exhibit a close similarity to those obtained with P2-FEM.

6.5 Future work

To the best of the author's knowledge, no analytical error analyses are available for nonlinear Black-Scholes problems, encompassing both a priori and a posteriori error estimates. The latter should include an adaptive grid strategy, which could enhance computational efficiency regarding both computational time and accuracy. While a priori error estimates are typically designed for linear problems, it is still feasible to conduct predictive analyses that bound the error from above, indicating the order of convergence in both time and space.

The generalization of NURBS weight parameters holds significance for a broad class of nonlinear problems encountered in financial engineering. It is widely acknowledged that computational time in numerical solutions of PDEs increases exponentially with spatial dimensions. Therefore, NURBS technology can be extended to higher-dimensional problems, such as the Heston or multi-asset models to achieve satisfactory accuracy and fast computational time.

With recent advancements in the IGA framework, Bernstein polynomial-based functions and T-splines are presenting the versatility of NURBS in specific tasks. Incorporating T-splines or Bézier curves could also be explored in future research endeavors.

Due to the computational limitations of the classical numerical approaches, especially when considering the portfolio of multiple assets, practically, it becomes less applicable due to the slowness of the computations. After the third dimension,

the variational methods or other discrete methods suffer from being computationally inefficient in achieving convergent results. Therefore, the recent advancements on physics-informed neural networks seems promising in dealing with higher dimensional problems, thus, the important research frontier found in mathematical finance is the treatment of the higher dimensional problem, which could also be realized in the future.

Bibliography

Y. Amanbek and M. F. Wheeler. A priori error analysis for transient problems using enhanced velocity approach in the discrete-time setting. *Journal of Computational and Applied Mathematics*, 361:459–471, 2019.

Y. Amanbek, G. Singh, G. Pencheva, and M. F. Wheeler. Error indicators for incompressible darcy flow problems using enhanced velocity mixed finite element method. *Computer Methods in Applied Mechanics and Engineering*, 363:112884, 2020.

M. Ammann, A. Kind, and C. Wilde. Simulation-based pricing of convertible bonds. *Journal of Empirical Finance*, 15(2):310–331, 2008.

A. Andalaft-Chacur, M. M. Ali, and J. G. Salazar. Real options pricing by the finite element method. *Computers and Mathematics with Applications*, 61(9):2863–2873, May 2011. doi: 10.1016/j.camwa.2011.03.070.

K. Andersson, A. Andersson, and C. W. Oosterlee. Convergence of a robust deep FBSDE method for stochastic control. *SIAM Journal on Scientific Computing*, 45 (1):A226–A255, Feb. 2023. doi: 10.1137/22m1478057.

J. Ankudinova and M. Ehrhardt. On the numerical solution of nonlinear Black–Scholes equations. *Computers and Mathematics with Applications*, 56(3): 799–812, Aug. 2008.

E. Ayache, P. Forsyth, and K. R. Vetzal. Valuation of convertible bonds with credit risk. *The Journal of Derivatives*, 11(1):9–29, 2003.

L. Bachelier. Théorie de la spéculation. *Annales scientifiques de l'École normale supérieure*, 17:21–86, 1900. doi: 10.24033/asens.476.

G. Barles and H. M. Soner. Option pricing with transaction costs and a nonlinear black-scholes equation. *Finance and Stochastics*, 2:369–397, 1998.

G. Barone-Adesi, A. Bermudez, and J. Hatgioannides. Two-factor convertible bonds valuation using the method of characteristics/finite elements. *Journal of Economic Dynamics and Control*, 27(10):1801–1831, Aug. 2003.

Y. Bazilevs, L. Veiga, J. Cottrell, T. Hughes, and G. Sangalli. Approximation isogeometric analysis: stability and error estimates for h-refined meshes. *Math. Models Methods Appl. Sci.*, 16:1–60, 01 2006.

F. Black and M. S. Scholes. The pricing of options and corporate liabilities. *Journal of Political Economy*, 81:637 – 654, 1973.

M. J. Brennan and E. S. Schwartz. Convertible bonds: Valuation and optimal strategies for call and conversion. *The Journal of Finance*, 32, 1977.

M. J. Brennan and E. S. Schwartz. Analyzing convertible bonds. *Journal of Financial and Quantitative Analysis*, 15, 1980.

R. Brown. A brief account of microscopical observations made in the months of june, july and august 1827, on the particles contained in the pollen of plants; and on the general existence of active molecules in organic and inorganic bodies. *The Philosophical Magazine*, 4(21):161–173, Sept. 1828. doi: 10.1080/14786442808674769.

J. Choi, M. Kwak, C. W. Tee, and Y. Wang. A Black–Scholes user's guide to the Bachelier model. *Journal of Futures Markets*, 42(5):959–980, Feb. 2022. doi: 10.1002/fut.22315.

C. C. Christara and N. C.-H. Leung. Option pricing in jump diffusion models with quadratic spline collocation. *Applied Mathematics and Computation*, 279:28–42, 2016. ISSN 0096-3003. doi: https://doi.org/10.1016/j.amc.2015.12.045. URL https://www.sciencedirect.com/science/article/pii/S0096300315300333.

C. C. Christara and R. Wu. Penalty and penalty-like methods for nonlinear HJB PDEs. *Applied Mathematics and Computation*, 425:127015, 2022.

R. Cont, N. Lantos, and O. Pironneau. A reduced basis for option pricing. *SIAM Journal on Financial Mathematics*, 2(1):287–316, Jan. 2011. doi: 10.1137/10079851x. URL https://doi.org/10.1137/10079851x.

J. A. Cottrell, T. J. R. Hughes, and Y. Bazilevs. *Isogeometric Analysis: Toward Integration of CAD and FEA*. Wiley Publishing, 1st edition, 2009.

C. de Boor. *A Practical Guide to Splines.*, volume 34. JSTOR, Jan. 1980. doi: 10.2307/2006241. URL https://doi.org/10.2307/2006241.

J. de Frutos. *A Finite Element Method for Two Factor Convertible Bonds*, pages 109–128. Springer US, Boston, MA, 2005. doi: 10.1007/0-387-25118-9_5.

E. Dremkova and M. Ehrhardt. A high-order compact method for nonlinear Black–Scholes option pricing equations of American options. *International Journal of Computer Mathematics*, 88(13):2782–2797, 2011.

D. Duffie and K. J. Singleton. Modeling term structures of defaultable bonds. *Review of Financial Studies*, 12(4):687–720, July 1999. ISSN 1465-7368. doi: 10.1093/rfs/12.4.687. URL http://dx.doi.org/10.1093/rfs/12.4.687.

A. Einstein. Über die von der molekularkinetischen Theorie der Wärme geforderte Bewegung von in ruhenden Flüssigkeiten suspendierten Teilchen. *Annalen der Physik*, 322(8):549–560, 1905. doi: 10.1002/andp.19053220806.

C. Fletcher. The group finite element formulation. *Computer Methods in Applied Mechanics and Engineering*, 37(2):225–244, 1983.

P. Forsyth, K. Vetzal, and R. Zvan. A finite element approach to the pricing of discrete lookbacks with stochastic volatility. *Applied Mathematical Finance*, 6(2): 87–106, 1999.

P. A. Forsyth and K. R. Vetzal. Quadratic Convergence for Valuing American Options Using a Penalty Method. *SIAM Journal on Scientific Computing*, 23(6):2095–2122, Jan. 2002.

R. Frey and A. Stremme. Market volatility and feedback effects from dynamic hedging. *Mathematical Finance*, 7(4):351–374, Oct. 1997. ISSN 1467-9965. doi: 10.1111/1467-9965.00036.

A. Golbabai, L. V. Ballestra, and D. Ahmadian. A highly accurate finite element method to price discrete double barrier options. *Computational Economics*, 44(2): 153–173, June 2013. doi: 10.1007/s10614-013-9388-5. URL https://doi.org/10.1007/s10614-013-9388-5.

J. Harrison and S. R. Pliska. Martingales and stochastic integrals in the theory of continuous trading. *Stochastic Processes and their Applications*, 11(3):215–260, Aug. 1981. doi: 10.1016/0304-4149(81)90026-0.

D. Higham. *An Introduction to Financial Option Valuation: Mathematics, Stochastics.*. Cambridge University Press, 2004.

T. Hughes, J. Cottrell, and Y. Bazilevs. Isogeometric analysis: CAD, finite elements, NURBS, exact geometry and mesh refinement. *Computer Methods in Applied Mechanics and Engineering*, 194(39-41):4135–4195, Oct. 2005. doi: 10.1016/j.cma.2004.10.008.

J. C. Hull. *Options, Futures, and Other Derivatives*. Prentice Hall, 9 edition, 2014.

J. Ingersoll. A contingent-claims valuation of convertible securities. *Journal of Financial Economics*, 4, may 1977.

K. Ito. On stochastic differential equations. 1951.

C. V. H. Jan De Spiegeleer, Wim Schoutens. *The Handbook of Hybrid Securities: Convertible Bonds, CoCo Bonds and Bail-In*. The Wiley Finance Series. Wiley, 1 edition, 2014.

P. J. Jan De Spiegeleer, Wim Schoutens. *The handbook of convertible bonds : pricing, strategies and risk management*. Wiley finance series. Wiley, 1 edition, 2011.

M. Jandačka and D. Ševčovič. On the risk-adjusted pricing-methodology-based valuation of vanilla options and explanation of the volatility smile. *Journal of Applied Mathematics*, 2005(3):235–258, 2005. ISSN 1687-0042. doi: 10.1155/jam.2005.235.

X. Jiang and Y. Lin. Relevant integrals of NURBS and its application in hull line element design. *Ocean Engineering*, 251:111147, May 2022. ISSN 0029-8018. doi: 10.1016/j.oceaneng.2022.111147.

R. Kazbek, Y. Erlangga, Y. Amanbek, and D. Wei. Pricing Convertible Bonds with the Penalty TF Model Using Finite Element Method. *Computational Economics*, May 2024. ISSN 1572-9974. doi: 10.1007/s10614-024-10625-1.

P. Kovalov and V. Linetsky. Valuing convertible bonds with stock price, volatility, interest rate, and default risk. *SSRN Electronic Journal*, 2008.

S. Kozpınar, M. Uzunca, and B. Karasözen. Pricing European and American options under Heston model using discontinuous Galerkin finite elements. *Mathematics and Computers in Simulation*, 177:568–587, Nov. 2020. doi: 10.1016/j.matcom.2020.05.022.

P. Kythe and D. Wei. *An Introduction to Linear and Nonlinear Finite Element Analysis*. Birkhäuser Boston, 2004. doi: 10.1007/978-0-8176-8160-9. URL https://doi.org/10.1007/978-0-8176-8160-9.

H. E. Leland. Option Pricing and Replication with Transactions Costs. *The Journal of Finance*, 40, 12 1985. doi: 10.2307/2328113. URL http://gen.lib.rus.ec/scimag/index.php?s=10.2307/2328113.

S. Lin and S.-P. Zhu. Numerically pricing convertible bonds under stochastic volatility or stochastic interest rate with an ADI-based predictor–corrector scheme. *Computers Mathematics with Applications*, 79(5):1393–1419, 2020. ISSN 0898-1221. doi: https://doi.org/10.1016/j.camwa.2019.09.003. URL https://www.sciencedirect.com/science/article/pii/S0898122119304444.

W. K. Liu, S. Li, and H. S. Park. Eighty years of the finite element method: Birth, evolution, and future. *Archives of Computational Methods in Engineering*, 29(6): 4431–4453, June 2022. doi: 10.1007/s11831-022-09740-9. URL https://doi.org/10.1007/s11831-022-09740-9.

K. Milanov and O. Kounchev. Binomial tree model for convertible bond pricing within equity to credit risk framework. *SSRN Electronic Journal*, 2012.

R. Mohammadi. Quintic B-spline collocation approach for solving generalized Black–Scholes equation governing option pricing. *Computers amp; Mathematics with Applications*, 69(8):777–797, Apr. 2015. ISSN 0898-1221. doi: 10.1016/j.camwa.2015.02.018.

C. W. Oosterlee and L. A. Grzelak. *Mathematical Modeling and Computation in Finance*. WORLD SCIENTIFIC (EUROPE), July 2019. doi: 10.1142/q0236. URL https://doi.org/10.1142/q0236.

L. Ortiz-Gracia and C. W. Oosterlee. Robust pricing of european options with wavelets and the characteristic function. *SIAM Journal on Scientific Computing*, 35(5):B1055–B1084, 2013. doi: 10.1137/130907288.

J. Pospíšil and V. Švígler. Isogeometric analysis in option pricing. *International Journal of Computer Mathematics*, 96(11):2177–2200, July 2018. doi: 10.1080/00207160.2018.1494826. URL https://doi.org/10.1080/00207160.2018.1494826.

R. Rannacher. Finite element solution of diffusion problems with irregular data. *Numerische Mathematik*, 43(2):309–327, 1984.

P. J. Roache. Code verification by the method of manufactured solutions. *Journal of Fluids Engineering*, 124, 2001.

C. R. J. Roger A. Horn. *Matrix Analysis*. Cambridge University Press, 2nd edition, 2013.

Y. H. A. Saedi and G. A. Tularam. A Review of the Recent Advances Made in the Black-Scholes Models and Respective Solutions Methods. *Journal of Mathematics and Statistics*, 14(1):29–39, Jan. 2018.

R. Sevilla and S. Fernández-Méndez. Numerical integration over 2D NURBS-shaped domains with applications to NURBS-enhanced FEM. *Finite Elements in Analysis and Design*, 47(10):1209–1220, Oct. 2011. ISSN 0168-874X. doi: 10.1016/j.finel.2011.05.011. URL http://dx.doi.org/10.1016/j.finel.2011.05.011.

L. Trefethen. *Finite Difference and Spectral Methods for Ordinary and Partial Differential Equations*. 1996.

C. Tsiveriotis, Kostas; Fernandes. Valuing convertible bonds with credit risk. *The Journal of Fixed Income*, 8, 09 1998.

D. Wei, Y. A. Erlangga, and G. Zhumakhanova. A finite element approach to the numerical solutions of Leland's model. *International Review of Economics &amp Finance*, 89:582–593, Jan. 2024. doi: 10.1016/j.iref.2023.07.076. URL https://doi.org/10.1016/j.iref.2023.07.076.

P. Wilmott. *Derivatives: The Theory and Practice of Financial Engineering*. Frontiers in Finance Series. Wiley, 1998.

M. Yousuf, A. Q. Khaliq, and B. Kleefeld. The numerical approximation of nonlinear Black–Scholes model for exotic path-dependent American options with transaction cost. *International Journal of Computer Mathematics*, 89(9):1239–1254, June 2012. doi: 10.1080/00207160.2012.688115. URL https://doi.org/10.1080/00207160.2012.688115.

S.-P. Zhu and J. Zhang. A new predictor–corrector scheme for valuing American puts. *Applied Mathematics and Computation*, 217(9):4439–4452, Jan. 2011.

S.-P. Zhu, S. Lin, and X. Lu. Pricing puttable convertible bonds with integral equation approaches. *Computers and Mathematics with Applications*, 75(8):2757–2781, 2018. ISSN 0898-1221. doi: https://doi.org/10.1016/j.camwa.2018.01.007. URL https://www.sciencedirect.com/science/article/pii/S0898122118300117.

W. Zhu and D. A. Kopriva. A Spectral Element Approximation to Price European Options with One Asset and Stochastic Volatility. *Journal of Scientific Computing*, 42(3):426–446, Oct. 2009. doi: 10.1007/s10915-009-9333-x. URL https://doi.org/10.1007/s10915-009-9333-x.

R. Zvan, P. Forsyth, and K. Vetzal. Discrete Asian barrier options. *The Journal of Computational Finance*, 3(1):41–67, 1999.

D. Černá and K. Fiňková. Option pricing under multifactor Black–Scholes model using orthogonal spline wavelets. *Mathematics and Computers in Simulation*, 220: 309–340, June 2024. ISSN 0378-4754.